

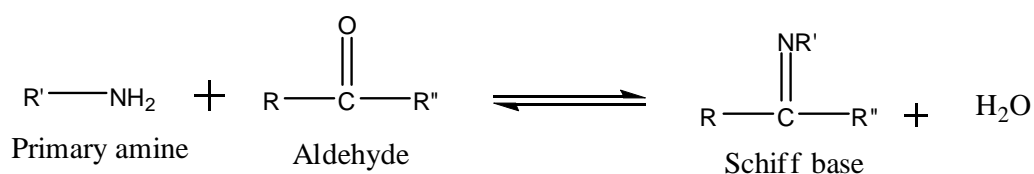
# **CHAPTER ONE**

## **INTRODUCTION**

## 1. Introduction

### 1.1 General review of Schiff bases

The condensation reaction between carbonyl group and amine leads to the formation of a Schiff base as defined by Hugo Schiff in 1864 [1]. The ability of Schiff bases to coordinate to metal ions, stabilize with metal ions in different oxidation states and control their catalytic transformations in many reactions makes them potential models for biological compounds. Their rate, equilibria and reaction mechanisms have been studied in many reactions [2,3] and one such example is given in Scheme 1 below:



where R, R' and R'' can be aliphatic or aromatic group

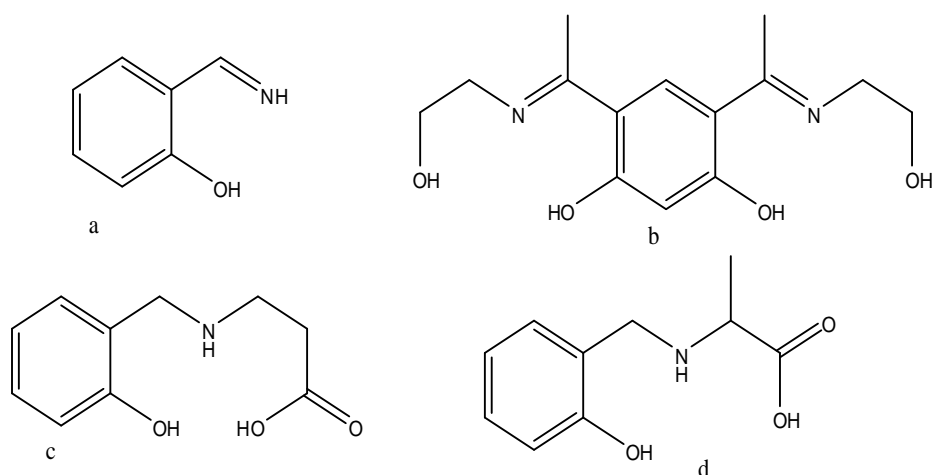
Scheme 1: Schiff base reaction pathway

Schiff bases play an important role in medicinal and inorganic chemistry as they show a wide spectrum of pharmacological applications due to their ability to bond with both transition and non-transition metal ions [4-6]. Their ability to form carbon-nitrogen bonds [7] also makes them important intermediates in a number of enzymatic reactions such as reactions involving interaction of an enzyme with amino acid or carbonyl group of the substrate. Among the mechanisms used by enzymes to catalyze reactions between organic molecules is through the formation of imines [8-10]. Schiff bases of aliphatic aldehyde are relatively unstable and are readily polymerized [11-14] while those of aromatic aldehyde having an effective conjugation system, are more stable [7,15,16]. Various studies have been conducted on the reaction of aromatic aldehydes [17] with aromatic and aliphatic amine and vice-versa. The imine chemistry since the time of discovery by Schiff in 1894

reported less literature on the quantitative studies of the reaction in cases where “R, R', and R'' are all hydrogen atoms or saturated alkyl groups” [13].

The polarographic studies on the equilibrium constant for imine formation in the reaction of ammonia and several amino acids with pyruvic acid and several aldehydes and ketones, have been reported [18,19]. Similar studies were carried out [20] to investigate the reaction of cyclopentanone and cyclohexanone with ammonia, methylamine, glycine, and other aliphatic amines. The ability of Schiff bases includes inducing chirality to the substrate, modifying the metal centered electronic factor and enhancing the solubility and stability of either homogeneous or heterogeneous catalyst [21, 22]. This coordination behavior of Schiff bases with metal ions has provided a means of extensive study of their properties since they are becoming increasingly relevant as biochemical, analytical and antimicrobial reagents.

However, the basic character of imine group and the presence of a phenolic group neighboring it in the back bone structure of the Schiff bases has led to the formation of stable complexes by simply donating a lone pair to the metal ion (Scheme 2a, b). Reduced Schiff bases, on the other hand, mainly act as a tridentate moiety, coordinating through the phenolate oxygen, imine nitrogen and carboxylate oxygen (Scheme 2c, and 2d). Meanwhile their binding mode can be confirmed by X-ray structures of their metal complexes.

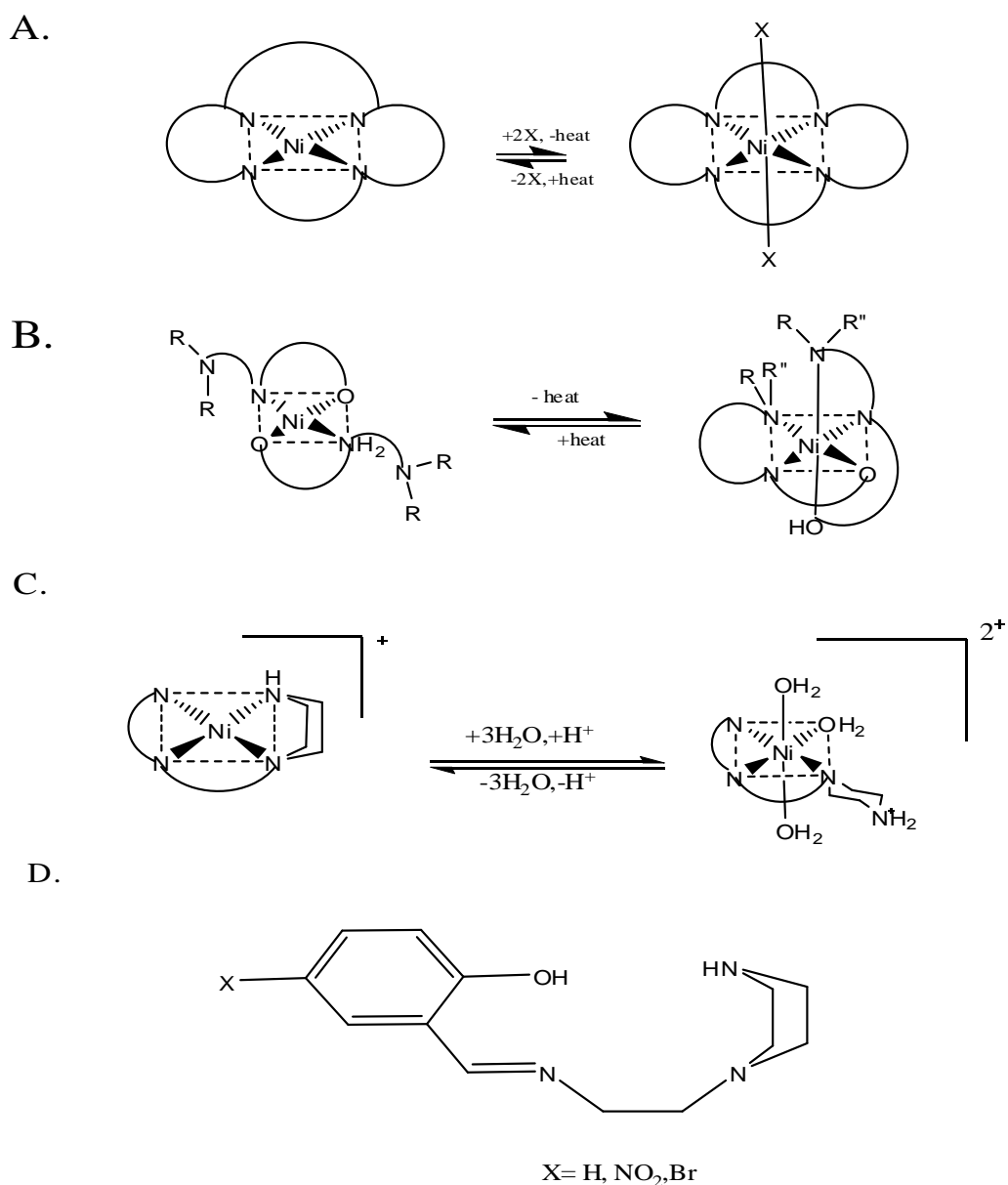


Scheme 2: (a) Salicylaldimine; (b) Keto-imine (c and d) reduced Schiff bases: of N-(2-hydroxybenzyl)-amino acid;

Schiff bases with chemotherapeutic applications have attracted the interest of many researchers [23]. Schiff base-metal complexes are the building block in coordination chemistry due to their high stability with most of the transition metals [26], easily synthesized, versatile and has a wide spectrum of applications [27,28]. Therefore, studies on novel metal-based compounds with therapeutic potentials became the area of intense investigation in biomedical and inorganic chemistry [29-31]. Moreover; many reports appeared on the syntheses, characterizations of Schiff bases and their metal complexes since the mid-nineteenth centuries [32]. Metal complexes of Schiff bases have occupied an important position in the development of coordination chemistry after the work of Jorgensen and Warner [33]. Ettlign isolated a dark green crystalline product from the reaction of cupric acetate and salicylaldehyde in aqueous ammonia [34]. Schiff prepared complexes of metal salicylaldehyde with primary amines and subsequently their metal complexes from the condensate of urea and salicylaldehyde. Delepine, 1899, prepared complexes by reacting metal acetate, salicylaldehyde and primary amine in alcohol and demonstrated 2:1 stoichiometry [35,36]. The first complex reported to have paramagnetic

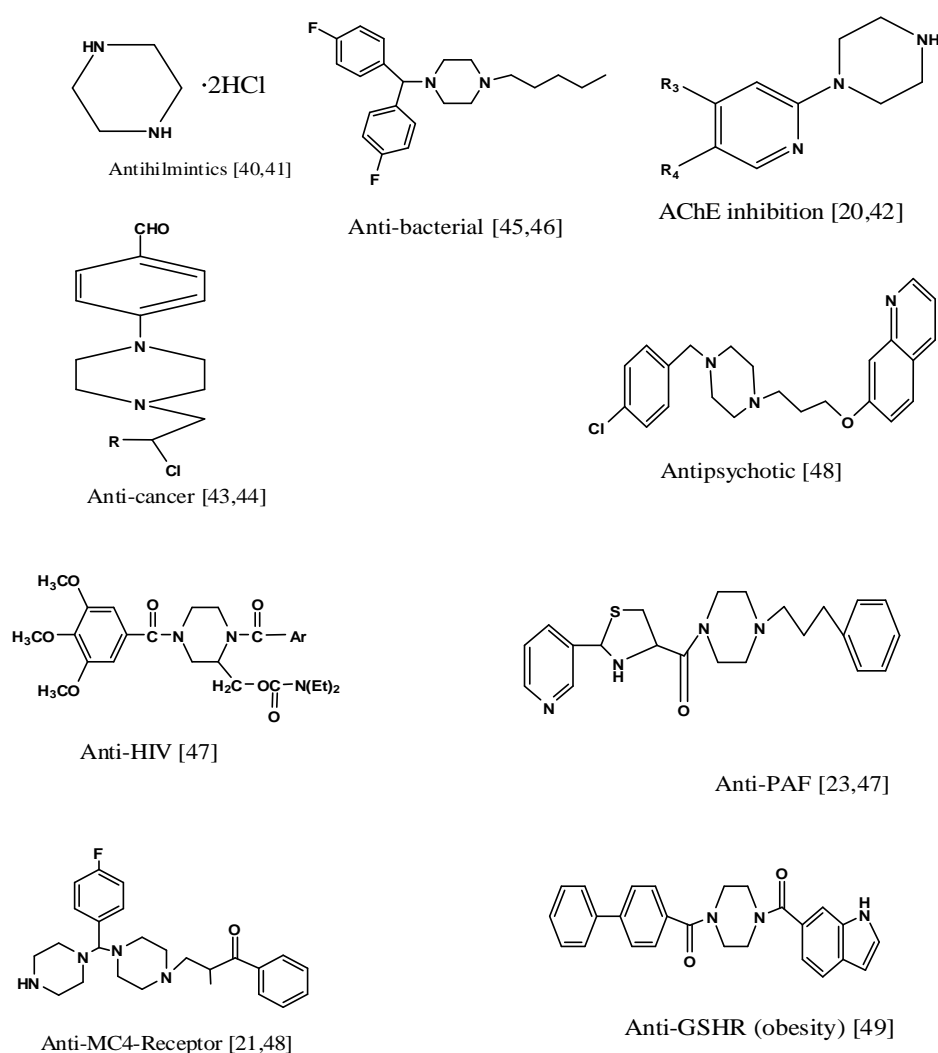
behavior was that of Ni(II), where it exists in  $\alpha$  and  $\beta$ -paramagnetic form at low temperature and  $\gamma$ -paramagnetic form at high-temperature [37,38]. This makes it possible for Ni atom to have the polymeric structure that involves sharing of the oxygen atoms. The structures of complexes of quadric-coordinated Ni(II) have also been studied [3,38], the controversy was on the assignment of tetrahedral stereochemistry strictly to four coordinate complexes based on their paramagnetism following Pauling criterion. In which case, the quadri-coordinated Ni(II) showed both paramagnetic and diamagnetic geometries.

Recently in 2003, Suman synthesized, characterized and studied the equilibrium changes for the first time on some 1-(2-salicylaldiminoethyl)piperazine Schiff bases with nickel(II) complex. The report [39] provided evidence for the existence of equilibrium in solution between the octahedral and planar forms of nickel(II) complexes (Scheme 3). The Schiff bases synthesized were coordinated through oxygen and nitrogen atoms to the central metal ion to form both chair and boat conformational geometries.



Scheme 3: Flexidentate behavior of Ni(II)-salicylaldiminoethylpiperazines complex.

Generally, the compounds containing piperazine moiety were found to show a wide spectrum of biological activities (Scheme 4). The activities reported are as anthelmintic [40,41], acetylcholinesterase inhibition [20,42], melanocortin-4-receptor (MC4-R) [21,48], anticancer [43,44], antibacterial [45,46], anti-PAF [23,47], anti-HIV [47], antipsychotics [48] and anti-obesity [49].



Scheme 4: Review of some biologically active piperazine compounds

## 1.2 Biological importance of Schiff bases and their metal complexes

Schiff bases continue to attract the interest of many researchers due to their ease of preparation and high affinity of coordination with transition metal ions to form solid complexes. Schiff bases are considered as potential chelators for superficial preparations of organometallic hybrid materials used for the study of molecule-based magnetism, material science [50], catalysis of reactions such as carboxylation, hydroformylation, oxidation, reduction and epoxidation, industrial processes, and complexation with some toxic metals [51]. Schiff base metal complexes exhibit potential biological activities which make them

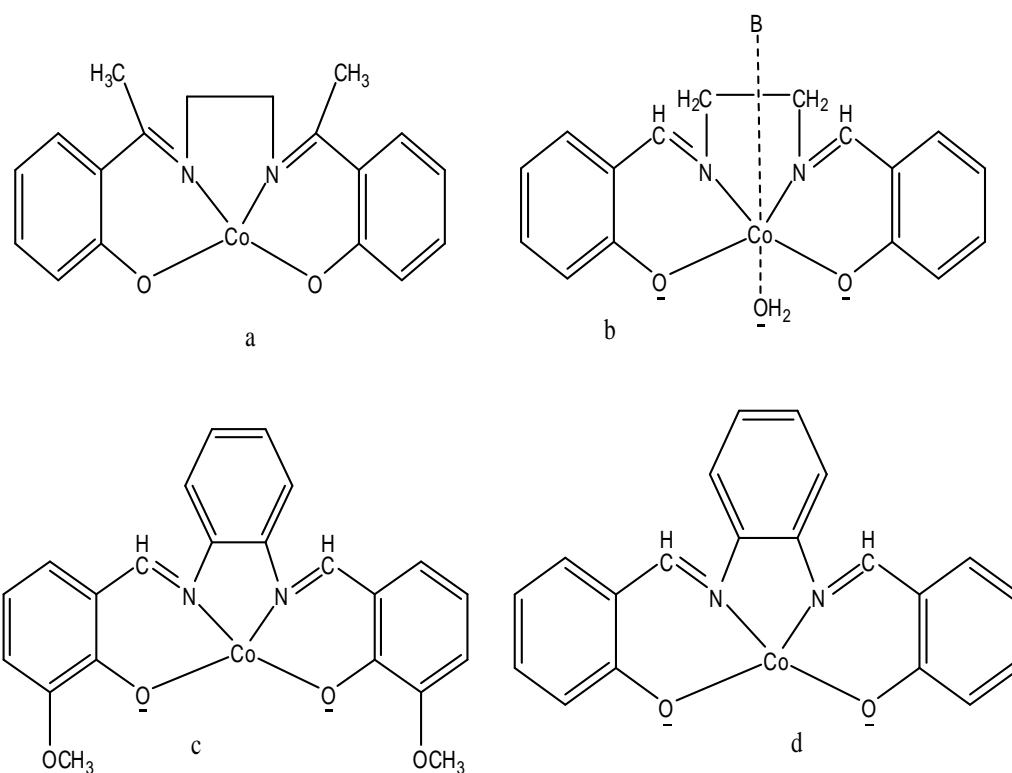
models for the study of enzymatic properties and they too appear to be important intermediates in a number of enzymatic reactions [52]. One of the most prevalent types of catalytic mechanisms in biochemical processes involves condensation of a primary amine in an enzyme, usually that of lysine residue with a carbonyl group of the substrate to form an imine or Schiff base [53,54]. Stereochemical studies [55-57] showed that Schiff bases formed from methylglyoxal and the amino groups of the lysine side chains of protein can bend back in such a way (towards the N-atom of peptide groups) that a charge transfer can occur between these groups and the oxygen atoms of the Schiff bases. Schiff bases derived from pyridoxal, and amino acids are considered very important ligands from biological point of view. Transition metal complexes of such ligands are important enzyme models. Certain polymeric Schiff bases have been reported to have anti-tumor activity [58]. Other biological roles of Schiff bases include transamination [59] and virus replication process [60] where the roles of metal ions are extremely important. The virus can penetrate into the host's cell only when it is mediated by some suitable metal ions. For example, zinc present in the cell wall of the bacterium E. coli can coordinate with the sulphur site present in the virus coating. By using any suitable metal complex such as  $\text{Cd}(\text{CN})_2$  which can preferably bind with the 'S' site as virus-(S)- $\text{Cd}(\text{CN})_2$ , the penetration of the viral DNA into the host cell can be arrested.

The literature has shown that copper and zinc metals are essentially required for virus replication process, hence by increasing or decreasing their concentration viral growth may be controlled [61,62]. However, anti-tumor and antibacterial activity of some Schiff bases has been attributed to their ability to chelate with trace transition metal [63]. Several explanations have been suggested for this enhancement in activity of metal complexation [64]. Generally, it was observed that transition metal complexes have greater activity and

less toxic effect [65] though; qualitative and quantitative variations in biological activities exists among the complexes depending on the metal ion or the ligand.

Moreover, one of the interesting features of Schiff base complexes is their ability to change in size, charge distribution, stereochemistry, redox potentials and other physical properties during chemical synthesis [66]. For example, metal complexes with divalent metal ions are well known (Scheme. 5) and their structure's changes from planar coordination Schiff base to non-planar tetrahedral coordination depending on the length of the methylene bridge which is normally determined by the oxidation state of the metal ion and the type of ligand used [35,36,67,68].

In particular, the complexes of bis(salicylaldehyde)ethylenediimine-cobalt-(II) (salcomines) and similar Schiff base complexes of Co(II) that are capable of reversibly coordinating with oxygen (Scheme. 5a-5d) have been extensively studied as “model compounds” to simulate natural oxygen carriers that contain transition metals, e.g., iron (myoglobin) and copper (heamocyanin). The Schiff bases in such di-oxygen carriers are usually tetra- or penta-dentate, and in the case of Co(II) [68], the resulting complex may have wide variations in structure, composition, and di-oxygen affinity. Di-oxygen-binding complexes based on Fe(II), Cu(I), Ni(II), and Mn(II) have been reported [68,69], but chelates of Co(II) displayed high tendencies for oxygen production due to the wide range of stabilities of cobalt di-oxygen complexes and the corresponding wide range of structures and properties available. The di-oxygen ligand binds in *trans* position to the axial base in which case the axial base that promote oxygenation may be aliphatic or aromatic (Scheme 5b)



Scheme 5: Salcomines

The binuclear copper(II) complexes with two metal ions in close proximity have been studied [70-72], their magnetic and redox properties were discussed [73, 74]. Such kind of copper complexes was reported to play a role in dioxygenase transport or activation, electron transfer, reduction of nitrogen oxides and hydrolytic chemistry [75,76]. However, the essentiality of copper for mammals was established as early as 1920s, but human copper deficiency was not well described until 1960s when Cordano and Graham [77,78] reviewed the treatment of severely malnourished infants treated with low-copper, milk-based diets.

### 1.3 Metals of the study

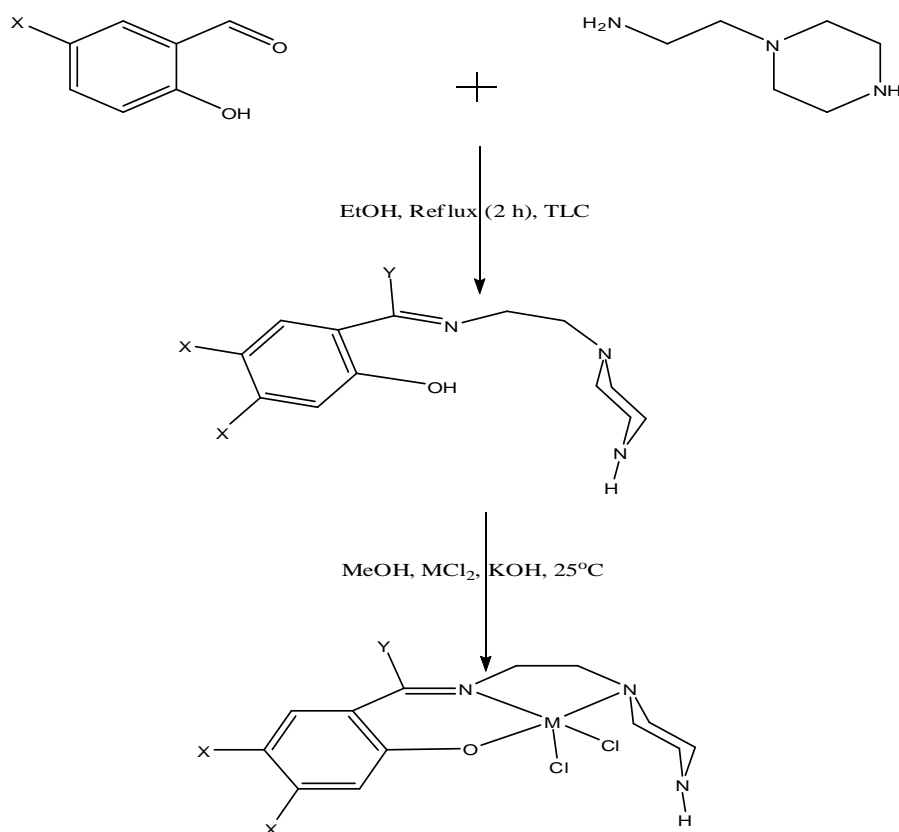
The relevance of metal ions in the living system makes it possible for many researches to be conducted in such a way to generate simple models for biologically occurring metal-

enzymes. The biological roles for the metal-elements used in this study are briefly described.

Copper is an essential element that serves as the cofactor for metalloenzymes, which binds iron to form transferrin, and binds plasma to form ceruloplasmin found in the liver [79]. Copper is involved in many biological systems [80-82], and this attracts the attention of many researchers to determine its mechanisms of absorption [82,83], distribution [84,85], metabolism and excretion [86,87]. The diseases caused by copper deficiency or copper in excess were also investigated [88,89].

Zinc, on the other hand, is also an essential element which plays an imperative role in cell-mediated immune functions. Zinc is employed as a cofactor for metallo-enzymes, superoxide dismutase, collagenase, alcohol dehydrogenase, alkaline phosphate and in spermatogenesis [90,91]. It is required for the proper functioning of mucosal cells and can arrest the advancement of gastrointestinal disease by free radical scavenging and interruption of the inflammatory process as an antioxidant and anti-inflammatory agent. Zinc deficiency can cause poor wound healing, loss of taste and smell, growth retardation and elevation in reactive oxygen species (ROS) [92,93]. Zinc complexes were reported to have anti-ulcer activity and used as drugs for the treatment of gastrointestinal injuries in Japan [31,93].

Cadmium, which was reported to have an extremely long biological half-life, was observed to complex with metallothionein (a cysteine rich protein), which is used to protect cells against the toxic effects of cadmium) [94-98]. Metallothionein is also a protein involved in cadmium transport from intestines to liver and from liver to kidneys [99-102]. Diverse factors affect cadmium absorption from the intestines. Generally, the compounds of this study were prepared according to Scheme 6 below:



Where X = H, OH, OCH<sub>3</sub>, Cl, Br and/or NO<sub>2</sub>. Y = H or CH<sub>3</sub>.  
M = Cu, Zn and Cd

Scheme 6: Synthetic route for the aldehydes and ketones Schiff bases of 2-(piperazin-1-yl)ethanamine

#### 1.4 Objectives of this study

In this study we report the synthesis, characterization, acute toxicity, anti-ulcer studies, antioxidant properties, anticancer evaluations and acetylcholinesterase inhibitory activities of the Schiff bases derived from the reflux condensation reaction of 2-(piperazin-1-yl)ethanamine with salicylaldehyde, 5-chlorosalicylaldehyde, 5-bromosalicylaldehyde, 5-nitrosalicylaldehyde, 5-hydroxysalicylaldehyde, 4-hydroxysalicylaldehyde, 5-methoxy salicylaldehyde, 4-methoxysalicylaldehyde, 1-(2-hydroxyphenyl)ethanone and 1-(2,4-dihydroxy phenyl)ethanone and their metal complexes of Cu(II), Zn(II) and Cd(II). The compounds were characterized by mass spectra, CHN, FTIR, <sup>1</sup>H NMR, <sup>13</sup>C NMR, UV-Visible, TGA, and X-ray diffraction analysis. The compounds prepared were screened for

biological evaluations according to the type and protocol of the experiments mentioned above.

# **CHAPTER TWO**

## **EXPERIMENTAL**

## **2. Experimental**

### **2.1 Materials**

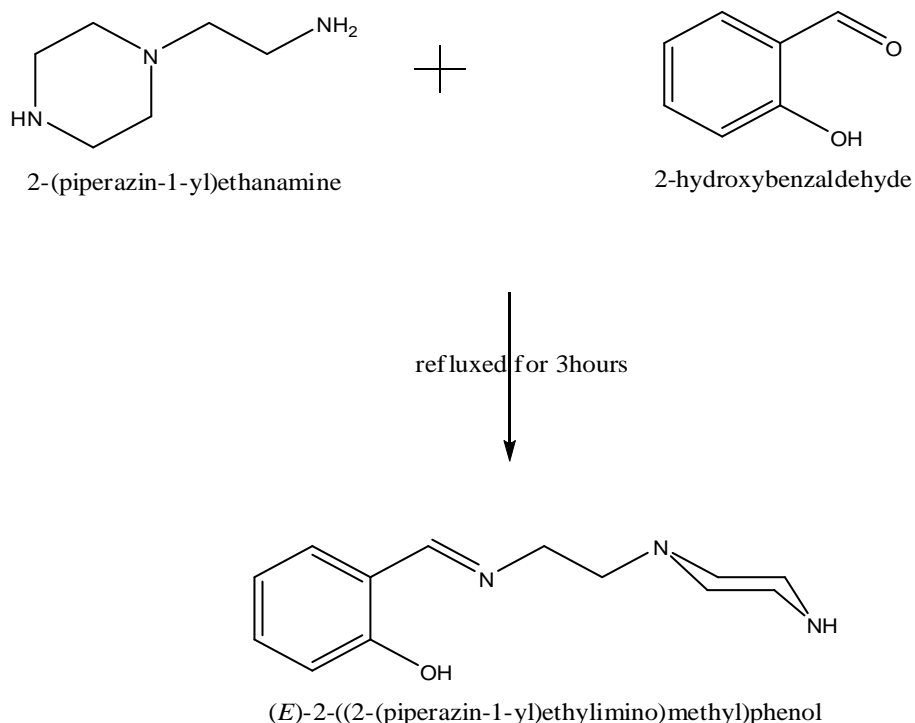
2-(piperazine-1-yl)ethanamine, salicylaldehyde, 5-chlorosalicylaldehyde, 5-bromosalicylaldehyde, 5-nitrosalicylaldehyde, 5-hydroxysalicylaldehyde, 4-hydroxysalicylaldehyde, 5-methoxysalicylaldehyde, 4-methoxysalicylaldehyde, 1-(2-hydroxyphenyl)ethanone and 1-(2,4-dihydroxyphenyl)ethanone were obtained from Merck Millipore, Kuala Lumpur, Malaysia and used without further purification. Solvents were of analytical grade and were distilled before use. All other reagents and chemicals were of analytical grade and used as received.

### **2.2 Methods**

#### **2.2.1 Preparation of Schiff base Ligands**

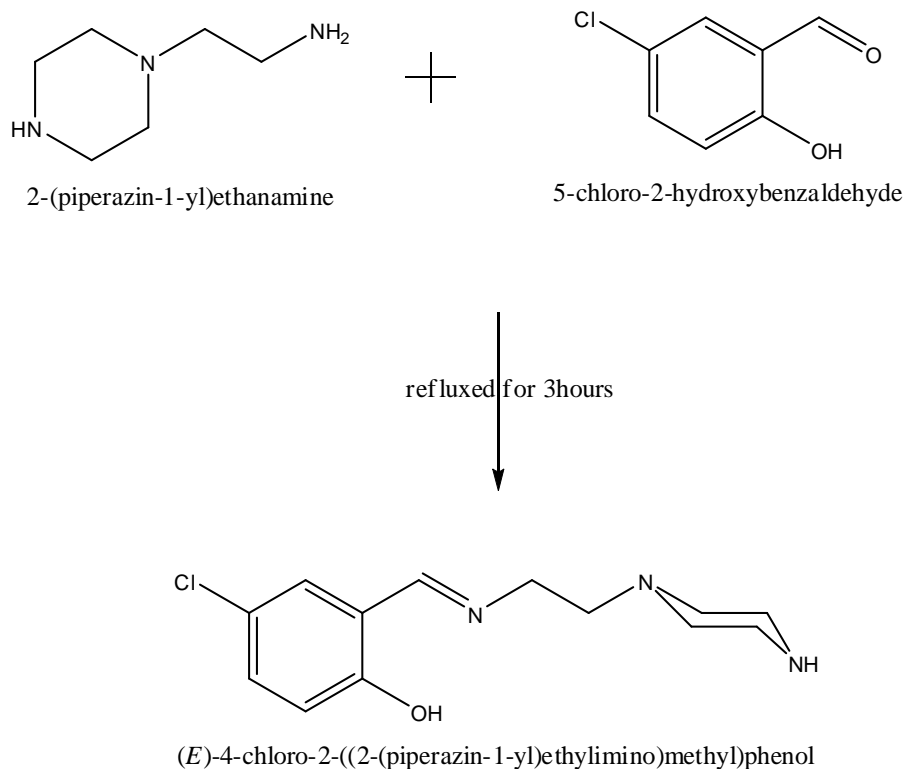
Two series of Schiff bases were prepared by the reaction of 2-(piperazine-1-yl)ethanamine with aldehydes (salicylaldehyde, 5-chlorosalicylaldehyde, 5-bromosalicylaldehyde, 5-nitrosalicylaldehyde, 5-hydroxysalicylaldehyde, 4-hydroxysalicylaldehyde, 5-methoxysalicylaldehyde, 4-methoxysalicylaldehyde,) and ketones (1-(2-hydroxyphenyl)ethanone and 1-(2,4-dihydroxyphenyl) ethanone) separately. The preparatory procedures are described below.

### 2.2.1.1 Preparation of (*E*)-2-((2-(piperazin-1-yl)ethylimino)methyl)phenol (LSP)



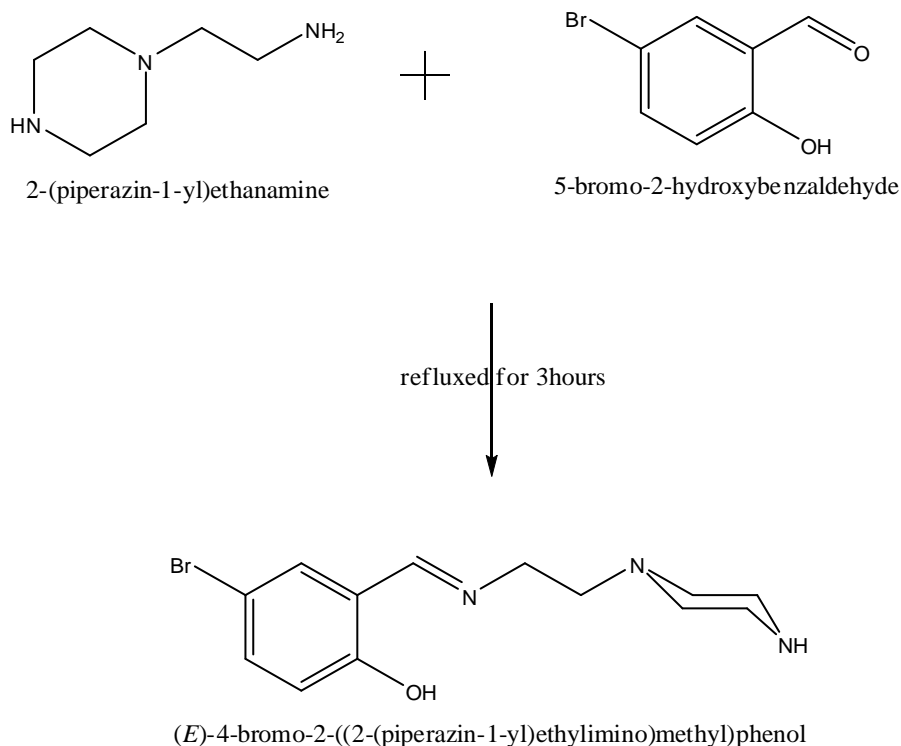
The compound 2-(piperazin-1-yl)ethanamine (2.58 g, 20 mmol) was dissolved in absolute ethanol and added drop wise to a stirred ethanolic solution of salicylaldehyde (2.44 g, 20 mmol) at room temperature and then refluxed for 3 h, to give an orange solution. The solution was concentrated using a rotary evaporator to form a red oil. The red oil became solid after leaving at room temperature two days [39] and the solid was dissolved in methanol by heating to 55 °C. Solid sodium perchlorate was added to the solution while it was hot to absorb the water and then filtered. A reddish-yellow solid appeared after concentrating and cooling. The solid product was collected by filtration, washed with water-ethanol mixture and dried in a vacuum desiccator. Yield (0.15 g, 64.4 %)

### 2.2.1.2 Preparation of (*E*)-4-chloro-2-((2-(piperazin-1-yl)ethylimino)methyl) phenol (LCS)



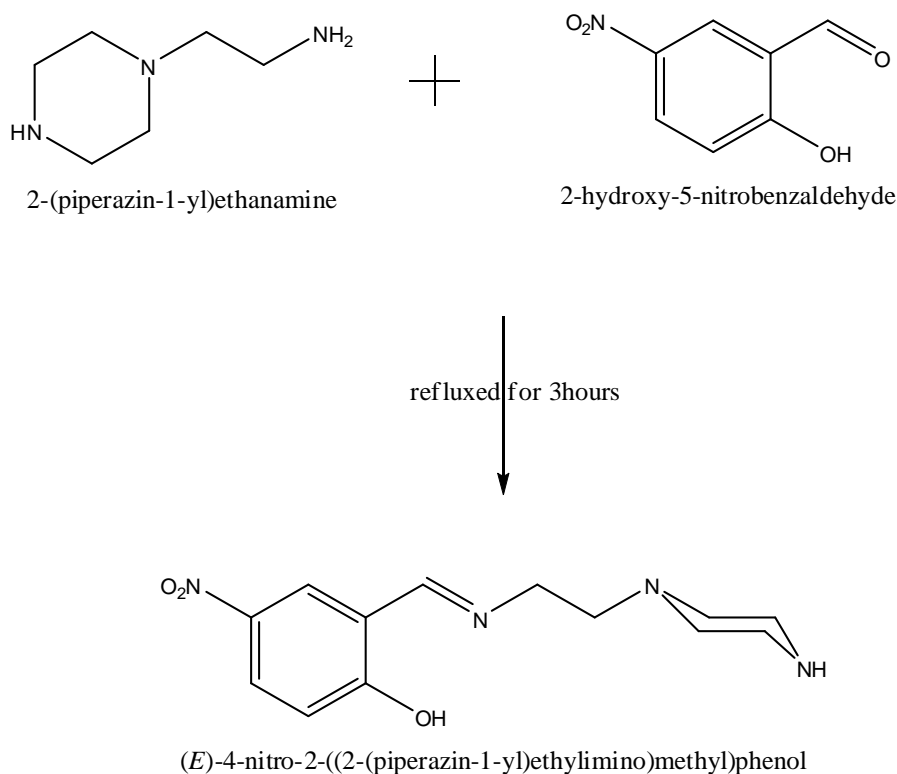
The compound 2-(piperazin-1-yl)ethanamine (2.58 g, 20 mmol) was dissolved in absolute ethanol and added drop wise to a stirred ethanolic solution of 5-chlorosalicylaldehyde (3.2 g, 20 mmol) at room temperature and then refluxed for 3 h, to give an orange solution. The solution was concentrated using a rotary evaporator to form a red oil. The red oil was kept in an oven at 75 °C overnight to give a brown solid. The solid product was recrystallized in methanol by heating to 60 °C. After concentrating and cooling, a yellowish solid was formed. The solid was collected by filtration, washed with methanol-water mixture and dried in vacuum. Yield (0.18 g, 67.4 %)

### 2.2.1.3 Preparation of (*E*)-4-bromo-2-((2-(piperazin-1-yl)ethylimino)methyl) phenol (LBS)



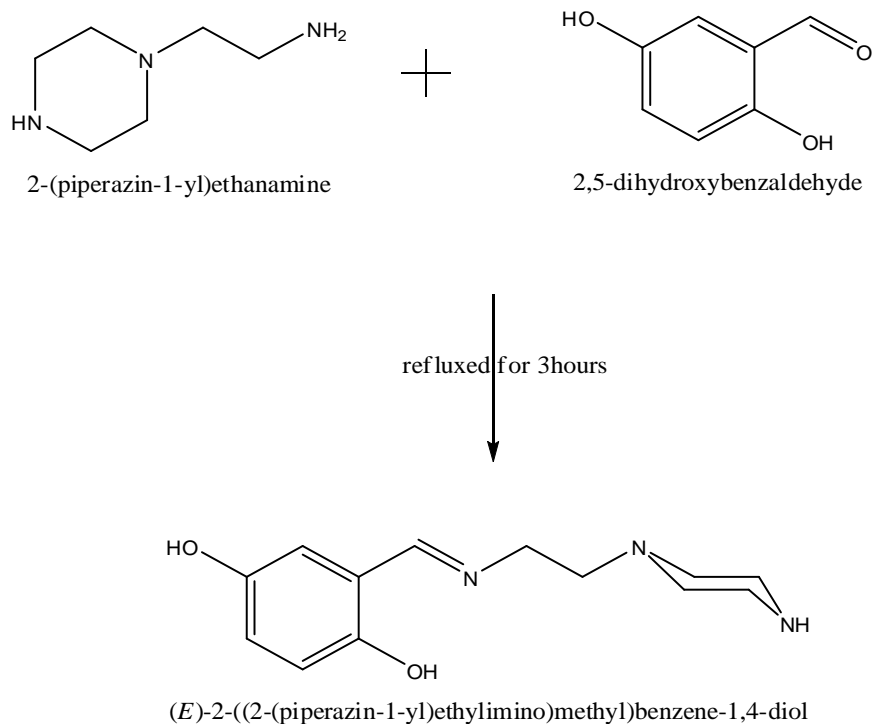
The compound 2-(piperazin-1-yl)ethanamine (2.58 g, 20 mmol) was dissolved in absolute ethanol and added drop wise to a stirred ethanolic solution of 5-bromosalicylaldehyde (4 g, 20 mmol) at room temperature and then refluxed for 3 h, to give an orange solution. The solution was concentrated using rotary evaporator to form a red oil [39]. The red oil was kept in an oven overnight at 75 °C to give deep yellow solid. The solid product was recrystallized in methanol at 60 °C, which after concentrating formed a red gel, and on addition of few drops of diethyl ether gave a solid. The solid product was collected by filtration, washed with methanol-water mixture and dried in vacuum. Yield (0.24 g, 76.9 %)

#### 2.2.1.4 Preparation of (*E*)-4-nitro-2-((2-(piperazin-1-yl)ethylimino)methyl)phenol (LNS)



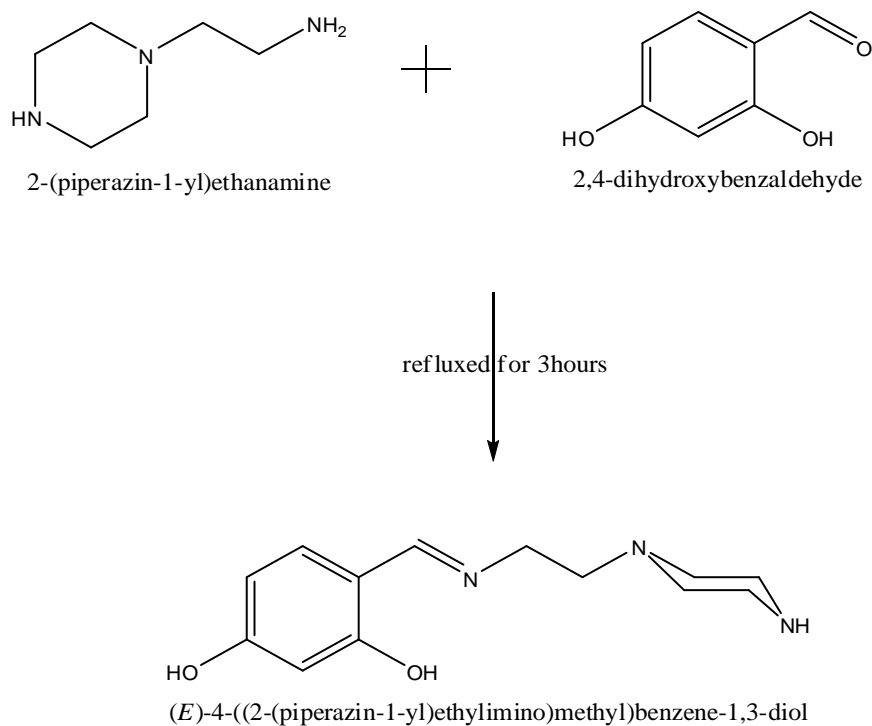
The compound 2-(piperazin-1-yl)ethanamine (2.58 g, 20 mmol) was dissolved in absolute ethanol and added drop wise to a stirred ethanolic solution of 5-nitrosalicylaldehyde (3.4 g, 20 mmol) at room temperature and then refluxed for 3 h, to give an orange solution. The solution was concentrated using a rotary evaporator to form red oil. The red oil becomes hygroscopic solid after three days in vacuum [39]. The hygroscopic solid was dissolved in methanol at 60 °C and a few drops of sodium perchlorate (taken in methanol) were added to the solution. After concentrating and cooling, red gel-like solid was formed, which was collected by adding a few drops of diethyl ether followed by filtration. Yield (0.21 g, 75.5 %),

### 2.2.1.5 Preparation of (*E*)-2-((2-(piperazin-1-yl)ethylimino)methyl)benzene-1,4-diol(LDH)



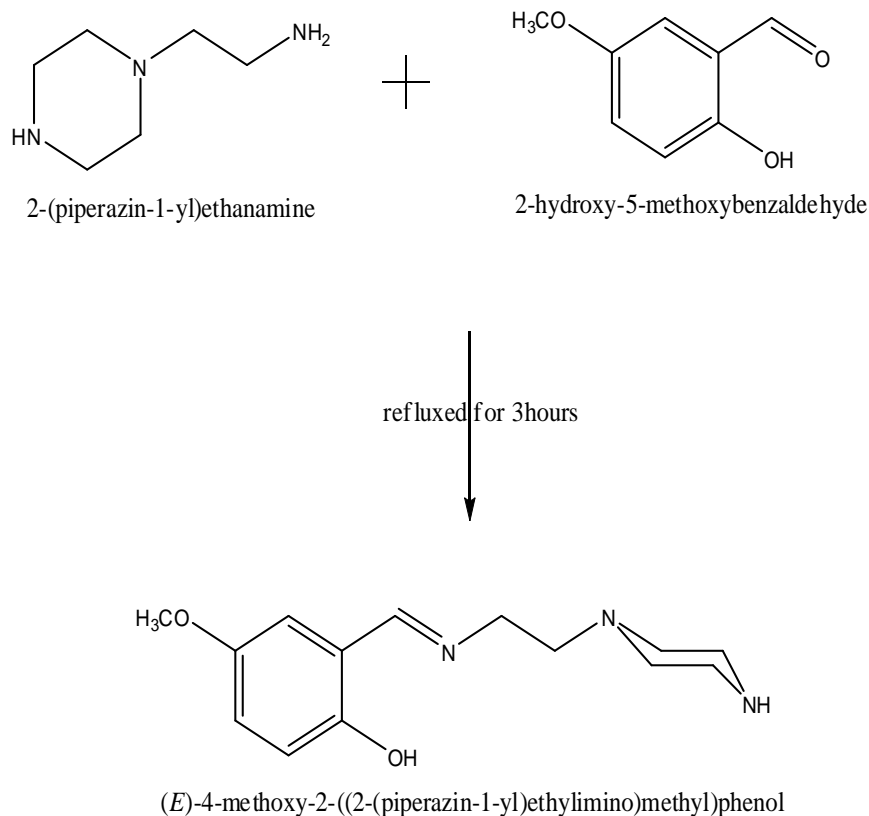
The compound 2-(piperazin-1-yl)ethanamine (2.58 g, 20 mmol) was dissolved in absolute ethanol and added drop wise to a stirred ethanolic solution of 5-hydroxysalicylaldehyde (2.8 g, 20 mmol) at room temperature and then refluxed for 3 h, to give a dark-brown solution. The solution was concentrated using rotary evaporator to give a light brown solid. The solid product was washed with ethanol, dried in vacuum and recrystallized in methanol. Yield (0.20 g, 84.1 %).

### 2.2.1.6 Preparation of (*E*)-4-((2-(piperazin-1-yl)ethylimino)methyl)benzene-1,3-diol (DHS)



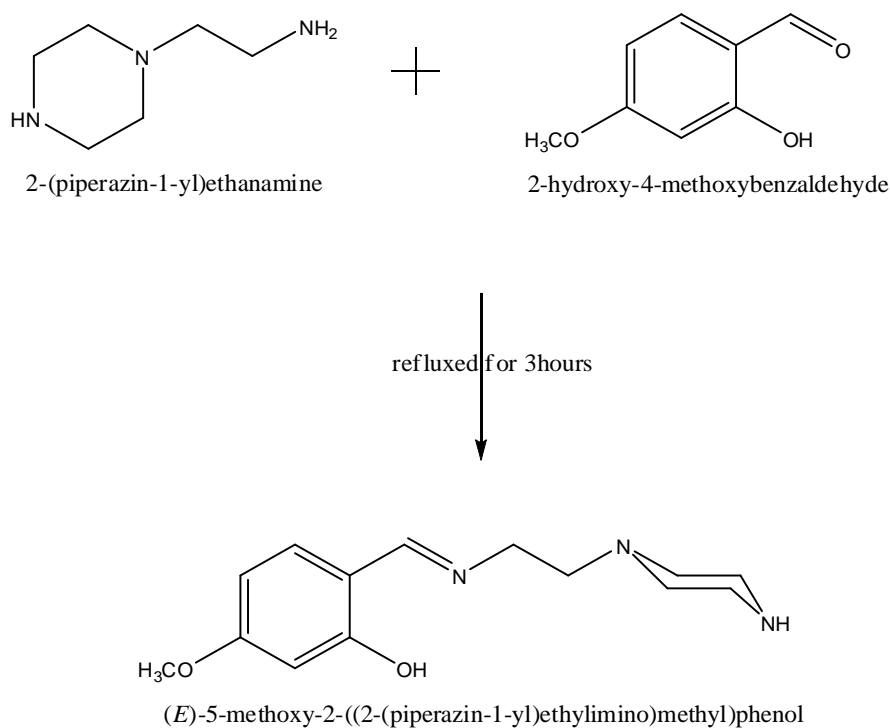
The compound 2-(piperazin-1-yl)ethanamine (2.58 g, 20 mmol) was dissolved in absolute ethanol and added drop wise to a stirred ethanolic solution of 5-hydroxysalicylaldehyde (2.8 g, 20 mmol) at room temperature and then refluxed for 3 h, to give a dark-brown solution. The solvent was removed using a rotary evaporator to give a brown solid. The solid product recrystallized in methanol. Yield (0.22 g, 88.1 %).

2.2.1.7 Preparation of (*E*)-4-methoxy-2-((2-(piperazin-1-yl)ethylimino)methyl) phenol (LHM)



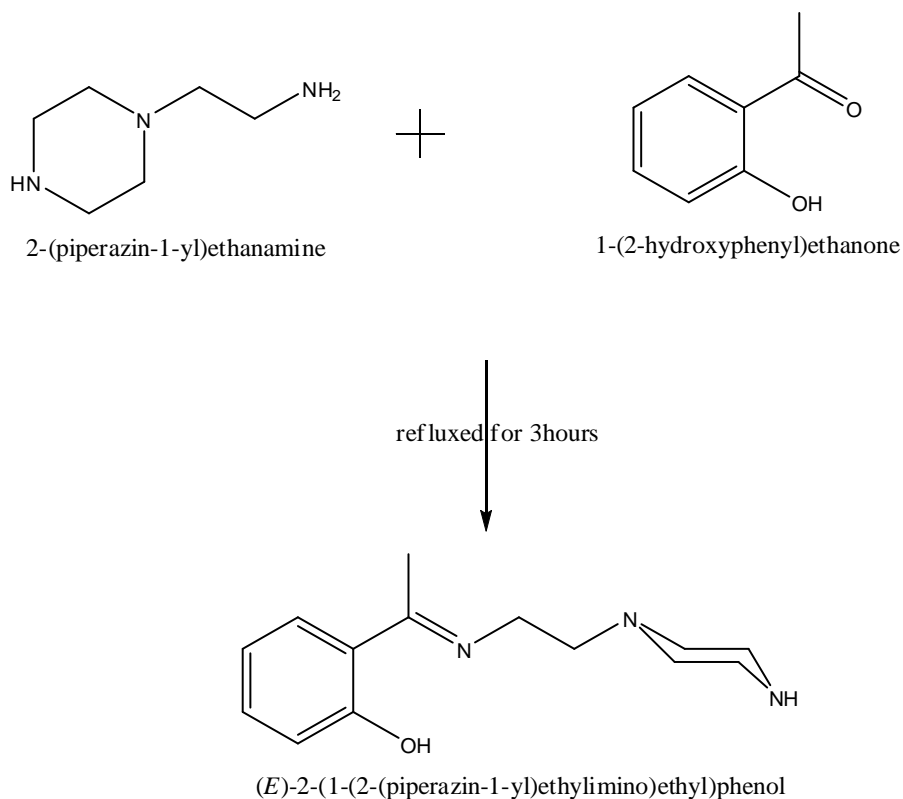
The compound 2-(piperazin-1-yl)ethanamine (2.58 g, 20 mmol) was dissolved in absolute ethanol and added drop wise to a stirred ethanolic solution of 5-methoxysalicylaldehyde (3.0 g, 20 mmol) at room temperature and then refluxed for 3 h, to give a pink solution. The solution was concentrated using a rotary evaporator to give a gel-like solid which upon addition of a few drops of distilled water gave a solid product. The solid product was removed by filtration, washed with ethanol-water mixture and dried in vacuum. Yield (0.18 g, 68.2 %).

2.2.1.8 Preparation of (*E*)-5-methoxy-2-((2-(piperazin-1-yl)ethylimino)methyl) phenol (HMS)



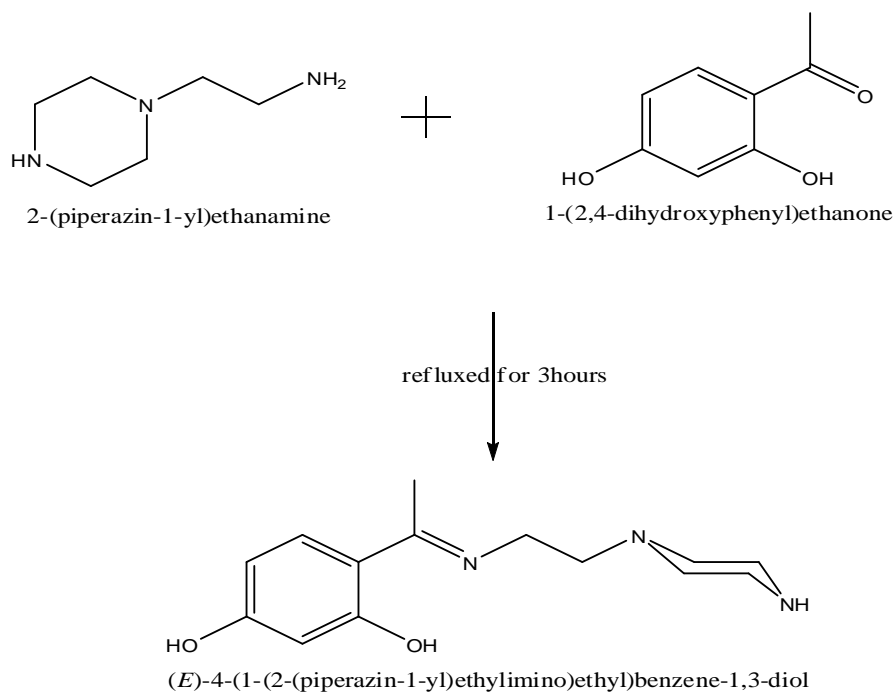
The compound 2-(piperazin-1-yl)ethanamine (2.58 g, 20 mmol) was dissolved in absolute ethanol and added drop wise to a stirred ethanolic solution of 5-methoxysalicylaldehyde (3.0 g, 20 mmol) at room temperature and then refluxed for 3 h, to a give pinkish solution. The solution was concentrated using a rotary evaporator to give gel-like solid, which was kept in an oven for 18 h at 45°C to give a reddish brown solid. The solid product was recrystallized in methanol. Yield (0.23 g, 87.1 %).

### 2.2.1.9 Preparation of (*E*)-2-(1-(2-piperazin-1-yl)ethylimino)ethyl phenol (2HP)



The compound 2-(piperazin-1-yl)ethanamine (2.58 g, 20 mmol) was dissolved in absolute ethanol and added drop wise to a stirred ethanolic solution of 1-(2-hydroxyphenyl)ethanone (2.8 g, 20 mmol) at room temperature and then refluxed for 3 h, to give a golden yellow solution. The solution was then evaporated using a rotary evaporator to form a yellow suspension which was filtered and washed with a methanol-water mixture. Yield (0.124 g, 50.2 %).

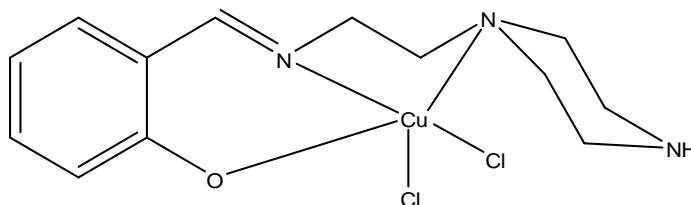
2.2.1.10 Preparation of (*E*)-4-(1-(2-piperazin-1-yl)ethylimino)ethyl)benzene-1,3-diol (DHP)



The compound 2-(piperazin-1-yl)ethanamine (2.58 g, 20 mmol) was dissolved in absolute ethanol and added drop wise to a stirred ethanolic solution of 1-(2,4-dihydroxyphenyl)ethanone (3.0 g 20 mmol) at room temperature and then refluxed for 3 h, to give an orange-yellow solution. The solution was then evaporated using a rotary evaporator to give an orange oil which after two days in vacuum produced a white hygroscopic solid. The solid product was dissolved in methanol at 50 °C and solid sodium perchlorate was added to the solution while still hot. After concentrating and cooling, pale yellow solid formed. The solid product was collected by filtration, washed with an ethanol-water mixture and dried in vacuum. Yield (0.132 g, 50.2 %).

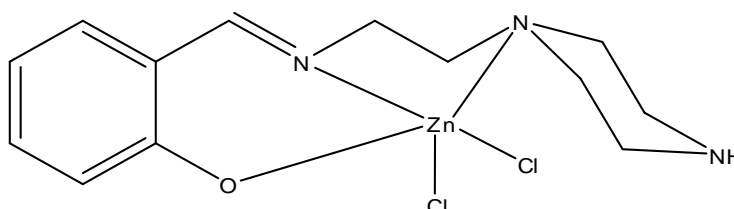
## 2.2.2 Preparation of the metal complexes

### 2.2.2.1 Preparation of Cu-(II)-(E)-2-((2-(piperazin-1-yl)ethylimino)methyl) phenol:



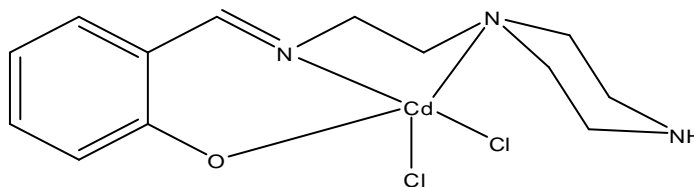
A methanolic solution of copper chloride dihydrate (0.17 g, 1 mmol) was mixed with the methanolic solution of the ligand LSP (0.23 g, 1 mmol) and stirred for 5 minutes at room temperature. A green precipitate was formed, filtered, washed with an ethanol-water mixture and dried in vacuum. The solid product was recrystallized in cold methanol-dichloromethane mixture.

### 2.2.2.2 Preparation of Zn-(II)-(E)-2-((2-(piperazin-1-yl)ethylimino)methyl) phenol:



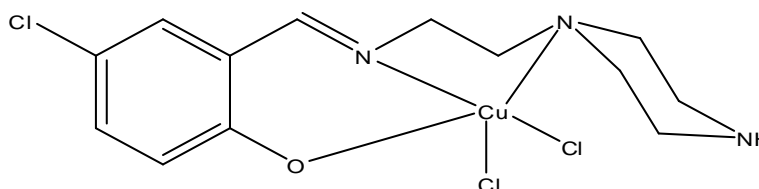
To a 25 mL methanolic solution of zinc chloride hydrate (0.14 g, 1 mmol), 25 mL methanolic solution of the ligand LSP (0.23 g, 1 mmol) was added and stirred for 5 minutes at room temperature. Pale-yellow precipitate appeared in the presence of a few drops of KOH. The solid product was filtered, washed with diethyl ether and dried in vacuum. Recrystallization from a cold solution of methanol-hexane mixture afforded needle-like crystals.

2.2.2.3 Preparation of Cd-(II)-(E)-2-((2-(piperazin-1-yl)ethylimino)methyl) phenol:  $[Cd(LSP)Cl_2]$



Cadmium chloride dihydrate (0.18 g, 1 mmol) was dissolved in methanol (25 mL) and added to a 25 mL solution of the ligand LSP (0.23 g, 1 mmol) in methanol. The mixture was stirred for about 5 minutes at room temperature. A white precipitate appeared on adding a few drops of diethylenetriamine. The precipitate was filtered, washed with ethanol and dried in a vacuum. Recrystallization from a cold solution of methanol-dichloromethane mixture afforded diffraction quality crystals.

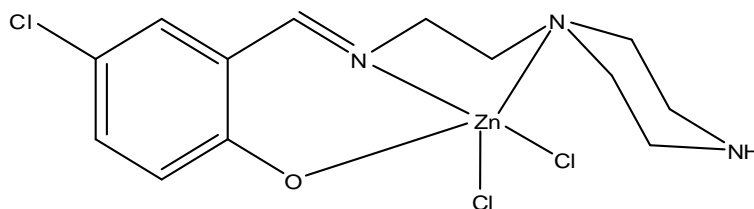
2.2.2.4 Preparation of Cu (II)-(E)-4-chloro-2-((2-(piperazin-1-yl)ethylimino)methyl)phenol:  $[Cu(LCS)Cl_2]$



Copper chloride dihydrate (0.17 g, 1 mmol) was dissolved in methanol (25 mL) and added to a stirred solution of the Schiff base LCS (0.27 g, 1 mmol) in methanol 25 mL at room temperature. A green precipitate was formed immediately; the mixture was further stirred for 5 minutes in the presence of KOH and then allowed to settle. The precipitate was removed by filtration, washed with ethanol and dried in vacuum. The solid product obtained was recrystallized from cold methanol-dichloromethane mixture.

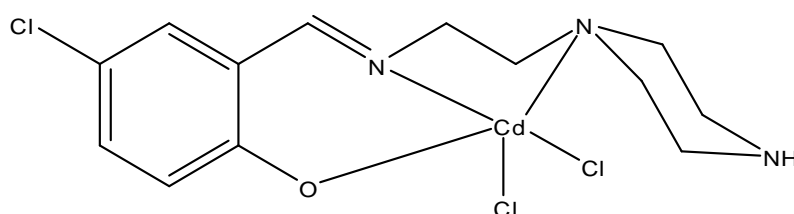
#### 2.2.2.5 Preparation of Zn(II)-(E)-4-chloro-2-((2-(piperazin-1-yl)ethylimino) methyl)phenol:

[Zn(LCS)Cl<sub>2</sub>]



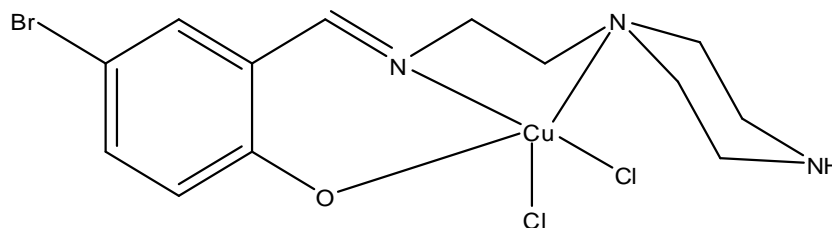
A measured amount of zinc chloride hydrate (0.14g, 1mmol) in methanol 25 mL was added to a 25 mL methanolic solution of the ligand LCS (0.27 g, 1 mmol) at room temperature and stirred. A few drops of KOH were added to the solution and then refluxed for three hours. A light orange solid appeared which was filtered and washed with a ethanol-water mixture. The product was recrystallized from a cold hexane-dichloromethane mixture.

#### 2.2.2.6 Preparation of Cd (II)-(E)-4-chloro-2-((2-(piperazin-1-yl)ethylimino) methyl)phenol: [Cd(LCS)Cl<sub>2</sub>]



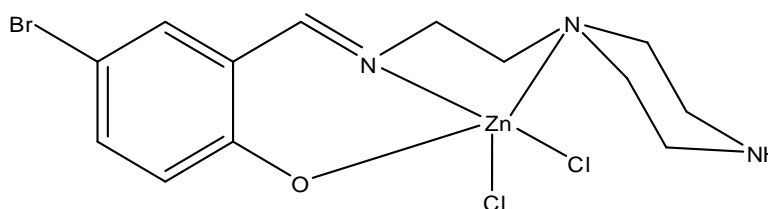
A measured quantity of cadmium chloride dihydrate (0.18 g, 1 mmol) prepared in 25 mL methanol was mixed with LCS (0.27 g, 1 mmol) in 25 mL methanol. The mixture was then stirred for five minutes at room temperature with a few drops of KOH. The orange solution was refluxed for 3 h which after concentrating and cooling gave a white precipitate. The precipitate was filtered, washed with ethanol and recrystallized in a cold methanol-acetone mixture.

2.2.2.7 Preparation of Cu (II)-(E)-4-bromo-2-((2-(piperazin-1-yl)ethylimino) methyl)phenol:  $[Cu(LBS)Cl_2]$



Copper chloride dihydrate (0.17 g, 1 mmol) was dissolved in methanol 25 mL and added to a stirred solution of the ligand LBS (0.3 g, 1 mmol) in 25 mL methanol at room temperature. Green precipitate was formed immediately and dissolved after stirring for 1 minute; the precipitate reformed on addition of a few drops of KOH in methanol and stirred continuously for 5 minutes. The precipitate was filtered, washed with methanol and dried in vacuum. The product was recrystallized from a cold methanol-chloroform mixture.

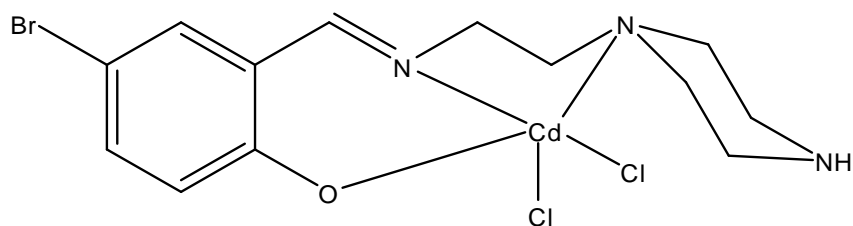
2.2.2.8 Preparation of Zn(II)-(E)-4-bromo-2-((2-(piperazin-1-yl)ethylimino) methyl)phenol:  $[Zn(LBS)Cl_2]$



A measured quantity of zinc chloride hydrate (0.14 g, 1 mmol) was dissolved in 25 mL methanol and added to a stirred solution of the ligand LBS (0.3 g, 1 mmol) in 25 mL methanol at room temperature. Pale yellow solid which formed was dissolved after being stirred for about 1 minute. A few drops of KOH were added and the mixture refluxed for three hours. A white solid was obtained after evaporating the solvent. The product was

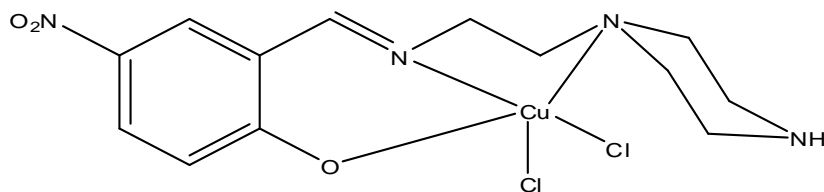
washed with an ethanol-water mixture, dried in vacuum desiccator and recrystallized in a cold dichloromethane-hexane mixture.

2.2.2.9 Preparation of *Cd(II)-(E)-4-bromo-2-((2-(piperazin-1-yl)ethylimino)methyl)phenol*:  $[Cd(LBS)Cl_2]$



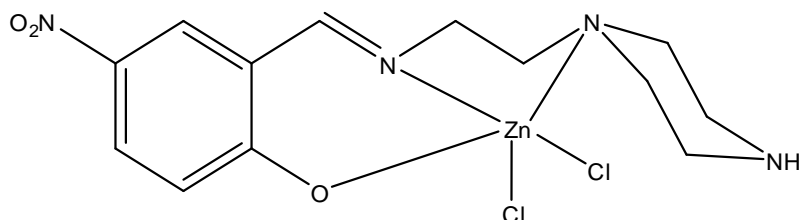
Cadmium chloride dihydrate (0.18 g, 1 mmol) was dissolved in 25 mL methanol and added to a stirred solution of the ligand LBS (0.3 g, 1 mmol) in 25 mL methanol at room temperature, white precipitate appeared immediately in the presence of KOH. The precipitate was filtered, washed with an ethanol and dried in the vacuum desiccator. The product was recrystallized in hexane.

2.2.2.10 Preparation of *Cu(II)-(E)-4-nitro-2-((2-(piperazin-1-yl)ethylimino)methyl)phenol*:  $[Cu(LNS)Cl_2]$



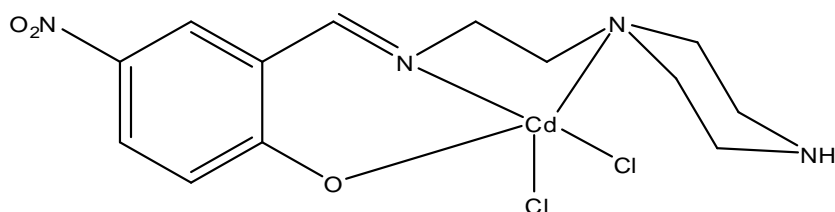
To the measured quantity of the Schiff base, LNS (0.28 g, 1 mmol) in 25 mL methanol, a solution of copper chloride dihydrate (0.17 g, 1 mmol) also in 25 mL methanol was added and stirred for five minutes. A deep green precipitate was formed after the addition of a few drops of KOH, which was collected by filtration, washed with ethanol and dried in vacuum. Recrystallization from cold methanol-dichloromethane mixture afforded a green solid.

2.2.2.11 Preparation of Zn(II)-(E)-4-nitro-2-((2-(piperazin-1-yl)ethylimino) methyl)phenol:



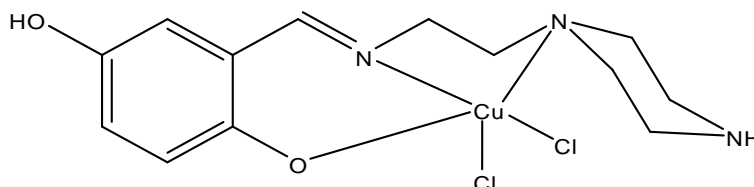
To a stoichiometric amount of the Schiff base, LNS (0.28 g, 1 mmol) in 25 mL methanol, a solution of zinc chloride hydrate (0.14 g, 1 mmol) also in 25 mL methanol was added and stirred for five minutes. A yellow precipitate was formed, which was filtered and the filtrate was concentrated under reduced pressure and kept for 48 hours to form orange microcrystalline solid. The crystals were collected by filtration and recrystallized from a methanol-dichloromethane mixture to afford diffraction quality crystals.

2.2.2.12 Preparation of Cd(II)-(E)-4-nitro-2-((2-(piperazin-1-yl)ethylimino) methyl)phenol:



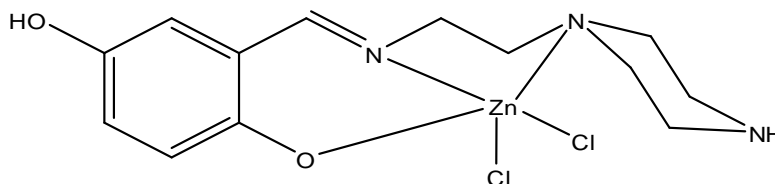
To the measured quantity of ligand, LNS (0.28 g, 1 mmol) in 25 mL methanol, a stirred solution of cadmium chloride dihydrate (0.18 g, 1 mmol) in 25 mL methanol was added with few a drops of KOH. Pale yellow precipitate was formed. The precipitate was filtered, washed with ethanol and dried in vacuum. The solid product was recrystallized in a cold dichloromethane.

2.2.2.13 Preparation of Cu (II)-(E)-2-((2-(piperazin-1-yl)ethylimino)methyl) benzene-1,4-diol: [Cu(LDH)Cl<sub>2</sub>]



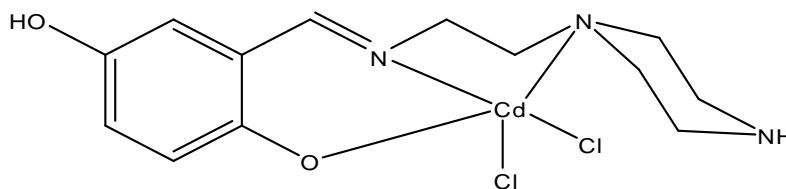
A 0.17 g of 1 mmol of copper chloride dihydrate was dissolved in 25 mL methanol and added to a solution of the ligand LDH (0.25 g, 1 mmol) followed by the addition of few drops of KOH and stirred at room temperature. A brownish red precipitate was obtained upon stirring for 5 minutes. The precipitate was filtered, washed with ethanol and dried in vacuum. Recrystallization was done in a cold methanol-acetone mixture.

2.2.2.14 Preparation of Zn(II)-(E)-2-((2-(piperazin-1-yl)ethylimino)methyl) benzene-1,4-diol: [Zn(LDH)Cl<sub>2</sub>]



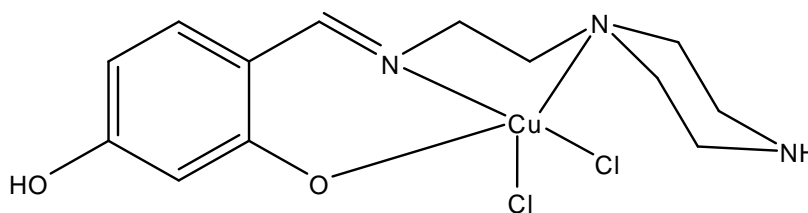
A stoichiometric amount of zinc chloride hydrate (0.14 g, 1 mmol) was dissolved in 25 mL methanol and mixed with the ligand LDH (0.25 g, 1 mmol) in 25 mL methanol. The mixture was stirred for five minutes in the presence of a few drops of KOH. Deep yellow precipitate was obtained. The precipitate was washed with distilled water and dried in vacuum. The filtrate was heated under reflux for 24 hours to give yellow microcrystalline solid. The solid crystals were collected by filtration and recrystallized in a cold methanol-acetone mixture to give quality crystals.

2.2.2.15 Preparation of Cd(II)-(E)-2-((2-(piperazin-1-yl)ethylimino)methyl) benzene-1,4-diol: [Cd(LDH)Cl<sub>2</sub>]



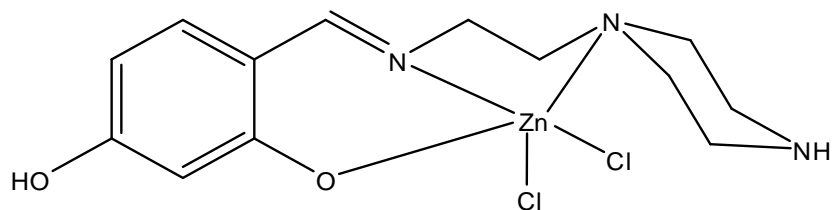
Cadmium chloride dihydrate (0.18 g, 1 mmol) was dissolved in 25 mL methanol and a solution of the ligand LDH (0.25 g, 1 mmol) in 25 mL methanol added dropwise. The mixture was stirred for five minutes and basified with a few drops of KOH to give a yellow precipitate. The precipitate was filtered, washed with distilled water and dried in vacuum. The filtrate was concentrated under reduced pressure and left at reflux temperature for 18 hours to produce golden-yellow microcrystalline solid. The crystals were collected by filtration and recrystallized in a cold dichloromethane-methanol mixture for X-ray diffraction analysis.

2.2.2.16 Preparation of Cu(II)-(E)-4-((2-(piperazin-1-yl)ethylimino)methyl) benzene- 1,3-diol: [Cu(DHS)Cl<sub>2</sub>]



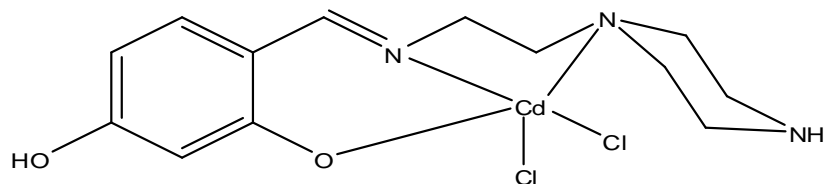
0.17 g, 1 mmol of copper chloride dihydrate was dissolved in 25 mL methanol and added to a stirred solution of the ligand DHS (0.25 g, 1 mmol) in 25 mL methanol at room temperature followed by 2-3 drops of KOH. A green precipitate was formed on stirring. The precipitate was filtered, washed with ethanol and dried in vacuum. The solid product was recrystallized in hexane.

2.2.2.17 Preparation of Zn(II)-(E)-4-((2-(piperazin-1-yl)ethylimino)methyl) benzene- 1,3-diol: [Zn(DHS)Cl<sub>2</sub>]



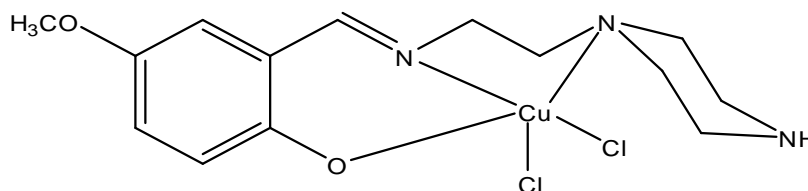
0.14 g, 1 mmol of zinc chloride hydrate was dissolved in 25 mL methanol and mixed with a stirred solution of the ligand DHS (0.25 g, 1 mmol) in 25 mL methanol at room temperature followed by a few drops of KOH. A yellow precipitate was formed on stirring. The precipitate was filtered, washed with ethanol and dried in vacuum. The solid product was recrystallized in a cold ethanol-water.

2.2.2.18 Preparation of Cd(II)-(E)-4-((2-(piperazin-1-yl)ethylimino)methyl) benzene- 1,3-diol: [Cd(DHS)Cl<sub>2</sub>]



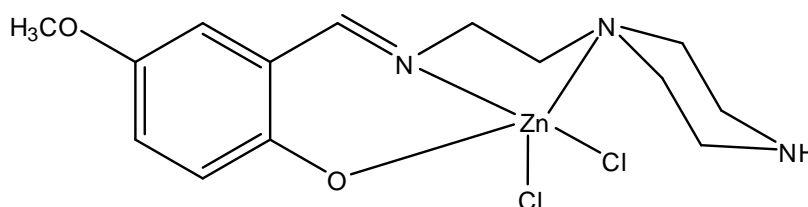
0.18 g of cadmium chloride dihydrate (1 mmol) was dissolved in 25 mL methanol and added to a stirred solution of the ligand DHS (0.25 g, 1 mmol) at room temperature followed by a few drops of KOH. Pale yellow precipitate was formed on stirring. The precipitate was filtered, washed with ethanol and dried in vacuum. The solid product was recrystallized from a cold methanol-chloroform mixture.

2.2.2.19 Preparation of Cu(II)(E)-4-methoxy-2-((2-(piperazin-1-yl)ethylimino) methyl) phenol:  $[Cu(LHM)Cl_2]$



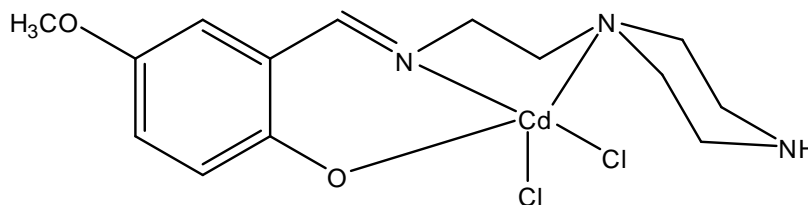
A weighed amount of copper chloride (0.17 g, 1 mmol) was dissolved in 25 mL methanol and added to 25 mL methanolic solution of the ligand LHM (0.26 g, 1 mmol) and stirred for five minutes. A few drops of KOH were added to basify the reaction. A green precipitate appeared immediately, which was filtered washed with ethanol and dried in vacuum. The solid product was recrystallized from an ethanol-water mixture.

2.2.2.20 Preparation of Zn(II)(E)-4-methoxy-2-((2-(piperazin-1-yl)ethylimino) methyl) phenol:  $[Zn(LHM)Cl_2]$



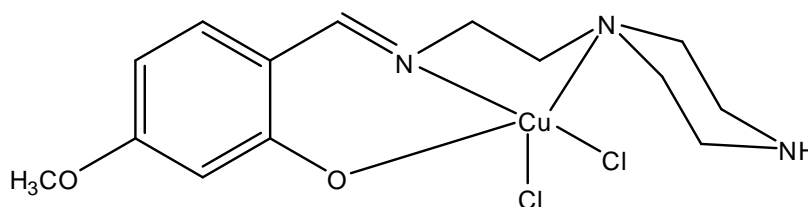
Zinc chloride hydrate (0.14 g, 1 mmol) was dissolved in 25 mL methanol and added gently into a stirred solution of the ligand LHM (0.26 g, 1 mmol) in 25 mL of methanol. The mixture was stirred for five minutes with the addition of a few drops of KOH to give light brown precipitate. The precipitate was filtered, washed with distilled water and dried in vacuum. Recrystallization was done in hexane.

2.2.2.21 Preparation of Cd(II)(E)-4-methoxy-2-((2-(piperazin-1-yl)ethylimino) methyl) phenol:  $[Cd(LHM)Cl_2]$



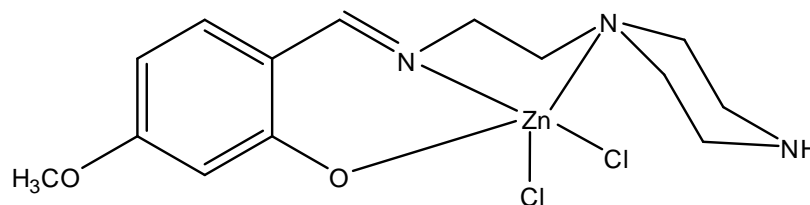
A cadmium chloride dihydrate (0.18 g, 1 mmol) methanolic solution (25 mL) was added gently into a stirred solution of the ligand LHM (0.26 g, 1 mmol) in 25 mL of methanol. The mixture was stirred for five minutes in the presence of a few drops of KOH. A brown precipitate was formed. The precipitate was filtered, washed with distilled water and dried in vacuum. The filtrate was concentrated in air for 48 hours to give brownish-orange microcrystalline solids. The crystals were collected by filtration and recrystallized in a cold dichloromethane-methanol mixture to afford diffraction quality crystals.

2.2.2.22 Preparation of Cu (II)-(E)-5-methoxy-2-((2-(piperazin-1-yl)ethylimino) methyl) phenol:  $[Cu(HMS)Cl_2]$



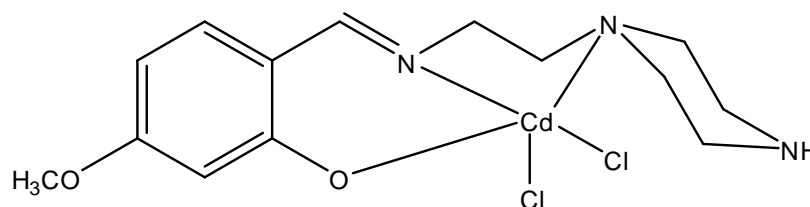
The ligand HMS (0.26 g, 1 mmol) was dissolved in 25 mL methanol and mixed with a stirred solution of copper chloride dihydrate (0.17 g, 1 mmol) in 25 mL methanol. A few drops of KOH were added and a green precipitate was formed. The precipitate was filtered, washed with an ethanol and dried in vacuum. Recrystallization was done in an ethanol-water mixture.

2.2.2.23 Preparation of Zn(II)-(E)-5-methoxy-2-((2-(piperazin-1-yl)ethylimino) methyl)phenol: [Zn(HMS)Cl<sub>2</sub>]



The ligand HMS (0.26 g, 1 mmol) was dissolved in 25 mL methanol and mixed with a stirred solution of zinc chloride hydrate (0.14 g, 1 mmol) in 25 mL methanol. A few drops of KOH were added to the reaction, and an orange precipitate was formed. The precipitate was filtered, washed with an ethanol-water mixture and dried in vacuum. The filtrate was concentrated under reduced pressure and heated under reflux for 48 hours to give microcrystalline solids. The solid crystals were collected by filtration and recrystallized in a cold methanol-chloroform mixture for diffraction analysis.

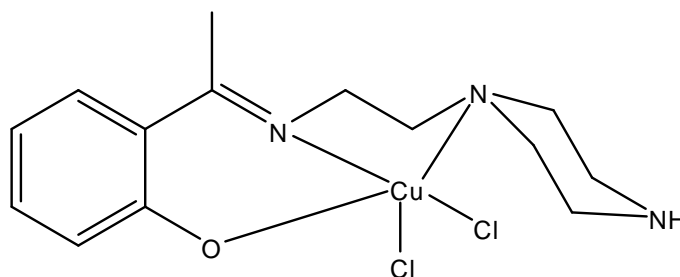
2.2.2.24 Preparation of Cd(II)-(E)-5-methoxy-2-((2-(piperazin-1-yl)ethylimino) methyl)phenol: [Cd(HMS)Cl<sub>2</sub>]



Cadmium chloride dihydrate (0.18g, 1 mmol) in 25 mL methanol was added to 25 mL methanolic solution of HMS ligand (0.26 g, 1 mmol) followed by a few drops of KOH. The mixture was stirred at room temperature to give the yellow-brownish precipitate. The precipitate was filtered, washed with ethanol and dried in vacuum. Recrystallization was carried out from an ethanol-water mixture.

2.2.2.25 Preparation of Cu (II)-(E)-2-(1-(2-piperazin-1-yl)ethylimino)ethyl phenol:

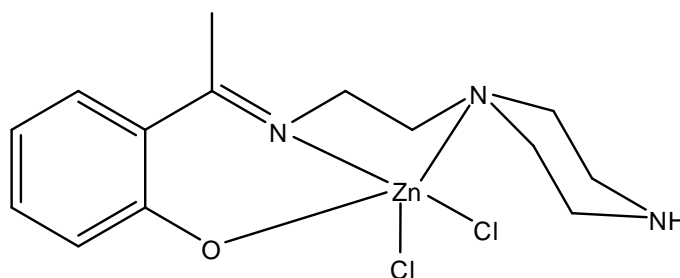
[Cu(2HP)Cl<sub>2</sub>]



Copper chloride dehydrate (0.17 g, 1 mmol) was dissolved in 25 mL methanol and added to 25 mL methanolic solution of the ligand 2HP (0.25 g, 1 mmol) with stirring in the presence of a few drops of KOH at room temperature to produce green precipitate. The precipitate was filtered, washed with ethanol and dried. The solid product was recrystallized in hexane.

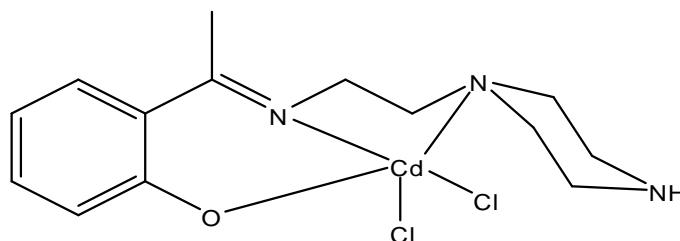
2.2.2.26 Preparation of Zn(II)-(E)-2-(1-(2-piperazin-1-yl)ethylimino)ethylphenol

[Zn(2HP)Cl<sub>2</sub>]



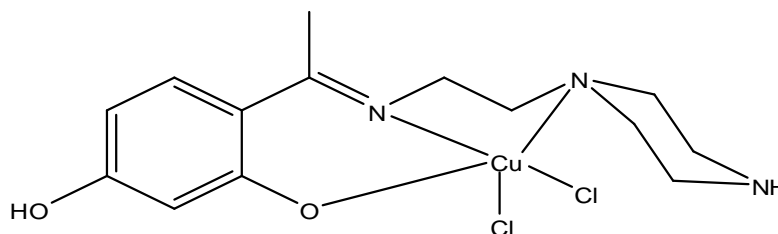
Zinc chloride hydrate (0.14 g, 1 mmol) in 25 mL methanol was added to 25 mL methanolic solution of 2HP ligand (0.25 g, 1 mmol) followed by a few drops of KOH. The mixture was stirred at room temperature to give a white precipitate. The precipitate was filtered, washed with ethanol and dried in vacuum. Recrystallization was done in an ethanol-water mixture.

2.2.2.27 Preparation of Cd(II)-(E)-2-(1-(2-piperazin-1-yl)ethylimino)ethylphenol  
[Cd(2HP)Cl<sub>2</sub>]



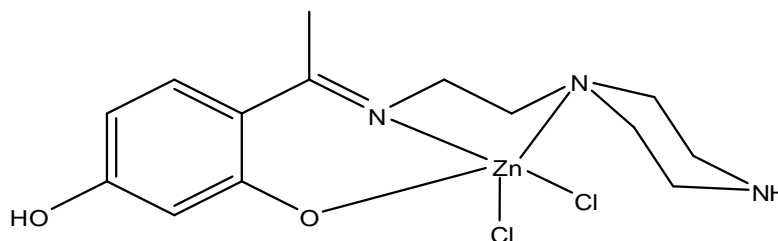
Cadmium chloride dihydrate (0.18 g, 1 mmol) in 25 mL methanol was added to a 25 mL methanolic solution of 2HP ligand (0.25 g, 1 mmol) followed by a few drops of KOH. The mixture was stirred at room temperature for one hour to give a pale yellow precipitate. The precipitate was filtered, washed with ethanol and dried in vacuum. Recrystallization was done in cold hexane.

2.2.2.28 Preparation of Cu (II)-(E)-4-(1-(2-piperazin-1-yl)ethylimino)ethyl benzene-1,3-diol: [Cu(DHP)Cl<sub>2</sub>]



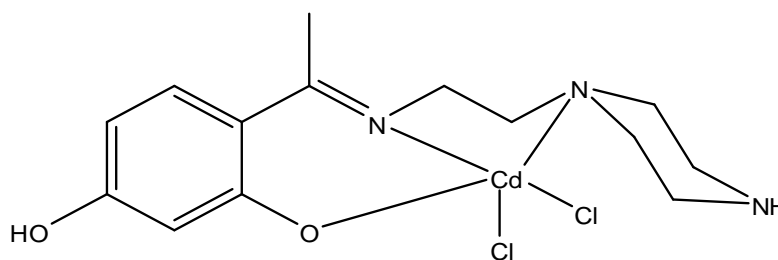
Copper chloride dehydrate (0.17 g, 1 mmol) was dissolved in 25 mL methanol and added to 25 mL stirred methanolic solution of DHP ligand (0.26 g, 1 mmol) in the presence of a few drops of KOH at room temperature to give green precipitate. The precipitate was filtered, washed with water and dried in vacuum. Recrystallization was done in hexane.

2.2.2.29 Preparation of Zn(II)-(E)-4-(1-(2-piperazin-1-yl)ethylimino)ethyl benzene-1,3-diol: [Zn(DHP)Cl<sub>2</sub>]



Zinc chloride dihydrate (0.14 g, 1 mmol) was dissolved in 25 mL methanol and mixed with 25 mL stirred methanolic solution of DHP ligand (0.26 g, 1 mmol) in the presence of a few drops of KOH at room temperature to give a light yellow precipitate. The precipitate was filtered, washed with water and dried in vacuum. Recrystallization was done in hexane.

2.2.2.30 Preparation of Cd(II)-(E)-4-(1-(2-piperazin-1-yl)ethylimino)ethyl benzene-1,3-diol: [Cd(DHP)Cl<sub>2</sub>]



Cadmium chloride (0.18 g, 1 mmol) was dissolved in 25 mL methanol and added to 25 mL stirred methanolic solution of DHP ligand (0.26 g, 1 mmol) in the presence of a few drops of KOH at room temperature to give a white precipitate. The precipitate was filtered, washed with water and dried in vacuum. Recrystallization was done in hexane.

### 2.2.3 Characterizations of the complexes

The synthesized complexes were characterized by the following spectroscopic techniques; Elemental analysis, solubility tests, mass spectroscopy, melting / decomposition points,

conductivity tests, infra-red,  $^1\text{H-NMR}$ ,  $^{13}\text{C-NMR}$ , UV-visible spectra, thermal analysis (TGA), and X-ray diffraction analysis.

#### *2.2.3.1 Elemental analysis*

The analysis of C, N and H was performed on the Schiff bases by weighing 10 mg of the sample and recording the reading on Costech ECS 4010 CHNSO analyzer (Valencia, USA).

#### *2.2.3.2 Solubility tests*

The solubility of the compounds was checked in water, ethanol, methanol, DMF, DMSO, chloroform, dichloromethane, hexane and other organic solvents for further analysis.

#### *2.2.3.3 Mass spectroscopy*

Mass spectra were determined only for the ligands using 20-30 ppm portion of each ligand and recording the reading on ABI 4800 Maldi TOF/TOF mass spectrophotometer (BIDMC Genomics, Proteomics And Bioinformatics Core, Boston, MA, USA) (LC-MS, ESI, 125.0 V).

#### *2.2.3.4. Melting / Decomposition points*

The melting and decomposition points determination were performed by inserting the powdered sample in glass capillary tubes and heating on a Gallen Kamp melting point apparatus (Calgary, Canada).

#### *2.2.3.5 Conductivity tests*

The conductivity of the compounds was measured in  $1 \times 10^{-3} \text{ mol/dm}^3$  DMF at 25-30°C using a digital conductivity meter, Jenway-4010, (Staffordshire ST15 OSA, UK). The molar conductivity was calculated according to the following relationship;

$$\Lambda_M = 1000L / M$$

Where  $\Lambda_M$  = molar conductance, L = specific conductance, M = molarity

#### 2.2.3.6 *Infra-red spectra*

Infra-red spectra were recorded at wave number range of 4000-400  $\text{cm}^{-1}$  on Perkin Elmer 2000 FTIR spectrophotometer using KBr pellets.

#### 2.2.3.7 *NMR spectra*

The spectra for  $^1\text{H}$  NMR and  $^{13}\text{C}$  NMR were recorded on ECA-400 higher performance NMR spectrophotometer using  $\text{DMSO-d}_6$  solvent and trimethylsilane (TMS) as internal standard.

#### 2.2.3.8 *UV-visible spectra*

The electronic spectra was obtained by dissolving the compounds in DMSO and the absorption band maxima recorded in the visible region from 200-900 nm using Perkin-Elmer-1650-UV-visible spectrophotometer.

#### 2.2.3.9 *Thermal analysis*

The thermo-gravimetric analysis was performed by weighing 10-20 mg of the sample and heating from 50-900  $^{\circ}\text{C}$  at the rate of 20  $^{\circ}\text{C min}^{-1}$  in nitrogen atmosphere. The analysis was performed on a TGA-4000 thermo analyzer.

#### 2.2.3.10 *X-ray structure determination*

Single crystals were obtained from ethanolic solutions of some of the metal complexes after slow evaporation at room temperature and analyzed on Bruker APEXII CCD diffractometer using  $\theta - 2\theta$  technique. The structural disorder and thermal motion were controlled by covering the analyzed crystals with a thin layer of light oil. The crystal data intensity for all the complexes was measured at  $\theta$  2.4-30.3 $^{\circ}$  range. The structures were analyzed according to Patterson method and refined using full matrix least square's procedure based on  $F^2$  using SHELXL-97 software.

# **CHAPTER THREE**

## **RESULTS AND DISCUSSION**

### 3. Characterization of the Schiff bases and their complexes

#### 3.1. Physical measurements

The results of elemental analysis showed good agreement between the experimental and the calculated values, which confirmed the formation of the Schiff bases under study. Both the Schiff bases and their complexes were tested for solubility and found to be more soluble in water, DMSO and DMF. The Liquid Chromatography-Electron Spray Ionization-Mass Spectrum (LC-ESI-MS) of the Schiff bases gave molecular ion peaks that correlate to the calculated formula weight of the corresponding ligand analyzed, thus proving the purity of the compounds [103]. The molar conductivity data of the compounds was obtained at approximately 0.1m in DMF to give ( $\Lambda_M$ ) values below the range of 1:1 electrolyte (i.e. 65-90  $\text{Scm}^2\text{mol}^{-1}$ ) [104], this proves the non-electrolytic behavior of the complexes synthesized (Appendix A, P156).

#### 3.2. Infra-red spectroscopy

##### 3.2.1. IR spectra of (E)-2-((2-(piperazin-1-yl)ethylimino)methyl)phenol (LSP) and its Cu, Zn and Cd complexes.

The IR spectra for all the Schiff bases and their complexes of Cu, Zn and Cd are shown in Tables 3.1-3.10 and Figures 3.1-3.40.

Table 3.1 IR spectral results for LSP and its complexes

Compound	$\nu$ (O-H /NH)	$\nu$ (C-H) (alp)	$\nu$ (C=N)	$\nu$ C-O	$\nu$ (C-H) (arom)	N (M-O)	$\nu$ (M-N)
LSP	3422	2941	1630	1278	762	-	-
[Cu(LSP)Cl <sub>2</sub> ]	3422	2944	1637	1297	763	615	586
[Zn(LSP)Cl <sub>2</sub> ]	3448	2824	1629	1308	768	530	419
[Cd(LSP)Cl <sub>2</sub> ]	3521	3126	1630	1307	780	597	456

The IR spectra of the LSP ligand had shown the characteristic iminic C=N band at 1636 cm<sup>-1</sup> and complete absence of a carbonyl group expected near 1700 cm<sup>-1</sup> which indicates the formation of imine bond (Schiff base) [105]. The strong and broad-band absorption at 3422 cm<sup>-1</sup> can be ascribed to hydrogen bond stretching of the phenolic group which is confirmed at 1278 cm<sup>-1</sup>. The aliphatic C-H appears at 2941cm<sup>-1</sup> and the aromatic C-H out of a plane was observed at 762 cm<sup>-1</sup> [106].

The spectra of [Cu(LSP)Cl<sub>2</sub>] shows a medium absorption of N-H stretching band at 3422 cm<sup>-1</sup> and a phenolate band at 1297 cm<sup>-1</sup>. The wavelengths appearing at 3422 cm<sup>-1</sup> and 1278 cm<sup>-1</sup> confirm the presence of a phenolic group in the ligand spectra [107]. This indicates deprotonation of the ligand and bonding of phenolic oxygen to the metal ion [108]. It is further supported by the shift of an iminic band from 1630 cm<sup>-1</sup> in the free ligand to 1637 cm<sup>-1</sup> in the complex which is attributable to the involvement of iminic nitrogen in bonding with metal ion. This deduction is supported by the appearance of bands at 615 cm<sup>-1</sup> due to Cu-O bonding and at 586 cm<sup>-1</sup> because of the Cu-N bond stretching vibrations [109]. Furthermore, similar observation was made in the spectra of the zinc complex except that the iminic band had shifted to a lower frequency of 1629 cm<sup>-1</sup> and the metal-phenolate (M-O) band appears at 530 cm<sup>-1</sup> while the metal-nitrogen (M-N) stretching vibrations was observed at the wave number 419 cm<sup>-1</sup>. The spectra of [Cd(LSP)Cl<sub>2</sub>] complex showed a band at 1630 cm<sup>-1</sup> which can be ascribed to deprotonated iminic -C=N-band due to

coordination with the metal ion [110]. Secondary amine of the piperazine moiety appears at  $3521\text{ cm}^{-1}$  which is confirmed at  $1156\text{ cm}^{-1}$  [111]. The phenolate band appears at  $1307\text{ cm}^{-1}$ , Cd-O at  $597\text{ cm}^{-1}$  and Cd-N band at  $456\text{ cm}^{-1}$  (Table 3.1 and Fig.3.1-3.4) (Appendix B).

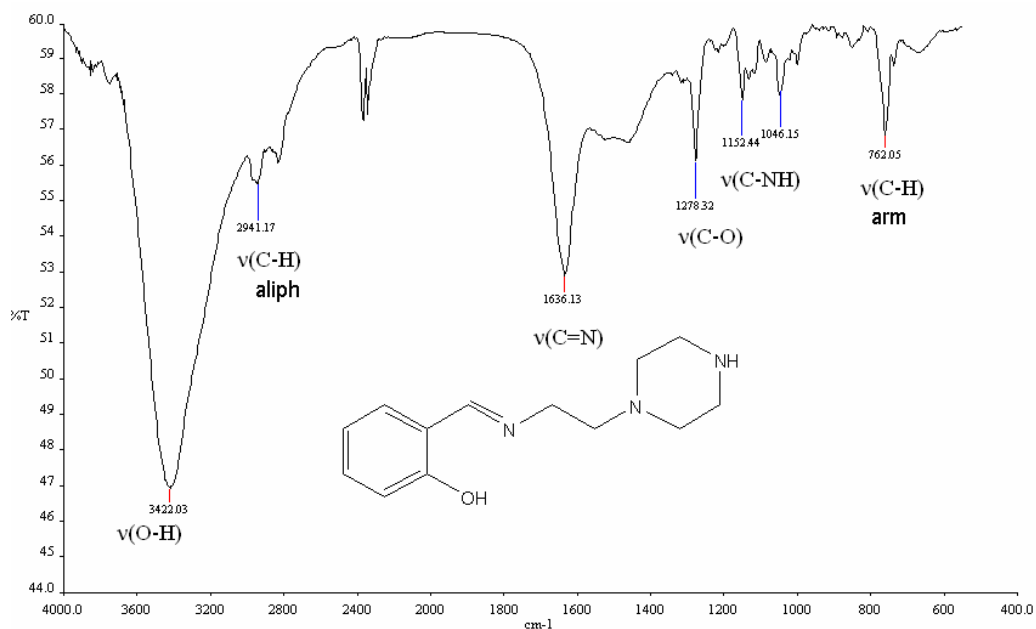


Figure.3.1 IR spectra of LSP ligand

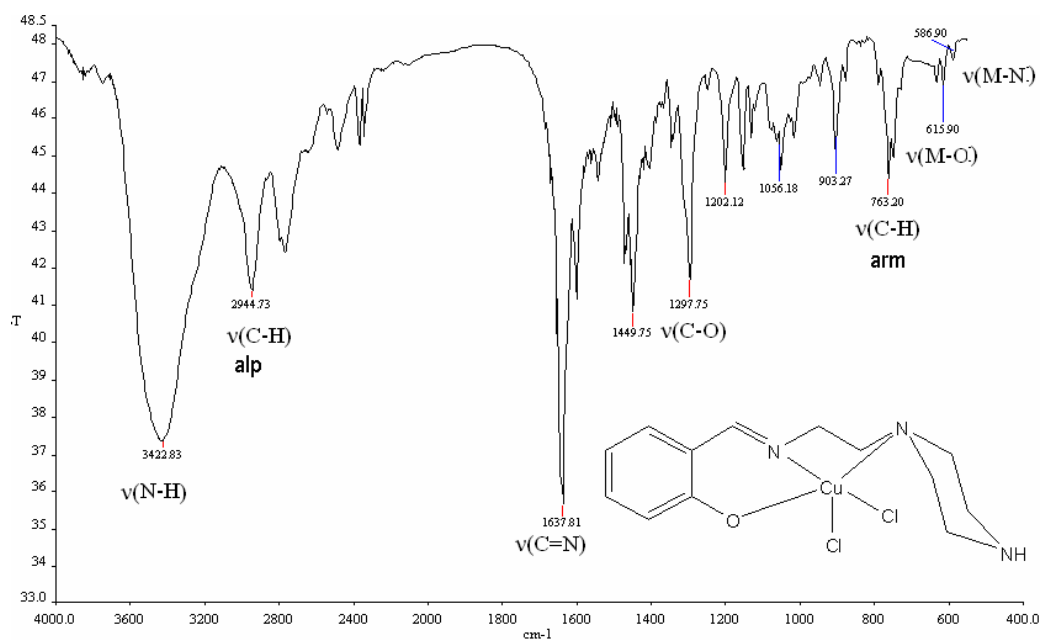


Figure 3.2 IR spectra of  $[\text{Cu}(\text{LSP})\text{Cl}_2]$  complex

3.2.2 IR spectra of (E)-4-chloro-2-((2-(piperazin-1-yl)ethylimino)methyl)phenol (LCS) and its complexes of Cu, Zn and Cd

Table 3.2 IR spectral results for LCS and its complexes

Compound	$\nu$ (O-H/NH)	$\nu$ (C-H) Alp	$\nu$ (C=N)	$\nu$ (C-O)	$\nu$ (C-H) Arom	$\nu$ (M-O)	$\nu$ (M-N)
LCS	3391	2975	1644	1296	708	-	-
[Cu(LCS)Cl <sub>2</sub> ]	3448	2930	1647	1304	708	495	416
[Zn(LCS)Cl <sub>2</sub> ]	3447	3135	1630	1314	705	647	581
[Cd(LCS)Cl <sub>2</sub> ]	3277	2947	1636	1277	714	647	597

The spectra of the ligand LCS show broad-band absorption at 3391 cm<sup>-1</sup> which can be attributed to phenolic stretching vibrations [112]. The aliphatic C-H stretching band appears at 2975 cm<sup>-1</sup> and no band can be associated to an aldehyde or carbonyl group. The iminic C=N band was observed at 1644 cm<sup>-1</sup>. This band appears at 1636 cm<sup>-1</sup> in the spectra of LSP ligand, indicating that the chlorine substituents on the phenolic ring have influenced the band position of imine in the ligand. In addition, C-O stretching vibration and out of a plane aromatic, C-H vibrations were shifted to 1296 cm<sup>-1</sup> and 708 cm<sup>-1</sup> bands respectively compared to their positions at 1278 cm<sup>-1</sup> and 762 cm<sup>-1</sup> observed in the spectra of LSP ligand. The spectra of Cu(LCS) has confirmed the deprotonation of phenolic O-H at 3448 cm<sup>-1</sup> which appears as a medium band in comparison with the strong and broad band that appears at 3391 cm<sup>-1</sup> in the ligand spectra. The iminic band also has shifted to 1647 cm<sup>-1</sup>. This indicates the participation of both phenolic oxygen and iminic nitrogen in complexation with metal ion [113]. This band is further confirmed at 1304 cm<sup>-1</sup> due to phenolate and supported by the appearance of new bands at 495 cm<sup>-1</sup> and 416 cm<sup>-1</sup> wave numbers that can be attributed to Cu-O and Cu-N stretching vibrations respectively [114]. The spectra of Zn complex showed iminic C=N band at 1630 cm<sup>-1</sup> and the phenolate C-O at 1314 cm<sup>-1</sup> indicating the deprotonation of O-H hydrogen due to coordination. This suggests that both C=N nitrogen and C-O oxygen are involved in the complex formation. This is

very clear when these bands are compared with the bands at  $1644\text{ cm}^{-1}$  for  $\text{HC}=\text{N}$  and the band at  $1296\text{ cm}^{-1}$  for  $\text{C}-\text{OH}$  in the spectra of the LCS ligand. The band regions that appeared at low wavelengths  $647\text{ cm}^{-1}$  and  $581\text{ cm}^{-1}$  can be allotted to  $\text{Zn}-\text{O}$  and  $\text{Zn}-\text{N}$  accordingly. Similar changes were observed in the spectra of  $\text{Cd}$  complex except that imine band appears at the frequency of  $1636\text{ cm}^{-1}$ , phenolate at  $1277\text{ cm}^{-1}$  and the bands due to  $\text{Cd}-\text{O}$  and  $\text{Cd}-\text{N}$  were observed at  $647\text{ cm}^{-1}$  and  $597\text{ cm}^{-1}$  respectively (Table 3.2 and Fig 3.5-3.8) (Appendix B).

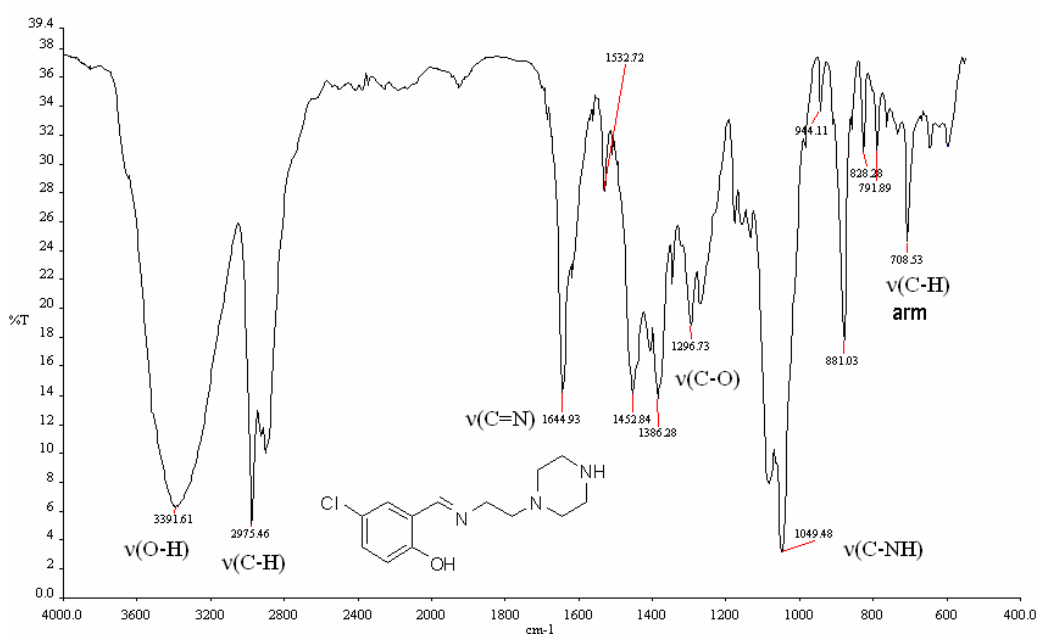


Figure 3.5 IR spectra of LCS ligand

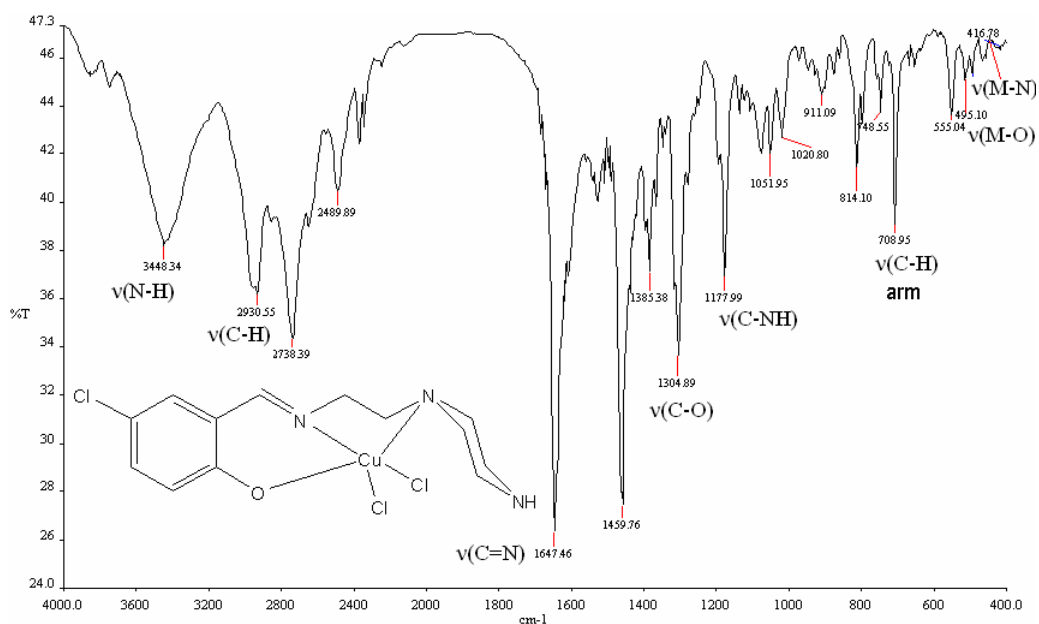


Figure 3.6 IR spectra of [Cu(LCS)Cl<sub>2</sub>] complex

### 3.2.3 IR spectra of (*E*)-4-bromo-2-((2-(piperazin-1-yl)ethylimino)methyl)phenol (LBS) and its complexes of Cu, Zn and Cd

Table 3.3 IR spectral results for LBS and its complexes

Compound	$\nu$ (O-H /NH)	$\nu$ (C-H) Alp	$\nu$ (C=N)	$\nu$ (C-O)	$\nu$ (C-H) Arom	$\nu$ (M-O)	$\nu$ (M-N)
LBS	3413	2820	1635	1278	623	-	-
[Cu(LBS)Cl <sub>2</sub> ]	3435	2957	1637	1303	749	640	590
[Zn(LBS)Cl <sub>2</sub> ]	3439	3140	1629	1313	684	634	580
[Cd(LBS)Cl <sub>2</sub> ]	3448	2813	1634	1308	680	633	588

The IR spectra of the ligand LBS exhibits a characteristic broad band at 3413 cm<sup>-1</sup> that can be assigned to the intermolecular hydrogen bond stretching of O-H. The imine band appears at similar frequency of 1635 cm<sup>-1</sup> in comparison with the band at 1636 cm<sup>-1</sup> observed in the spectra of LSP. This shows that chloride substituents have a high effect on imine position in Schiff bases than bromide. The phenolic C-O stretching appears at 1278 cm<sup>-1</sup> and aromatic C-H bending was observed at 623 cm<sup>-1</sup>. The spectra of copper complex of this ligand shows a shift in the imine position to the band of 1637 cm<sup>-1</sup> which is presumably due to complexation. In the same manner, the phenolic C-O has shifted to 1303



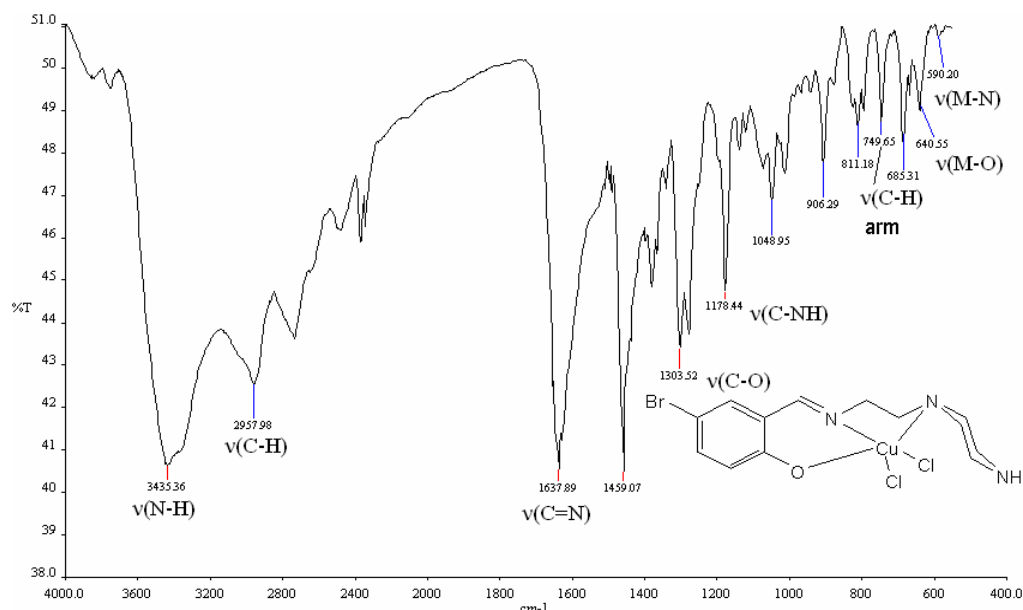


Figure 3.10 IR spectra of [Cu(LBS)Cl<sub>2</sub>] complex

### 3.2.4 IR spectra of (*E*)-4-nitro-2-((2-(piperazin-1-yl)ethylimino)methyl)phenol

(LNS) and its complexes of Cu, Zn and Cd

Table 3.4 IR spectral results for LNS and its complexes

Compound	$\nu$ (O-H /NH)	$\nu$ (C-H) Alp	$\nu$ (C=N)	$\nu$ (C-O)	$\nu$ (C-H) Arom	$\nu$ (M-O)	$\nu$ (M-N)
LNS	3423	2935	1637	1321	755	-	-
[Cu(LNS)Cl <sub>2</sub> ]	3448	2957	1648	1321	757	651	562
[Zn(LNS)Cl <sub>2</sub> ]	3448	2830	1638	1319	699	505	416
[Cd(LNS)Cl <sub>2</sub> ]	3448	2854	1649	1317	700	644	584

The stretching vibration observed at 3423 cm<sup>-1</sup> in the spectra of LNS ligand can be attributed to the overlap between the hydrogen bonding of O-H and N-H stretching [116]. The imine stretching vibration appears at 1637 cm<sup>-1</sup>. This is very close to the position of the iminic band in the spectra of the LSP ligand. The phenolic C-O band appears at 1321 cm<sup>-1</sup> and the band region at 755 cm<sup>-1</sup> can be afforded to aromatic C-H. The complex [Cu(LNS)Cl<sub>2</sub>] shows absorption at a medium band of 3448 cm<sup>-1</sup> which corresponds to the

stretching vibration of the piperazine secondary amine N-H [117]. The notable spectral change observed in the LNS ligand after coordination with copper ion, is the high-frequency shift of an imine band to  $1648\text{ cm}^{-1}$ . This is supported by the appearance of a new  $651\text{ cm}^{-1}$  that corresponds to Cu-O stretching and another band at  $562\text{ cm}^{-1}$  which can be attributed to Cu-N stretching vibrations. Similar descriptions can be made for the spectra of Zn and Cd complexes except that the new band at  $505\text{ cm}^{-1}$  is due to Zn-O and the band at  $416\text{ cm}^{-1}$  can be assigned to Zn-N stretching vibrations whereby the bands at  $644\text{ cm}^{-1}$  and  $584\text{ cm}^{-1}$  in the spectra of cadmium complex can be ascribed to Cd-O and Cd-N stretching respectively (Table 3.4, Fig. 3.13-3.16). The band due to piperazine C-N appears at  $1132\text{ cm}^{-1}$  [118] (Appendix B).

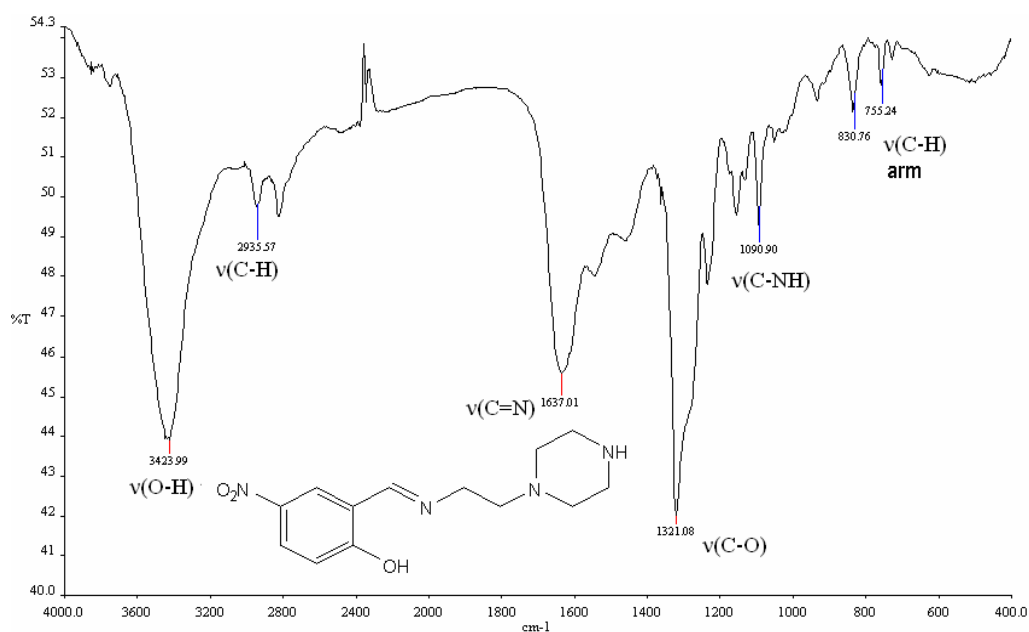


Figure 3.13 IR spectra of LNS ligand

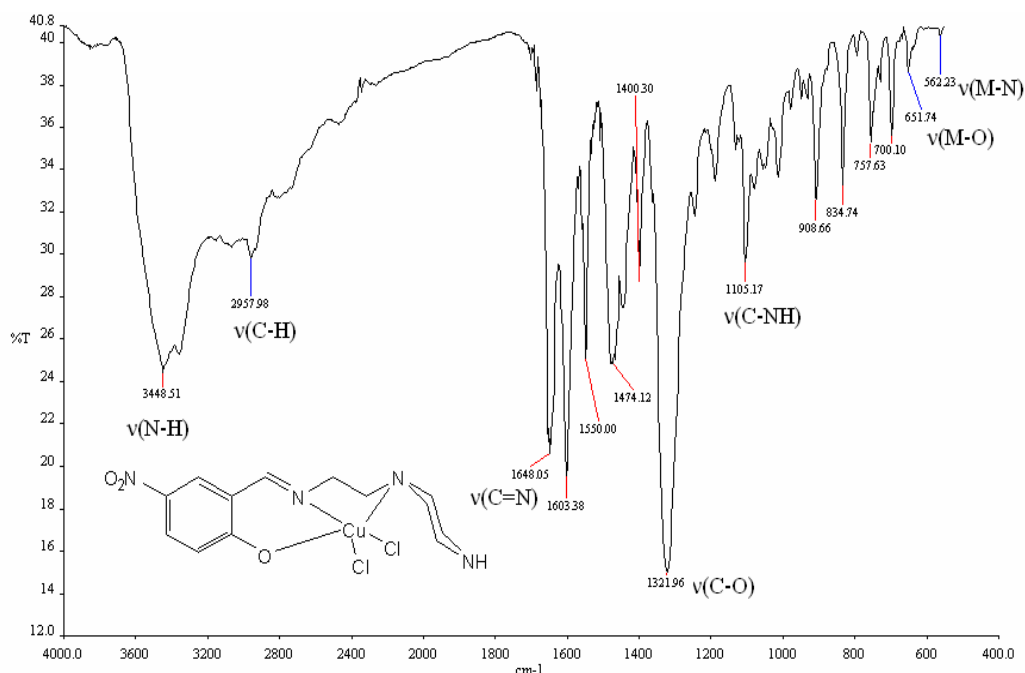


Figure 3.14 IR spectra of [Cu(LNS)Cl<sub>2</sub>] complex

3.2.5 IR spectra of (*E*)-2-((2-(piperazin-1-yl)ethylimino)methyl)benzene<sup>-1,4-diol</sup> (LDH) and its complexes of Cu, Zn and Cd

Table 3.5 IR spectral results for LDH and its complexes

Compound	v (O-H) /NH	v (C-H) Alp	v (C=N)	v (C-O)	v (C-H) Arom	v (M-O)	v (M-N)
LDH	3450	2963	1616	1250	794	-	-
[Cu(LDH)Cl <sub>2</sub> ]	3267	2833	1639	1293	680	591	420
[Zn(LDH)Cl <sub>2</sub> ]	3057	2821	1624	1300	615	517	461
[Cd(LDH)Cl <sub>2</sub> ]	3524	2957	1604	1267	708	570	441

The band region observed at 3450 cm<sup>-1</sup> in the spectra of LDH ligand can be due to coupled absorptions of piperazinic N-H and intermolecular hydrogen bonding of O-H. The aliphatic C-H appears at 2963 cm<sup>-1</sup>, HC=N stretching vibrations at 1616 cm<sup>-1</sup>, phenolic C-OH at 1250 cm<sup>-1</sup> and aromatic out of a plane C-H emerges at 799 cm<sup>-1</sup> as expected. The spectra of copper complex displayed complete absence of O-H broad band and displayed the piperazinic N-H band at 3267 cm<sup>-1</sup> due to deprotonation upon complexation. The aliphatic

C-H band has shifted to a lower frequency of  $2833\text{ cm}^{-1}$  whereby the bands due to HC=N stretching and phenolic C-O vibrations considerably shifts to high frequency of  $1639\text{ cm}^{-1}$  and  $1293\text{ cm}^{-1}$  respectively. The aromatic out of a plane C-H appears at  $680\text{ cm}^{-1}$  and the new bands that emerge at  $591\text{ cm}^{-1}$  and  $420\text{ cm}^{-1}$  are due to Cu-O and Cu-N stretchings correspondingly. For the spectra of zinc complex of this ligand, comparable increase in frequency were observed about  $8$  to  $50\text{ cm}^{-1}$  and this has been related to changes in the C=N and C-O bands respectively due to coordination. However, the aromatic out of plane C-H has shifted to a lower frequency by  $134\text{ cm}^{-1}$  whereby the new band at  $517\text{ cm}^{-1}$  can be assigned to Zn-O and that at  $461\text{ cm}^{-1}$  is attributable to Zn-N stretching. The spectra of the cadmium complex further confirm the N-H stretching at  $3524\text{ cm}^{-1}$  and complete absence of O-H band. The iminic HC=N appears at  $1604\text{ cm}^{-1}$  signifying a decrease in the bond order due to complexation. The phenolic C-OH appears deprotonated after coordination and shifts to a lower frequency of  $708\text{ cm}^{-1}$ . The new bands at  $570\text{ cm}^{-1}$  and  $441\text{ cm}^{-1}$  can be ascribed to Cd-O and Cd-N vibrations accordingly [119] (Table 3.5, Fig. 3.17-3.20) (Appendix B).

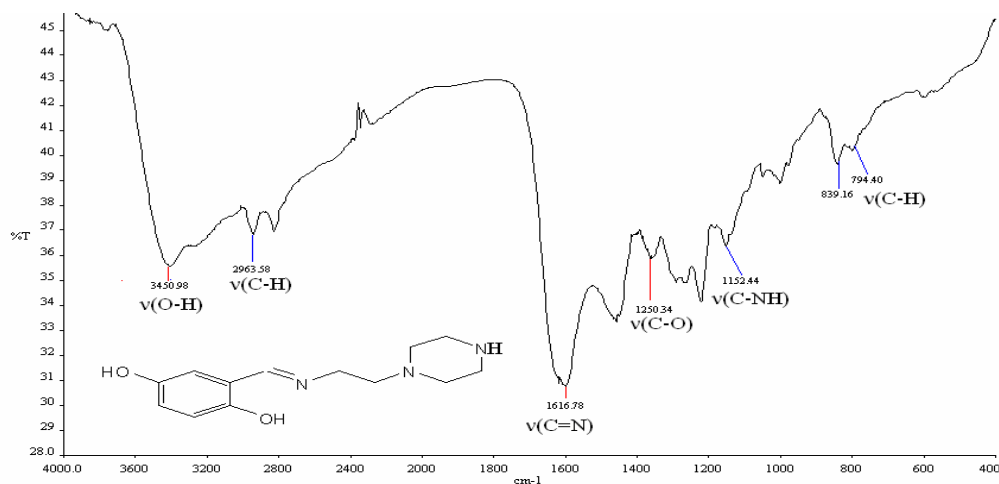


Figure 3.17 IR spectra of LDH ligand

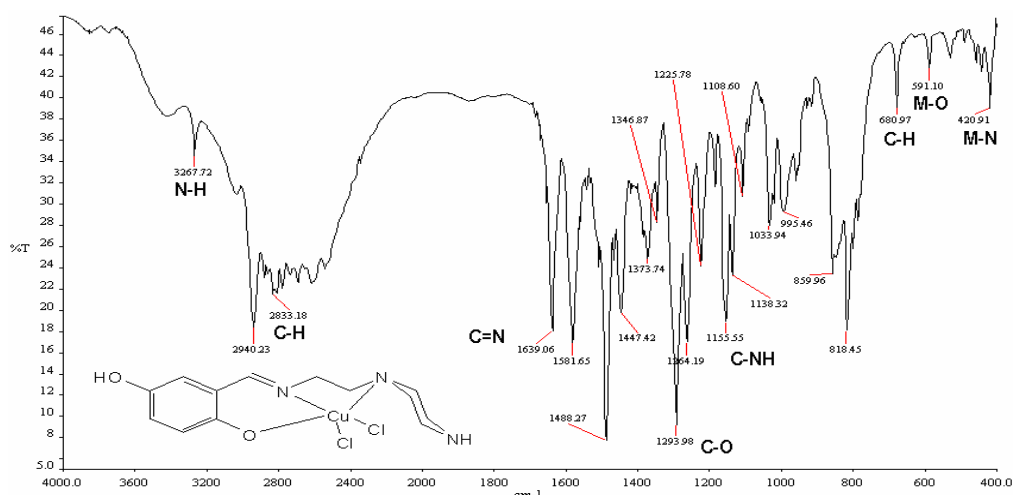


Figure 3.18 IR spectra of  $[\text{Cu}(\text{LDH})\text{Cl}_2]$  complex

3.2.6 IR spectra of (*E*)-4-((2-(piperazin-1-yl)ethylimino)methyl)benzene-1,3-diol (DHS) and its complexes of Cu, Zn and Cd

Table 3.6 IR spectral results for DHS and its complexes

Compound	$\nu$ (O-H /NH)	$\nu$ (C-H) Alp	$\nu$ (C=N)	$\nu$ (C-O)	$\nu$ (C-H) Alp	$\nu$ (M-O)	$\nu$ (M-N)
DHS	3410	2946	1598	1222	794	-	-
$[\text{Cu}(\text{DHS})\text{Cl}_2]$	3357	2957	1618	1228	636	514	455
$[\text{Zn}(\text{DHS})\text{Cl}_2]$	3431	2834	1595	1224	765	623	591
$[\text{Cd}(\text{DHS})\text{Cl}_2]$	3423	2845	1618	1217	627	598	461

Akin to the previously described LDH ligand, the ligand DHS also establishes superimposed spectral bands of N-H and O-H stretching vibrations at  $3410\text{ cm}^{-1}$ . The aliphatic C-H band appears at  $2946\text{ cm}^{-1}$  and iminic HC=N band resonates at  $1598\text{ cm}^{-1}$  while phenolic (C-OH), and the out of a plane aromatic (C-H) bands are observed at  $1222\text{ cm}^{-1}$  and  $794\text{ cm}^{-1}$  respectively. The spectra of copper complex indicates band regions expected to have emanated from the coordination of the binding sites of the ligand to the metal ion [120]. The shift of imine band C=N by  $20\text{ cm}^{-1}$  indicates coordination of imine nitrogen to copper [121]. This is further supported by the shift of C-O band by  $6\text{ cm}^{-1}$  to

form phenolate. This coordination is confirmed by the appearance of new bands at  $514\text{ cm}^{-1}$  and  $455\text{ cm}^{-1}$  due to Cu-O and Cu-N stretching frequencies respectively [122]. In comparison with the spectra of the ligand, zinc complex exhibits a low-frequency shift of C=N by  $3\text{ cm}^{-1}$  which indicates the participation of imine nitrogen in the coordination to zinc atom. In addition, the shift of C-O band to  $1224\text{ cm}^{-1}$  corresponds to the deprotonation of O-H and formation of Zn-O bond [123]. These changes were further ascertained at the bands  $623\text{ cm}^{-1}$  and  $591\text{ cm}^{-1}$  which can be attributed to Zn-O and Zn-N respectively. In the case of cadmium complex, the involvement of a deprotonated phenolic moiety in complexation was ascertained by the shift of C-O stretching band from  $1222\text{ cm}^{-1}$  in the free ligand to a lower frequency of  $1217\text{ cm}^{-1}$ . This suggests the weakening of C-O bond and formation of the stronger Cd-O bond [124]. The shift of the imine band to  $1618\text{ cm}^{-1}$  in the cadmium spectra also indicates coordination of imine nitrogen to Cd. This is further supported by the appearance of bands at  $598\text{ cm}^{-1}$  due to Cd-O and another band at  $461\text{ cm}^{-1}$  due to Cd-N stretching (Table 3.6, Fig. 3.21-3.24) (Appendix B).

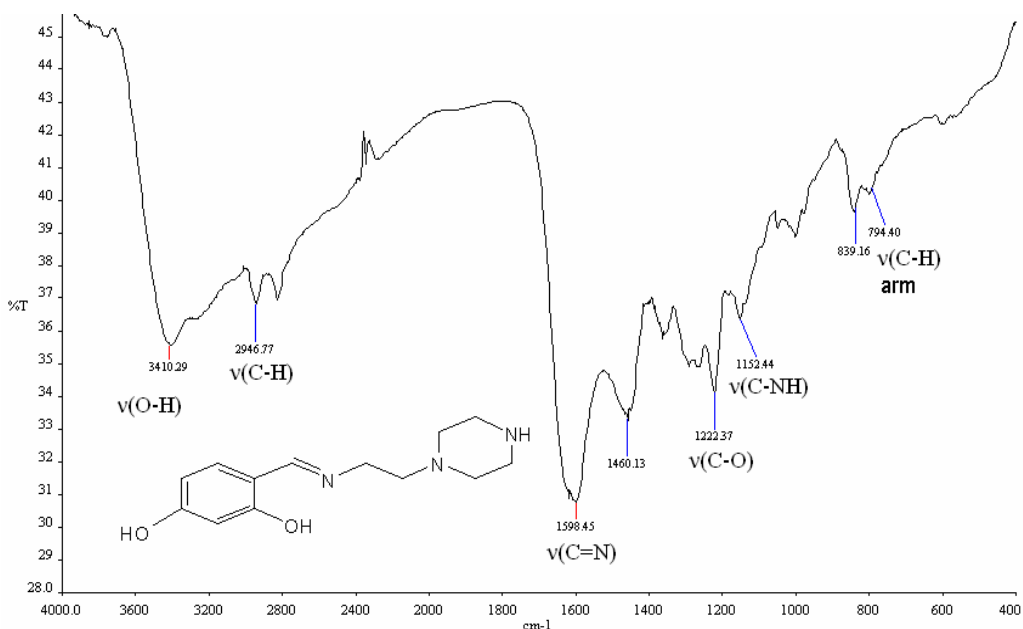


Figure 3.21 IR spectra of DHS ligand

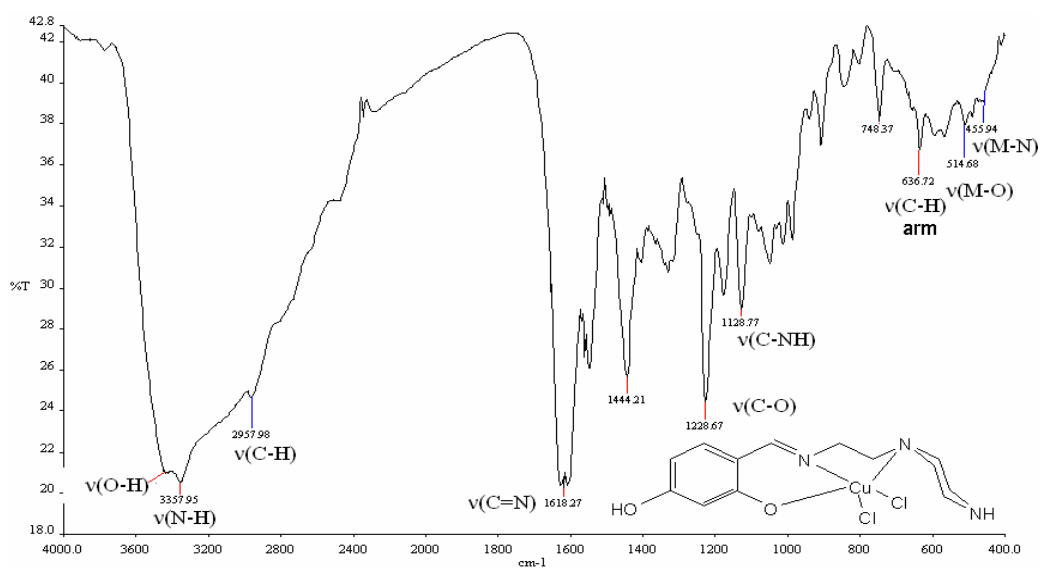


Figure 3.22 IR spectra of [Cu(DHS)Cl<sub>2</sub>] complex

3.2.7 IR spectra of (*E*)-4-methoxy-2-((2-(piperazin-1-yl)ethylimino)methyl) phenol (LHM) and its complexes of Cu, Zn and Cd

Table 3.7 IR spectral results for LHM and its complexes

Compound	$\nu$ (O-H /NH)	$\nu$ (C-H) Alp	$\nu$ (C=N)	$\nu$ (C-O)	$\nu$ (C-H) Arom	$\nu$ (M-O)	$\nu$ (M-N)
LHM	3423	2941	1624	1223	788	-	-
[Cu(LHM)Cl <sub>2</sub> ]	3434	2952	1639	1296	774	495	467
[Zn(LHM)Cl <sub>2</sub> ]	3448	2964	1609	1222	796	592	472
[Cd(LHM)Cl <sub>2</sub> ]	3467	3082	1627	1212	797	587	461

The strong and broad band shown by the ligand LHM spectra at 3423 cm<sup>-1</sup> can be ascribed to double resonance absorption [125] of phenolic O-H and piperazine N-H stretching vibrations. The ligand also manifests a characteristic iminic C=N band at 1624 cm<sup>-1</sup>. Band regions at 1223 cm<sup>-1</sup> can be attributed to phenolic C-O stretching [126] whereby the out of a plane aromatic C-H stretching appears at 788 cm<sup>-1</sup>. From the spectral data presented in Table 3.7, it can be concluded that piperazine N-H stretching band superimposes with O-H stretching band in all the spectra of the Schiff bases. However, this band slightly changes due to deprotonation upon complexation. For example, the medium band at 3434 cm<sup>-1</sup> in

the spectra of copper complex appears as a broad band at  $3423\text{ cm}^{-1}$  in the ligand spectra. The iminic  $\text{C}=\text{N}$  shifts to  $1639\text{ cm}^{-1}$  due to coordination between Cu and nitrogen. This is further supported by the deprotonation that leads to the formation of phenolate  $\text{C}-\text{O}$  stretching with increased frequency by  $73\text{ cm}^{-1}$ . The coordination of both imine nitrogen and the phenolate oxygen was confirmed by the appearance of new bands at  $495\text{ cm}^{-1}$  and  $467\text{ cm}^{-1}$  which can be attributed to  $\text{Cu}-\text{O}$  and  $\text{Cu}-\text{N}$  accordingly. Similar description can be made to the spectra of zinc complex despite the shift of imine  $\text{C}=\text{N}$  to a lower frequency due to reduced electron density that follows bonding of imine nitrogen to the metal ion. This is in agreement with the new bands at  $592\text{ cm}^{-1}$  due to  $\text{Zn}-\text{O}$  and at  $472\text{ cm}^{-1}$  due to  $\text{Zn}-\text{N}$  [127]. The spectra of cadmium complex also demonstrated a shift of iminic  $\text{C}=\text{N}$  at  $1627\text{ cm}^{-1}$  and of phenolic,  $\text{C}-\text{O}$  at  $1212\text{ cm}^{-1}$ . These changes can be assigned to the coordination of ligand to the metal ion. This is further supported by the appearance of a new band at  $587\text{ cm}^{-1}$  due to  $\text{Cd}-\text{O}$  stretching and another band at  $461\text{ cm}^{-1}$  that is assignable to  $\text{Cd}-\text{N}$  stretching vibrations [128] (Table 3.7, Fig. 3.25-3.28) (Appendix B).

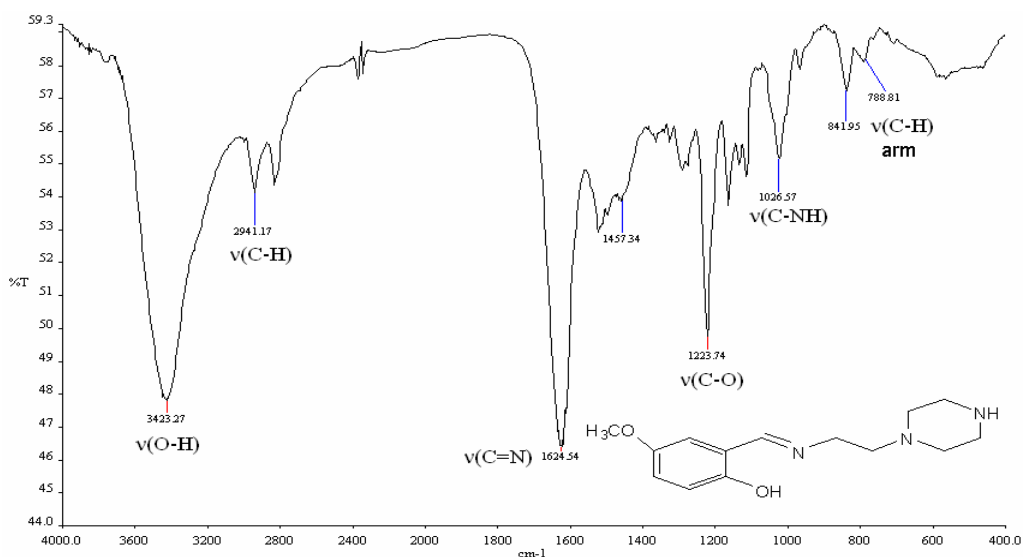


Figure 3.25 IR spectra of LHM ligand

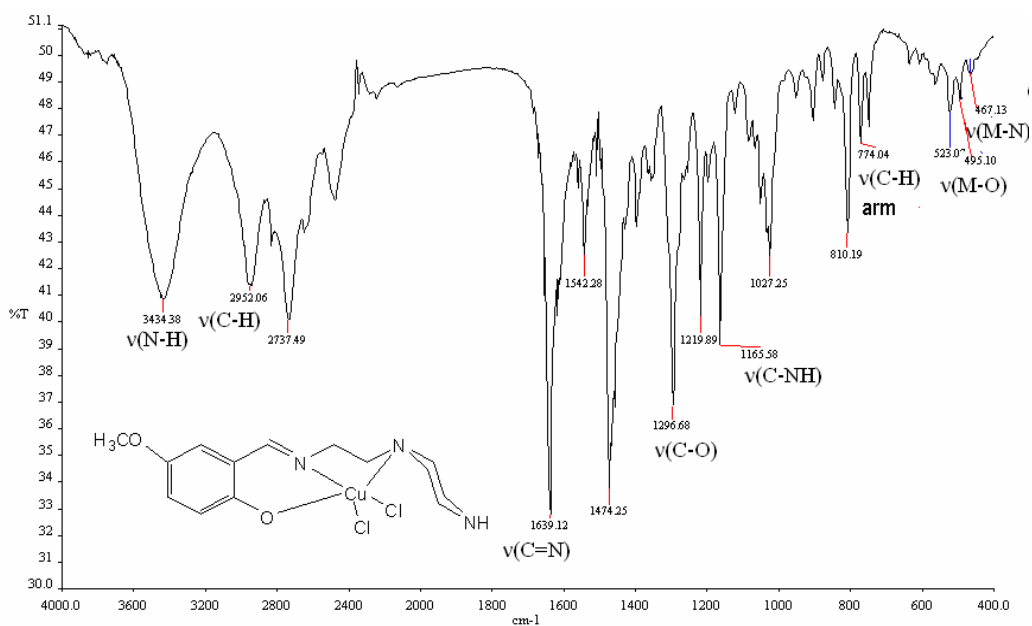


Figure 3.26 IR spectra of [Cu(LHM)Cl<sub>2</sub>] complex

3.2.8 IR spectra of (*E*)-5-methoxy-2-((2-(piperazin-1-yl)ethylimino)methyl) phenol (HMS) and its complexes of Cu, Zn and Cd

Table 3.8 IR spectral results for HMS and its complexes

Compound	$\nu$ (O-H /NH)	$\nu$ (C-H) Alp	$\nu$ (C=N)	$\nu$ (C-O)	$\nu$ (C-H) Arom	$\nu$ (M-O)	$\nu$ (M-N)
HMS	3423	2941	1625	1225	788	-	-
[Cu(HMS)Cl <sub>2</sub> ]	3416	2956	1605	1224	745	508	419
[Zn(HMS)Cl <sub>2</sub> ]	3466	2969	1606	1219	796	592	486
[Cd(HMS)Cl <sub>2</sub> ]	3450	3082	1627	1212	797	567	461

The broad band that appears at 3423 cm<sup>-1</sup> in the spectra of HMS ligand can be assigned to double vibration due to OH and N-H as described earlier. A prominent band at 1625 cm<sup>-1</sup> is ascribed to the imine C=N vibrations, this absorption is very close to the band observed in the spectra of the LHM ligand thus suggesting comparable electron density on the aromatic ring of the two analogue ligands. The phenolic C-O stretching band appears at 1225 cm<sup>-1</sup> and the band at 788 cm<sup>-1</sup> is due to aromatic C-H out of plane absorption. The spectra of the copper complex of this ligand exhibits N-H stretching at 3416 cm<sup>-1</sup> which is expected due

to the deprotonation of phenolic O-H after complexation. The iminic C=N had also shifted to a lower frequency of  $1605\text{ cm}^{-1}$  owing to iso-electronic behavior that is anticipated at an imine link [129]. The coordination of imine nitrogen and phenolate oxygen to the metal ion was further established by the appearance of new bands at  $508\text{ cm}^{-1}$  due to Cu-O and the band at  $419\text{ cm}^{-1}$  that corresponds to Cu-N stretching. Similar explanation can be made to zinc complex except that Zn-O and Zn-N bands appears at increased wavelengths of  $592\text{ cm}^{-1}$  and  $486\text{ cm}^{-1}$  respectively [130]. In the case of the cadmium complex, the expected bands of the coordination sites were observed at a high frequency in comparison with the spectra of the free ligand. The piperazine N-H vibrations appears at  $3450\text{ cm}^{-1}$  and iminic C=N shifts to  $1627\text{ cm}^{-1}$ . The phenolate C-O band appears at a low wave number of  $1212\text{ cm}^{-1}$  suggesting the formation of Cd-O bond. This is confirmed due to the new wavelengths found at  $567\text{ cm}^{-1}$  and  $461\text{ cm}^{-1}$  that can be assigned to Cd-O and Cd-N vibrations respectively (Table 3.8, Fig. 3.29-3.32) (Appendix B).

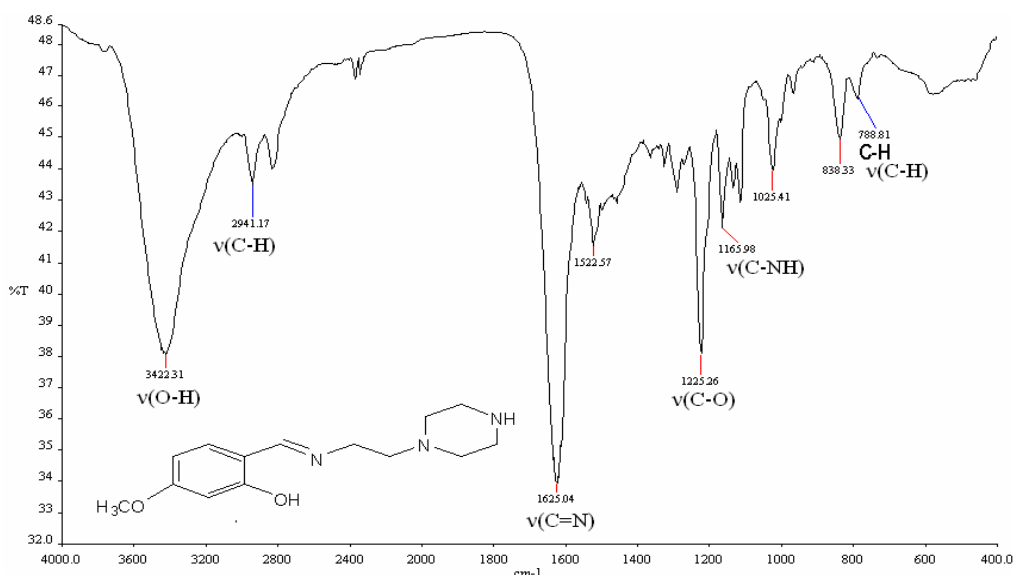


Figure 3.29 IR spectra of HMS ligand

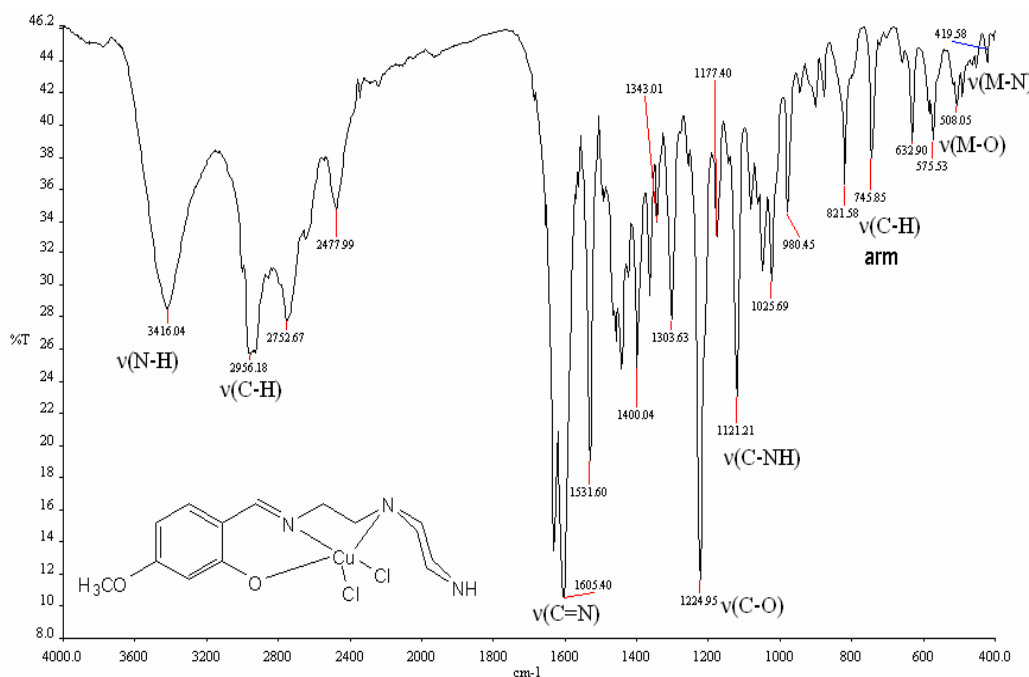


Figure 3.30 IR spectra of [Cu(HMS)Cl<sub>2</sub>] complex

### 3.2.9 IR spectra (E)-2-(1-(2-piperazin-1-yl)ethylimino)ethyl phenol (2HP) and its complexes of Cu, Zn and Cd

Table 3.9 IR spectral results for 2HP and its complexes

Compound	v (O-H /NH)	v (C-H) Alp	v (C=N)	v (C-O)	v (C-H) Arom	v (M-O)	v (M-N)
2HP	3394	2949	1616	1302	753	-	-
[Cu(2HP)Cl <sub>2</sub> ]	3448	2952	1599	1234	706	584	509
[Zn(2HP)Cl <sub>2</sub> ]	3497	2945	1608	1220	775	539	455
[Cd(2HP)Cl <sub>2</sub> ]	3520	2945	1610	1303	750	618	503

The infra red spectral data for the ligand 2HP shows a strong and broad band at 3394 cm<sup>-1</sup> due to overlaid absorptions of N-H stretching and phenolic O-H. The iminic C=N stretching band appears at 1616 cm<sup>-1</sup> whereby the phenolic C-O stretching and the aromatic out of a plane C-H vibrations were observed at 1302 cm<sup>-1</sup> and 753 cm<sup>-1</sup> respectively. In the copper complex of this ligand, a sharp broad band appears at 3448 cm<sup>-1</sup> which is attributable to piperazine N-H stretching vibration [131]. The iminic C=N band shifts to a

lower frequency of  $1599\text{ cm}^{-1}$  due to the decrease in the N atom charge density and the partial delocalization of charge into the C=N bond on coordination to the metal ion [132]. The phenolate C-O stretching also appears at the lower wavelengths symptomatic of the weakening of C-O bond and coordination to the metal. This is further proved by the appearance of new bands at  $584\text{ cm}^{-1}$  which corresponds to Cu-O vibrations and at  $509\text{ cm}^{-1}$  that can be assigned to Cu-N stretching. A similar description can be made to the spectra of zinc complex. Furthermore, the bands due to Zn-O and Zn-N appear at the lower frequency of  $539\text{ cm}^{-1}$  and  $455\text{ cm}^{-1}$  respectively as described. In the case of cadmium complex, the iminic C=N band appears at the lower frequency as expected due to reduced electron density. The phenolic C-O band slightly shifts to  $1303\text{ cm}^{-1}$  due to complexation. The Cd-O stretching band appears at a frequency of  $618\text{ cm}^{-1}$  while the M-N band was observed at  $503\text{ cm}^{-1}$  (Table 3.9, Fig. 3.33-3.36) (Appendix B).

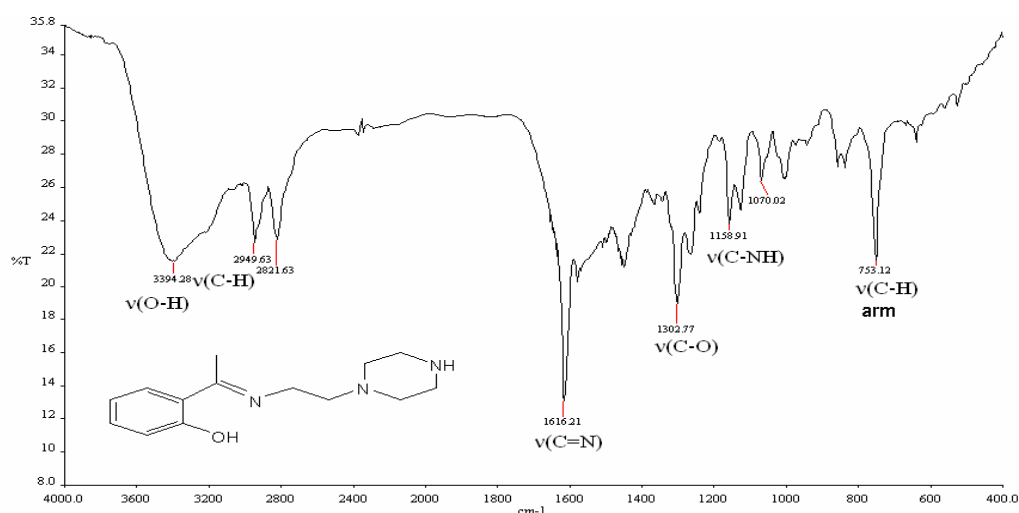


Figure 3.33 IR spectra of 2HP ligand

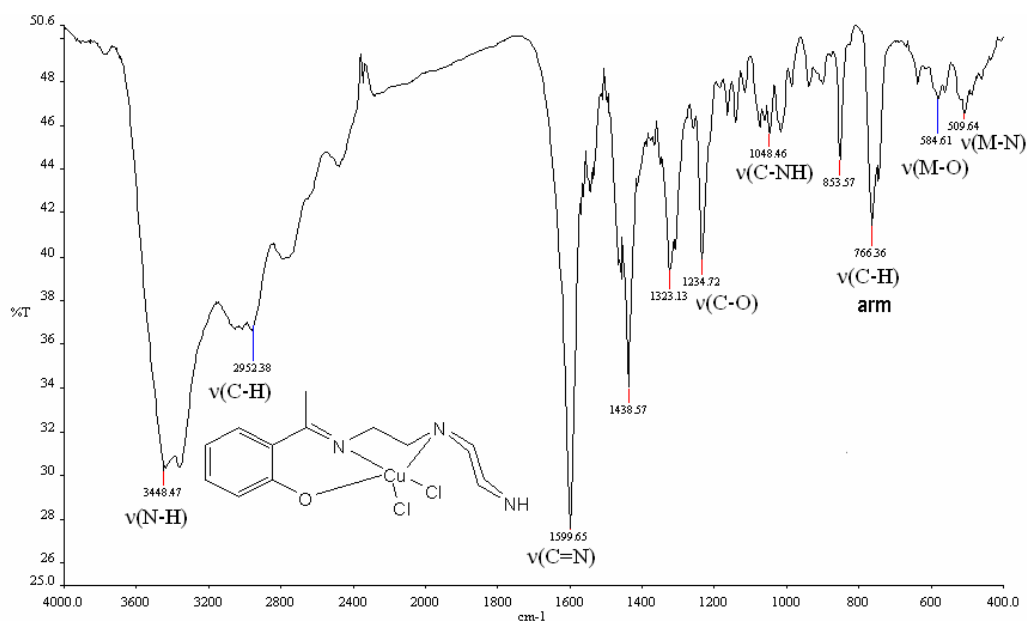


Figure 3.34 IR spectra of  $[\text{Cu}(\text{2HP})\text{Cl}_2]$  complex

3.2.10 IR spectra of (*E*)-4-(1-(2-piperazin-1-yl)ethylimino)ethyl)benzene-1,3-diol (DHP) and its complexes of Cu, Zn and Cd

Table 3.10 IR spectral results for DHP and its complexes

Compound	$\nu$ (O-H /NH)	$\nu$ (C-H) Alp	$\nu$ (C=N)	$\nu$ (C-O)	$\nu$ (C-H) Arom	$\nu$ (M-O)	$\nu$ (M-N)
DHP	3371	2957	1610	1286	792	-	-
$[\text{Cu}(\text{DHP})\text{Cl}_2]$	3402	2969	1594	1247	750	507	451
$[\text{Zn}(\text{DHP})\text{Cl}_2]$	3490	2951	1586	1263	805	585	457
$[\text{Cd}(\text{DHP})\text{Cl}_2]$	3512	2965	1608	1277	810	690	562

In the IR spectrum of the ligand DHP, the broad absorption band at  $3371\text{ cm}^{-1}$  was assigned to the stretching vibration of the intermolecular hydrogen bonding of phenolic O-H. The iminic C=N stretching vibrations appears at  $1610\text{ cm}^{-1}$  while the phenolic C-O stretching band is found at  $1286\text{ cm}^{-1}$ . The piperazine N-H was obscured by the two hydroxyl group's presence in the aromatic ring. The copper complex of this ligand also manifested a band region at  $3402\text{ cm}^{-1}$  due to double resonance of the O-H groups and piperazine N-H

stretching vibrations. The iminic C=N band shifts to a lower frequency of 1594  $\text{cm}^{-1}$  as predicted owing to coordination of the imine nitrogen with the metal ion. This is supported by the shift of phenolic C-O band to a lower frequency of 1247  $\text{cm}^{-1}$ , thus weakening the hydrogen bond due to the formation of stronger M-O bond [133]. The band at 507  $\text{cm}^{-1}$  corresponds to Cu-O band stretching, and that at 451  $\text{cm}^{-1}$  is assigned to Cu-N vibration. Same description can be made on the spectra of zinc and cadmium complexes except that the Zn-O band appears at 585  $\text{cm}^{-1}$  which is comparably lower frequency than Cd-O band that emerges at 610  $\text{cm}^{-1}$  [134]. Similar decrease in wavelengths is observed for Zn-N and Cd-N bands, which appears at 457  $\text{cm}^{-1}$  and 562  $\text{cm}^{-1}$  respectively (Table 3.10, Fig. 3.37-3.40).

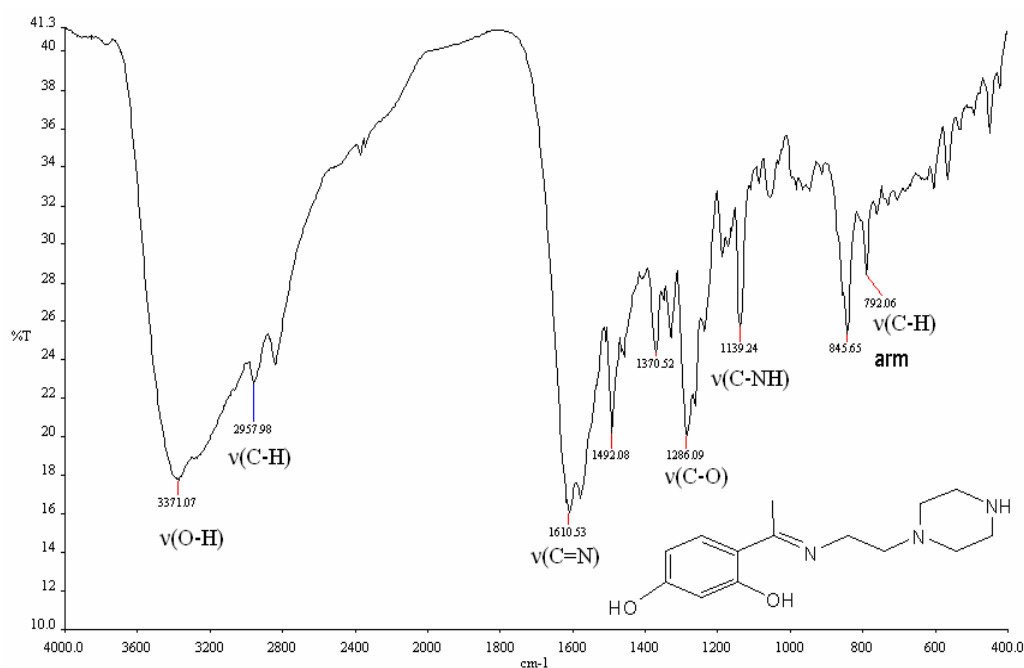


Figure 3.37 IR spectra of DHP ligand

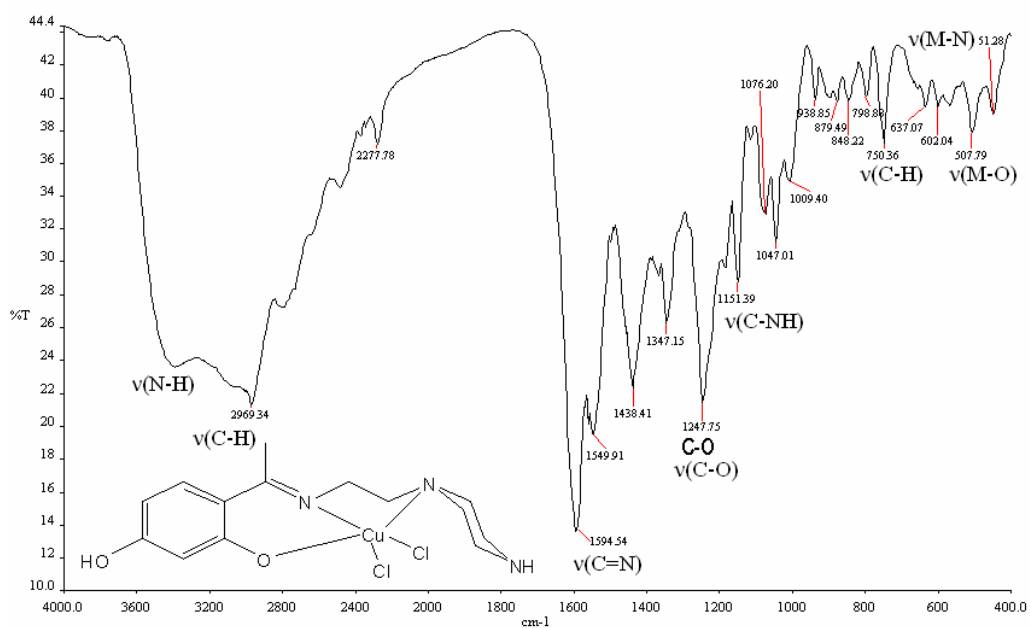


Figure 3.38 IR spectra of [Cu(DHP)Cl<sub>2</sub>] complex

### 3.3 Proton NMR spectrums of the Schiff bases and their metal complexes

The <sup>1</sup>H NMR spectra of the ligands and their Zn and Cd complexes were recorded in dimethylsulphoxide-d<sub>6</sub> using tetramethylsilane (TMS) as an internal standard. The signals observed due to chemical shifts were expressed in ppm as shown in Tables 11-20 and Figures 3.41-3.60.

3.3.1. <sup>1</sup>H NMR spectra of (*E*)-2-((2-(piperazin-1-yl)ethylimino)methyl)phenol (LSP) and its Zn and Cd complexes.

Table 3.11 <sup>1</sup>H NMR spectral data for LSP and its complexes, δ (ppm)

Compound	Ha	3Hb	Hc	Hd	He	arH
LSP	2.10	2.44-2.70	3.22-3.48	8.49	7.45	6.8-7.4
[Zn(LSP)Cl <sub>2</sub> ]	2.02	3.01-2.64	3.15-3.46	8.22	-	6.3-7.2
[Cd(LSP)Cl <sub>2</sub> ]	2.04	2.83-2.70	3.51-3.71	8.21	-	6.2-7.0
[Cu(LSP)Cl <sub>2</sub> ]	Paramagnetic					

The <sup>1</sup>H NMR spectrum of the ligand LSP and its complexes of Zn and Cd were recorded in dimethylsulphoxide-d<sub>6</sub>. The spectra of the ligand exhibits a singlet signal in the region δ 8.49 which has been ascribed to imine proton (-HC=N-) (Hd) [135] (Table 3.11). This signal in the spectra of zinc and cadmium were down field to δ 8.22 and δ 8.21

respectively, which presumably indicates the bonding of imine with the metal ions through nitrogen [136]. The chemical shift at  $\delta$  7.45 can be assigned to the hydrogen bonding of phenolic O-H (He) in the ligand which appears as broad peak that presumably exchange with D<sub>2</sub>O. This peak is absent in the spectra of the complexes due to deprotonation of the phenolic group. The multiplet peaks observed at  $\delta$  6.8-7.4 in the ligand spectra can be attributable to the shifts of aromatic protons (arH) [137]. These signals shift down field due to coordination of phenolic hydrogen with the metal ion [138] and appear at  $\delta$  6.3-7.2 in the spectra of zinc complex and at  $\delta$  6.2- 7.0 in the spectra of cadmium complex. Peaks observed at the  $\delta$  2.5-2.56 in all the spectra can be due to solvent (DMSO) (Table 3.11 and Figures 3.41-3.43) (Appendix C).

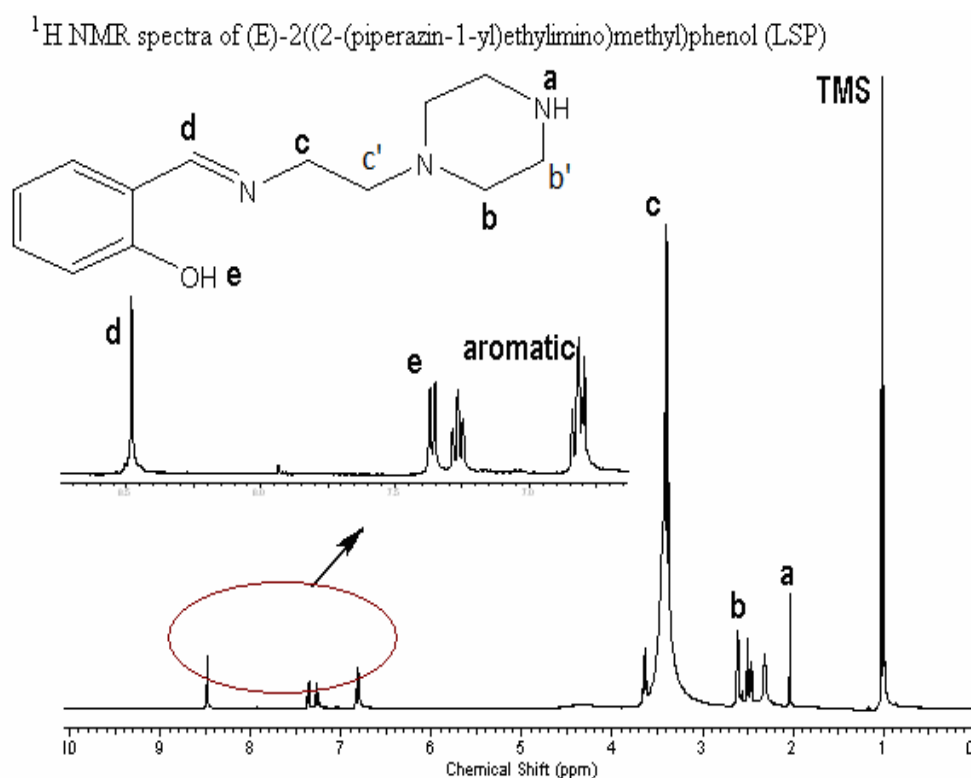


Figure 3.41 <sup>1</sup>H NMR spectra of LSP ligand.

3.3.2. <sup>1</sup>H NMR spectra of (E)-4-chloro-2-((2-(piperazin-1-yl)ethylimino)methyl) phenol (LCS) and its Zn and Cd complexes.

Table 3.12 <sup>1</sup>H NMR spectral data for LCS and its complexes δ (ppm)

Compound	Ha	Hb	Hc	Hd	He	arH
LCS	2.34	2.43-2.81	3.22-3.62	8.21	7.20	6.7-7.1
[Zn(LCS)Cl <sub>2</sub> ]	2.10	2.52-2.62	3.28-3.64	7.80	-	6.1-6.8
[Cd(LCS)Cl <sub>2</sub> ]	2.32	2.41-2.61	3.19-3.59	7.95	-	6.0-6.9
[Cu(LCS)Cl <sub>2</sub> ]	Paramagnetic					

The spectral data of <sup>1</sup>H NMR of the ligand LCS showed a broad signal at δ 7.20, which can be attributed to hydrogen bonding of phenolic O-H (He); this band is down field compared to its position in the LSP ligand which can presumably be due to substituents effect [139]. The absence of this signal in the spectra of zinc and cadmium complexes confirms the replacement of phenolic proton by metal ion and the formation of metal-phenolate bond. The aromatic protons (arH) appear as doublet at the δ range 6.1-6.8 in zinc spectra and at δ 6.0-6.9 in the spectra of cadmium. These protons resonate at the frequency of δ 6.7-7.1 in the ligand spectra which indicates rearrangements of protons due to complex formation. A singlet peak observed at δ 8.21 in the spectra of the ligand can be ascribed to iminic proton. This signal shifts to low field frequency of δ 7.8 in zinc spectra and appears at δ 7.95 in the cadmium spectra due to complexation. In addition, the methylene (Hb, Hb', Hc and Hc') protons showed resonance frequency at δ range 2.41-3.64 which could be attributed to the conformational rearrangements of the piperazine group due to axial and equatorial hydrogens that coupled differently [140] to form chair conformational geometry as confirmed by X-ray diffraction analysis. The signals at 2.48-2.54 observed in all the spectra were ascribed to the DMSO solvent (Table 3.12, Fig. 3.44-3.46) (Appendix C).

<sup>1</sup>H NMR spectra of (E)-4-chloro-2-((2-(piperazin-1-yl)ethylimino)methyl)phenol (LCS)

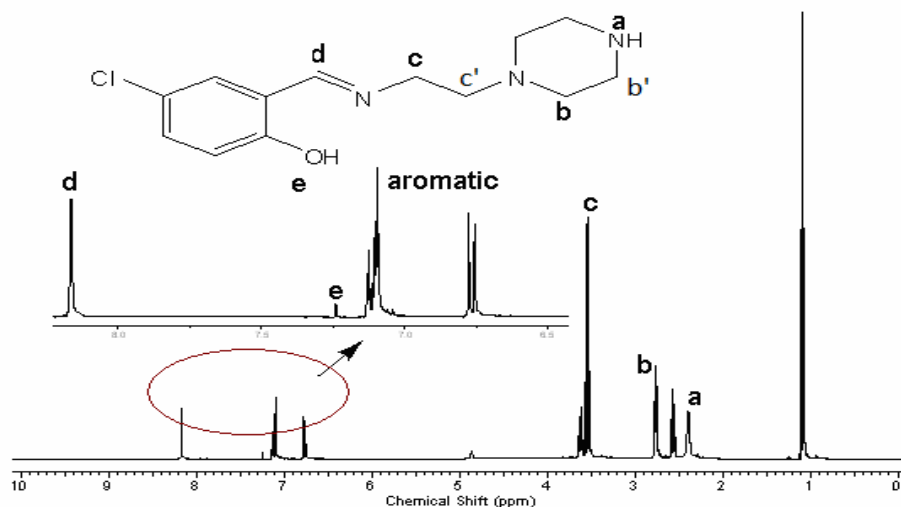


Figure 3.44 <sup>1</sup>H NMR spectra of LCS ligand.

3.3.3. <sup>1</sup>H NMR spectra of (E)-4-bromo-2-((2-(piperazin-1-yl)ethylimino)methyl) phenol (LBS) and its Zn and Cd complexes.

Table 3.13 <sup>1</sup>H NMR spectral data for LBS and its complexes  $\delta$  (ppm)

Compound	Ha	Hb	Hc	Hd	He	arH
LBS	2.17	2.69-2.70	2.91-3.74	8.29	7.34	6.87-7.22
[Zn(LBS)Cl <sub>2</sub> ]	2.25	2.58-3.03	3.11-3.39	8.17	-	6.45-7.72
[Cd(LBS)Cl <sub>2</sub> ]	2.04	2.81-3.57	2.97-3.41	8.54	-	6.34-7.61
[Cu(LBS)Cl <sub>2</sub> ]	Paramagnetic					

In the proton, NMR spectra of LBS ligand, the signal at  $\delta$  7.34 can be attributed to intermolecular hydrogen bonding of phenolic O-H (He) [141]. These signals disappear in the spectra of zinc and cadmium complexes due to metal-phenolate coordination. A singlet shift that appear at  $\delta$  8.29 in the ligand spectra can be assigned to  $\text{-HC=N-}$  group (Hd). After complexation, this signal has shifted to a lower frequency of  $\delta$  8.17 in the spectra of zinc complex and to a higher frequency of 8.54 in the spectra of cadmium due to changes in the electron density of phenolic ring. This also affects the position of aromatic protons (arH) which resonates at  $\delta$  range 6.87-7.22 in the free ligand and shifts to  $\delta$  range of 6.45-7.72 and 6.34-7.61 in the spectra of zinc and cadmium complexes respectively after chelation. The methylene protons Hb, Hb', Hc and Hc' appeared as double peaks at  $\delta$  range

2.58-3.74 due to multiplicities of peaks emanating from the neighboring methyl groups in the ligand spectra. These signals shifted to a higher frequency range  $\delta$  3.03-3.57 in zinc and cadmium spectra, thus suggesting the structural rearrangements involved upon chelation [142]. In addition, the piperazine N-H in the spectra of zinc complex shows a signal at  $\delta$  2.25, which may be due to the non-involvement of piperazine secondary nitrogen in bonding with metal. Also, this signal was observed at a decreased frequency of  $\delta$  2.04 in the spectra of cadmium which require similar elucidation (Table 3.13, Fig. 3.47-3.49) (Appendix C).

<sup>1</sup>H NMR spectra of (E)-4-bromo-2-((2-(piperazin-1-yl)ethylimino)methyl)phenol (LBS)

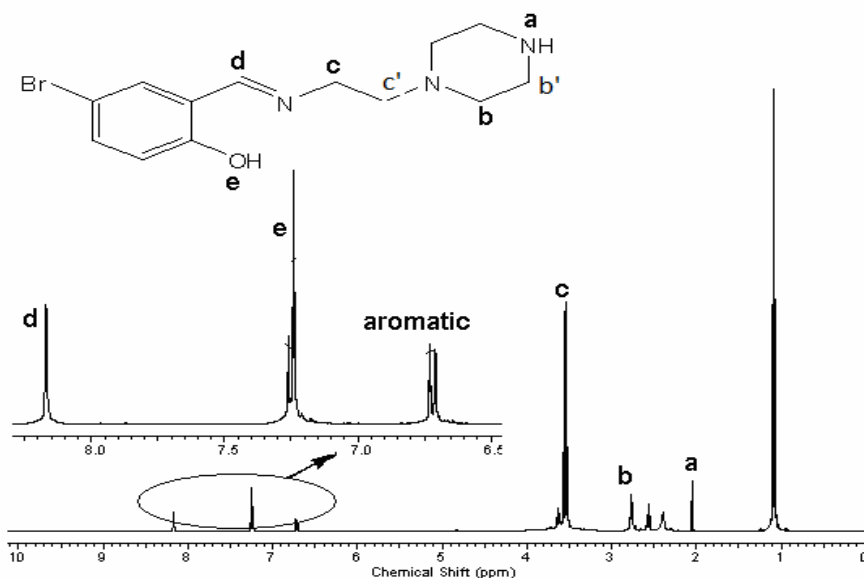


Figure 3.47 <sup>1</sup>H NMR spectra of LBS ligand.

### 3.3.4. <sup>1</sup>H NMR spectra of (E)-4-nitro-2-((2-(piperazin-1-yl)ethylimino)methyl) phenol (LNS) and its Zn and Cd complexes.

Table 3.14 <sup>1</sup>H NMR spectral data for LNS and its complexes  $\delta$  (ppm)

Compound	Ha	Hb	Hc	Hd	He	arH
LNS	2.04	2.39-2.81	2.95-3.50	8.52	8.13	7.42-8.13
[Zn(LNS)Cl <sub>2</sub> ]	2.28	2.48-2.91	3.17-3.69	8.48	-	6.59-8.31
[Cd(LNS)Cl <sub>2</sub> ]	2.03	2.52-2.80	2.66-3.43	8.60	-	6.39-8.16
[Cu(LNS)Cl <sub>2</sub> ]	Paramagnetic					

The  $^1\text{H}$  NMR spectra of the ligand LNS exhibited sharp and broad singlet peaks at  $\delta$  2.04 and 8.13 due to N-H of the piperazine moiety (Ha) and phenolic proton (He) respectively. The iminic HC=N (Hd), also appeared as singlet at  $\delta$  8.52. In the spectra of its zinc complex, a down field chemical shift was noticed at  $\delta$  8.48 which can be attributed to iminic HC=N, this signal appeared up-field at  $\delta$  8.60 in the spectra of cadmium and was ascribed to the changes in electron density resulted [143] from coordination. Both complexes showed complete disappearance of O-H signal in their spectra. Signals due to aromatic protons (arH) were observed at  $\delta$  range 7.42-8.13 in the ligand spectra. These signals appear at  $\delta$  range 6.59-8.31 and 6.39-8.16 in the spectra of zinc and cadmium complexes respectively thus, supporting the changes observed in the position of HC=N due to complexation [144]. The peaks at  $\delta$  range were assigned to the solvent DMSO while those small peaks at 3.92 can be attributed to the impurities (Table 3.14, Fig. 3.50-3.52) (Appendix C).

$^1\text{H}$  NMR spectra of (E)-4-nitro-2-((2-(piperazin-1-yl)ethylimino)methyl)phenol (LNS)

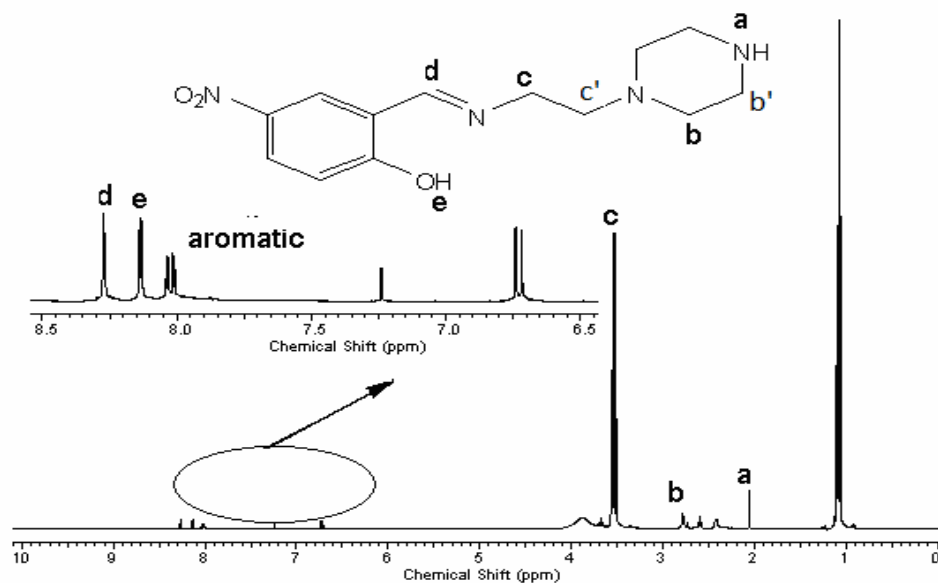


Figure 3.50  $^1\text{H}$  NMR spectra of LNS ligand.

3.3.5. <sup>1</sup>H NMR spectra of (E)-2-((2-(piperazin-1-yl)ethylimino)methyl)benzene-1,4-diol (LDH) and its Zn and Cd complexes.

Table 3.15 <sup>1</sup>H NMR spectral data for LDH and its complexes δ (ppm)

Compound	Ha	Hb	Hc	Hd	He	arH
LDH	2.02	2.77-2.83	3.15-3.78	8.42	7.96	6.54-6.83
[Zn(LDH)Cl <sub>2</sub> ]	2.04	2.43-2.67	3.32-3.63	8.56	8.27	6.28-8.44
[Cd(LDH)Cl <sub>2</sub> ]	2.05	2.71-2.86	3.19-3.60	8.36	8.24	6.43-8.17
[Cu(LDH)Cl <sub>2</sub> ]	Paramagnetic					

The <sup>1</sup>H NMR spectral data of the ligands LDH show a signal that can be assignable to aromatic protons (arH) at the δ range of 6.54–6.83. The broad peaks observed at δ 7.96 could be due to O-H (He) protons of the phenolic groups [145]. The singlet peak that appeared at δ 8.42 can be attributed to the imine protons (Hd). The chemical shift due to CH<sub>2</sub> protons (Hb, Hb', Hc and Hc') appear at the δ range of 2.43-3.78 whereby the piperazine N-H protons (Ha) appeared as broad peak at δ 2.02. Comparably, these signals in the spectra of zinc complex has shifted to higher frequencies as a result of complexation [109], whereby the HC=N proton (Hd) shifts up-field to δ 8.56, and the signal due to O-H group was observed at δ 8.27. The aromatic protons emerge at δ range of 6.28-8.44. This high-frequency shift of aromatic protons can presumably be due to non-involvement of the tertiary nitrogen of a piperazine moiety as confirmed by x-ray diffraction analysis. Similar chemical shifts are noticed in the spectra of cadmium complex except that the position of iminic HC=N appears at a low frequency of δ 8.36 when compared to the signal at δ 8.42 in the spectra of the free ligand. This is expected due to the reduction in electron density that resulted from complex formation [146]. The multiplet peaks signals at δ range of 6.43-8.17 could be assigned to aromatic protons, which are expected to have arisen from the possible

changes in bond order [147]. The multiplet peaks that appeared at  $\delta$  2.48-2.54 could be due to the solvent DMSO or impurities (Table 3.15, Fig. 3.53-3.55) (Appendix C).

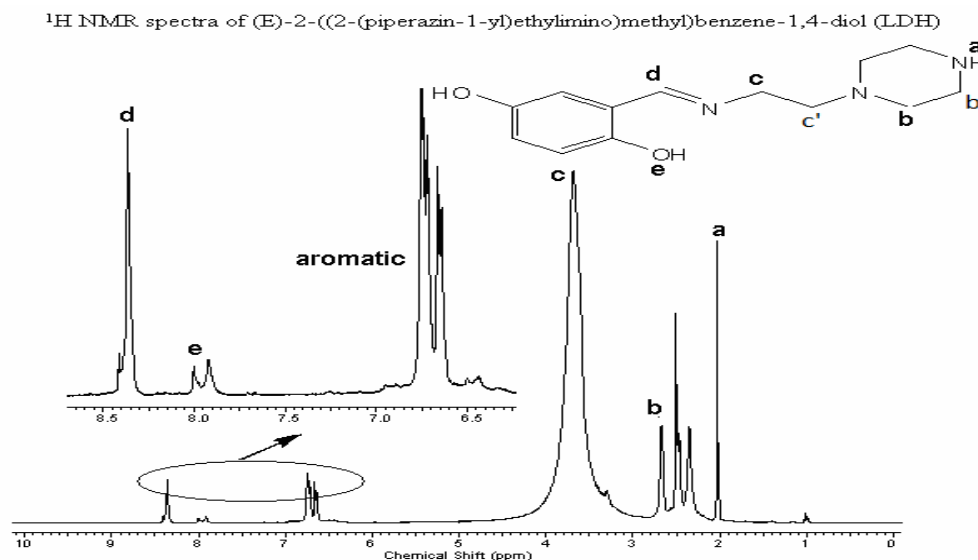


Figure 3.53 <sup>1</sup>H NMR spectra of LDH ligand.

### 3.3.6. <sup>1</sup>H NMR spectra of (E)-2-((2-(piperazin-1-yl)ethylimino)methyl)benzene-1,3-diol (DHS) and its Zn and Cd complexes.

Table 3.16 <sup>1</sup>H NMR spectral data for DHS and its complexes  $\delta$  (ppm)

Compound	Ha	Hb	Hc	Hd	He	arH
DHS	2.02	2.67-2.86	3.21-3.64	8.42	10.31	6.64-7.91
[Zn(DHS)Cl <sub>2</sub> ]	2.34	2.74-3.21	2.98-3.56	8.15	6.81	6.10-6.31
[Cd(DHS)Cl <sub>2</sub> ]	2.94	2.79-3.62	3.65-3.98	8.52	4.72	6.34-7.62
[Cu(DHS)Cl <sub>2</sub> ]	Paramagnetic					

The <sup>1</sup>H NMR spectra of the ligand DHS exhibited broad signals due to intermolecular hydrogen bond O-H (He) at  $\delta$  10.31. The iminic HC=N (Hd) appeared as a singlet at the chemical shift  $\delta$  8.42 which is similar with its analogue LDH ligand. This indicated that the change in the position of aromatic ring substituents (OH) has little effect on the imine center [148]. The aromatic protons (arH) appeared at  $\delta$  6.64-7.91. In the <sup>1</sup>H NMR spectra of zinc complex of this ligand, both iminic HC=N and the out of a plane OH groups were deshielded due to coordination of the ligand with the metal ion and appear at  $\delta$  8.15 and  $\delta$

6.81 respectively [149]. The aromatic protons also shift to a lower field  $\delta$  range 6.10-6.31. This is attributable to the conformational changes that are expected upon complexation. Similar changes were observed in the spectra of cadmium complex where the iminic HC=N position shifted slightly. However, this signifies the possible coordination of the tertiary nitrogen of a piperazine moiety contrary to what was observed in its analogue compound described above (Table 3.16, Fig. 3.56-3.58) (Appendix C).

<sup>1</sup>H NMR spectra of (E)-4-((2-(piperazin-1-yl)ethylimino)methyl)benzene-1,3-diol (DHS)

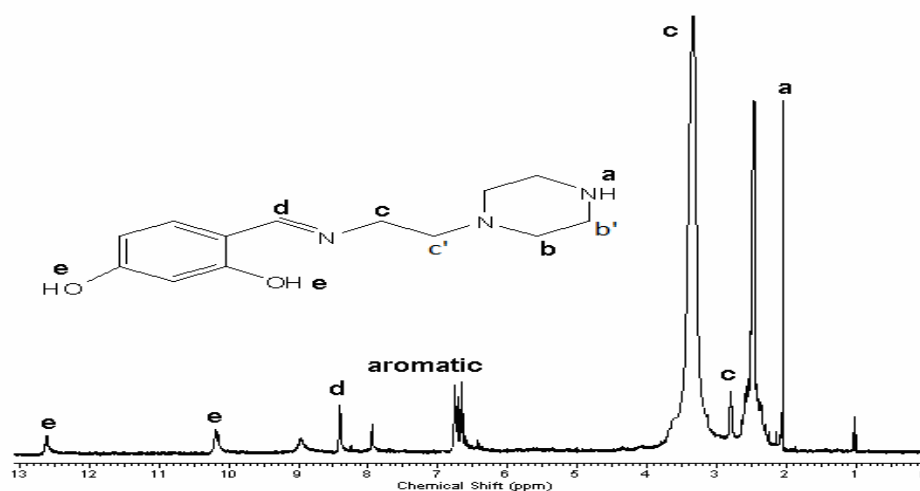


Figure 3.56 <sup>1</sup>H NMR spectra of DHS ligand.

### 3.3.7. <sup>1</sup>H NMR spectra of (E)-4-methoxy-2-((2-(piperazin-1-yl)ethylimino)methyl) phenol (LHM) and its Zn and Cd complexes.

Table 3.17 <sup>1</sup>H NMR spectral data for LHM and its complexes  $\delta$  (ppm)

Compound	Ha	Hb	Hc	Hd	He	arH
LHM	2.32	2.43-2.75	3.29-3.65	8.44	7.92	6.59-7.28
[Zn(LHM)Cl <sub>2</sub> ]	2.46	3.27-3.39	3.22-3.61	8.21	-	6.46-6.84
[Cd(LHM)Cl <sub>2</sub> ]	2.04	2.84-3.46	3.66-3.76	8.23	-	6.24-8.05
[Cu(LHM)Cl <sub>2</sub> ]	Paramagnetic					

The proton NMR spectra for the ligand LHM displayed a sharp singlet at  $\delta$  8.44 that can be assignable to iminic HC=N (Hd). The phenolic OH (He) appeared as broad signal at  $\delta$  7.92 while the aromatic protons (arH) resonate at  $\delta$  range 6.59-7.28. However, the spectra of

zinc complex demonstrate a low field chemical shift at  $\delta$  8.21 that can be attributed to the coordination of imine nitrogen with the metal ion. Absence of OH signal in this spectrum also confirms the involvement of phenolic (C-O) oxygen in bonding with the metal ion [150]. The CH<sub>2</sub> signals (Hb, Hb', Hc and Hc') that appear at  $\delta$  range 2.43-3.65 in the ligand spectra are observed to have shifted to  $\delta$  range 3.27-3.61. These structural adjustments that occur due to complexation further affects the position of the aromatic protons which appear at  $\delta$  range 6.46-6.84 [151]. The spectra of cadmium complex reveals high-field shifts due to aromatic proton in the  $\delta$  range 6.24-8.05 but the position of iminic HC=N remained relatively the same at  $\delta$  8.23. In addition, the CH<sub>2</sub> protons resonate at a frequency range  $\delta$  2.84-3.76. In both spectra, there is no evidence for the coordination of piperazine secondary amine N-H to the metal ion (Table 3.17, Fig. 3.59-3.61) (Appendix C).

<sup>1</sup>H NMR spectra of (E)-4-methoxy-2-((2-(piperazin-1-yl)ethylimino)methyl)phenol (LHM)

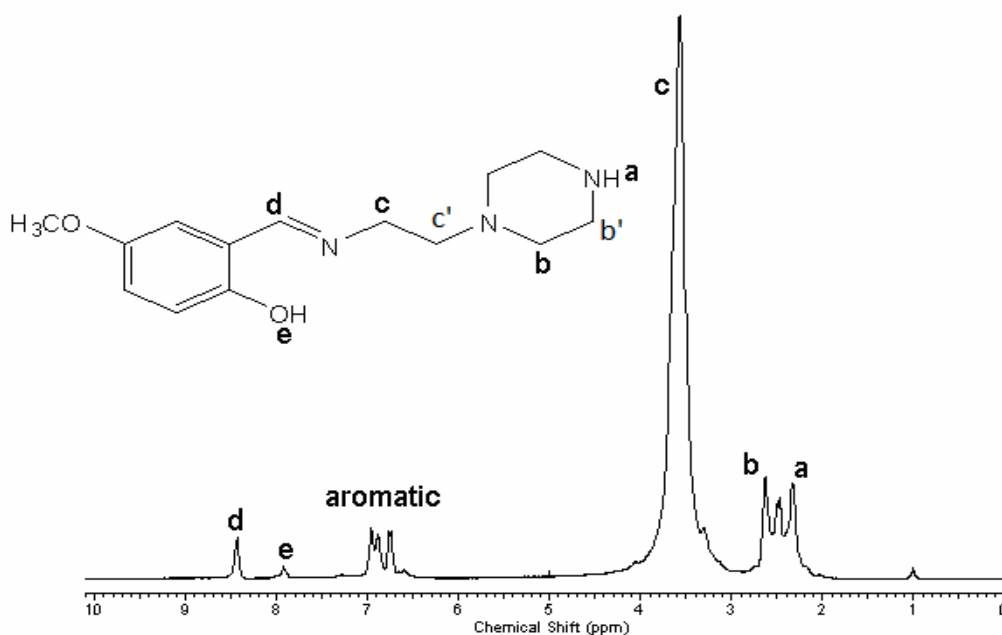


Figure 3.59 <sup>1</sup>H NMR spectra of LHM ligand.

3.3.8. <sup>1</sup>H NMR spectra of (E)-5-methoxy-2-((2-(piperazin-1-yl)ethylimino)methyl) phenol (HMS) and its Zn and Cd complexes.

Table 3.18 <sup>1</sup>H NMR spectral data for HMS and its complexes δ (ppm)

Compound	Ha	Hb	Hc	Hd	He	arH
HMS	2.36	2.53-2.89	2.73-3.04	8.16	10.91	7.32-7.85
[Zn(HMS)Cl <sub>2</sub> ]	2.01	2.79-3.05	3.17-3.57	8.08	-	6.01-7.42
[Cd(HMS)Cl <sub>2</sub> ]	2.00	2.51-2.87	3.39-3.52	8.14	-	6.02-7.50
[Cu(HMS)Cl <sub>2</sub> ]	Paramagnetic					

Akin to the previously described ligand, the <sup>1</sup>H NMR spectra of HMS ligand display a signal at δ 8.16 due to an imine HC=N (Hd). The phenolic O-H (He) appeared as broad peak at δ 10.91. Similar signals appeared at δ 10.31 and 12.26 in the spectra of LDH and DHS ligands respectively, which were presumably attributed to the phenolic OH proton. With this, it can be concluded that electron donating substituents on the phenolic ring provide similar shield effects to the phenolic proton (O-H) [152]. Furthermore, the spectra of zinc and cadmium complexes obtained from HMS ligand shows a down field at the position of iminic protons when compared with the spectra of the free ligand. This suggests de-shielding of the imine proton due to complexation with the metal ion through nitrogen [153]. The aromatic protons (arH) appeared at δ range 6.01-7.42 and δ 6.02-7.50 in the spectra of zinc and cadmium complexes respectively (Table 3.18, Fig. 3.62-3.64). This down field shift could be assigned to the contribution of piperazine tertiary amine nitrogen in coordination with the metal ion as confirmed by x-ray diffraction (Appendix C).

<sup>1</sup>H NMR spectra of (E)-4-methoxy-2-((2-(piperazin-1-yl)ethylimino)methyl)phenol (HMS)

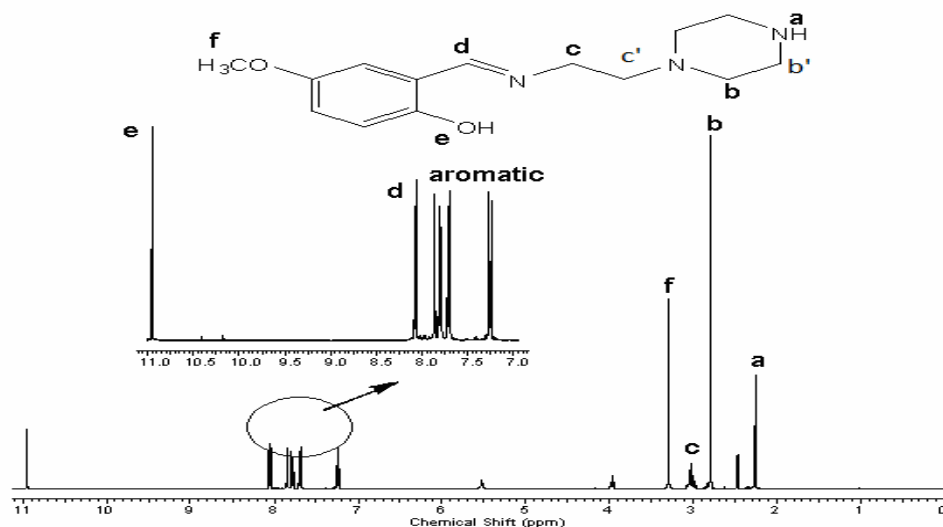


Figure 3.62 <sup>1</sup>H NMR spectra of HMS ligand.

3.3.9. <sup>1</sup>H NMR spectra of *E*-2-(1-(2-piperazin-1-yl)ethylimino)ethyl phenol (2HP) and its Zn and Cd complexes.

Table 3.19 <sup>1</sup>H NMR spectral data for 2HP and its complexes  $\delta$  (ppm)

Compound	Ha	Hb	Hc	Hd	He	arH
2HP	1.82	2.45-2.72	2.98-3.22	1.21	7.17	6.18-7.0
[Zn(2HP)Cl <sub>2</sub> ]	2.01	2.46-2.95	3.26-3.59	2.19	-	6.37-7.80
[Cd(2HP)Cl <sub>2</sub> ]	2.31	2.69-3.12	3.38-3.79	2.03	-	6.17-7.46
[Cu(2HP)Cl <sub>2</sub> ]	Paramagnetic					

The <sup>1</sup>H NMR spectrum of 2HP ligand exhibited a broad peak signal at  $\delta$  7.17 due to intermolecular hydrogen bonding of phenolic OH (He) [154]. The signal due to an imine HC=N (Hd) was observed shielded at very low field  $\delta$  1.21 by the methyl group, which is distinctive of ketone derived Schiff bases [155]. The aromatic protons showed their resonance signals at  $\delta$  range 6.18-7.0 while the signals of CH<sub>2</sub> (Hb, Hb', Hc and Hc') protons were observed at  $\delta$  range 2.45-3.79. The position of the imine HC=N- in zinc and cadmium complexes had expectedly shifted to  $\delta$  2.19 and  $\delta$  2.03 respectively. This is up-field when compared with the spectra of the ligand before coordination. Similar chemical

shifts appear in the position of aromatic protons at  $\delta$  range 6.37-7.80 in the spectra of zinc complex and at  $\delta$  range 6.17-7.46 in the spectra of cadmium complex. These high-frequency shifts of aromatic protons are noticeable in the spectra of the complexes of this ligand. This indicated the non-participation of piperazine tertiary nitrogen in coordination with the metal and that the central metal ion binds only to the imine nitrogen and phenolic oxygen [156]. The multiplet peak at  $\delta$  2.51 could be assigned to the solvent DMSO (Table 3.19, Fig. 3.65-67) (Appendix C).

<sup>1</sup>H NMR spectra of (E)-2-(1-(piperazin-1-yl)ethylimino)ethylphenol (2HP)

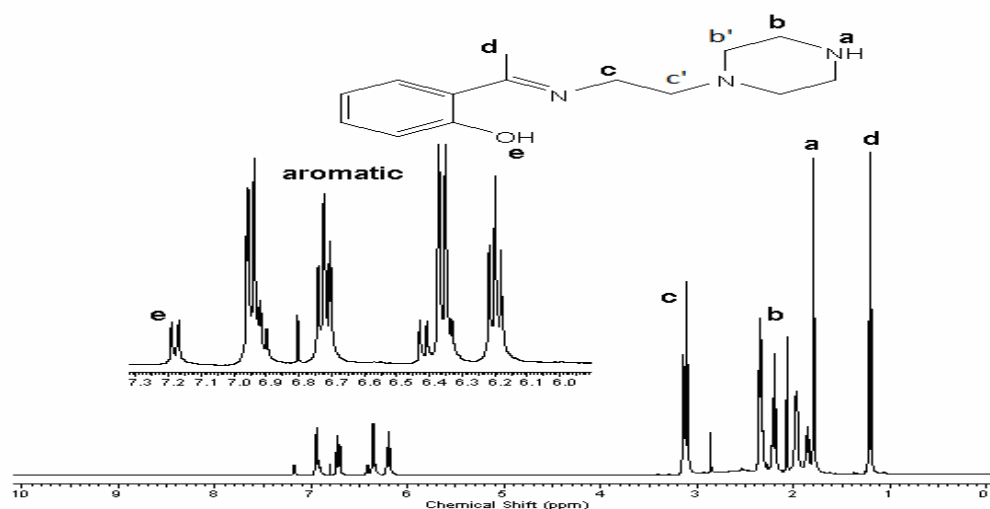


Figure 3.65 <sup>1</sup>H NMR spectra of 2HP ligand

3.3.10. <sup>1</sup>H NMR spectra of (E)-2-(1-(2-piperazin-1-yl)ethylimino)ethyl benzene-1,3-diol (DHP) and its Zn and Cd complexes.

Table 3.20 <sup>1</sup>H NMR spectral data for DHP and its complexes  $\delta$  (ppm)

Compound	Ha	Hb	Hc	Hd	He	arH
DHP	2.92	2.82-3.24	2.96-3.46	1.86	11.21	6.18-7.0
[Zn(DHP)Cl <sub>2</sub> ]	2.31	2.84-3.45	2.89-3.57	2.08	7.62	6.02-6.56
[Cd(DHP)Cl <sub>2</sub> ]	2.30	2.91-3.24	2.78-3.87	2.00	7.87	6.10-7.95
[Cu(DHP)Cl <sub>2</sub> ]	Paramagnetic					

The <sup>1</sup>H NMR spectra of the Schiff base DHP showed a broad peak at  $\delta$  11.21, this correspond to the hydroxyl groups (He) originating from the ligand structure. The imine

signal (Hd) was obscured at  $\delta$  1.86 as observed in the previous ligand (2HP). The resonance due to aromatic protons was observed at the frequency range  $\delta$  6.18-7.0 [147]. The piperazine N-H (Ha) appeared at  $\delta$  2.92 as broad peak, and the signals of CH<sub>2</sub> (Hb, Hb', Hc and Hc') protons were displayed at  $\delta$  range 2.82-3.87. As expected, the spectra of zinc and cadmium complexes showed singlet peaks at  $\delta$  2.08 and  $\delta$  2.0 respectively, which could be assigned to the imine shift due to complexation [157]. The broad signal of phenolic O-H appeared down field at  $\delta$  7.62 and  $\delta$  7.87 in the spectra of zinc and cadmium complexes respectively when compared with the spectra of the ligand. This is due to the deprotonation of phenolic O-H that is expected to reduce the electron density after complexation. The aromatic protons are observed at  $\delta$  range 6.02-6.56 in the spectra of zinc and at  $\delta$  range 6.10-7.95 in the cadmium complex spectra [150]. However, no clear spectral evidence for the involvement of piperazine tertiary nitrogen was noticed upon complexation with metal the atoms (Table 3.20, Fig. 3.68-70) (Appendix C). The copper complexes of all the Schiff bases synthesized did not exhibit clear spectrum. This can be due to the paramagnetic nature of copper ion which presumably interferes with the proton spectra.

<sup>1</sup>H NMR spectra of (E)-4-(1-(2-(piperazin-1-yl)ethylimino)ethyl)benzene-1,3-diol (DHP)

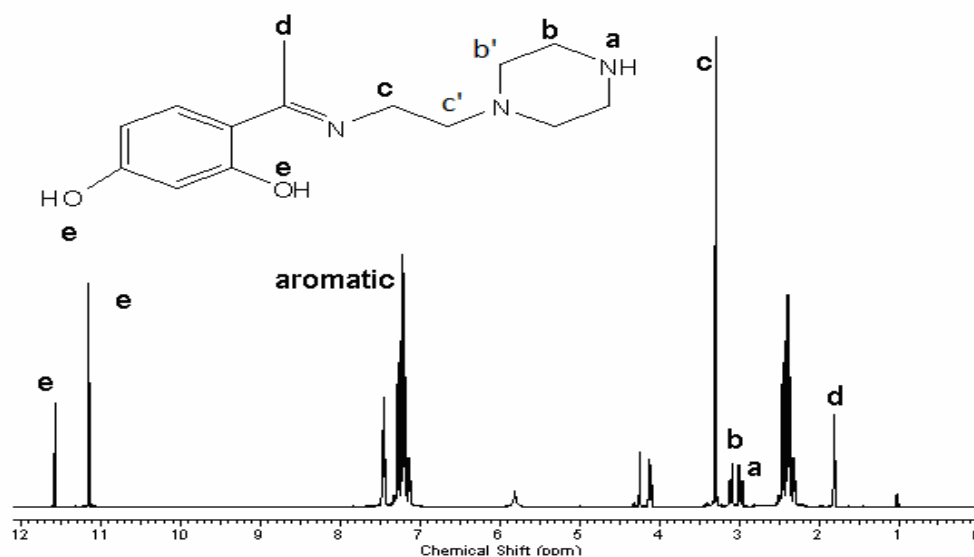


Figure 3.68 <sup>1</sup>H NMR spectra of DHP ligand.

### 3.4 <sup>13</sup>C NMR spectrums of the Schiff bases and their metal complexes

#### 3.4.1 <sup>13</sup>C NMR spectra of (E)-2-((2-(piperazin-1-yl)ethylimino)methyl)phenol (LSP) and its Zn and Cd complexes.

Table 3.21 <sup>13</sup>C NMR spectral data for LSP and its complexes  $\delta$  (ppm)

Compound	C1	C7	C8	C9	C10	C11	arC
LSP	161.4	163.3	58.8	46.2	32	19	118-132
[Zn(LSP)Cl <sub>2</sub> ]	-	170.2	50.7	44.6	32	28	114-138
[Cd(LSP)Cl <sub>2</sub> ]	-	174.4	54.4	44.8	38	28	121-139
[Cu(LSP)Cl <sub>2</sub> ]			Paramagnetic				

In the <sup>13</sup>C NMR spectra of the ligand LSP the signal that appeared at  $\delta$  163.3 could be attributed to imine C=N carbon (C7) while the signal at  $\delta$  161.4 can be assigned to phenolic C-OH (C1). The chemical shifts due to methylene CH<sub>2</sub> (C8, C9, C10 and C11) appeared at  $\delta$  range 20-58.8. The multiplet signal observed at  $\delta$  40 can be attributed to double resonance due to DMSO<sub>d6</sub>/CH<sub>2</sub> absorptions [158] whereby the peak at  $\delta$  59 can be attributed to impurities. In addition, the aromatic carbon atoms show resonance at  $\delta$  range 118-132. In the spectra of zinc complex of this ligand, new signal was observed at  $\delta$  170.2 due to double resonance absorptions by phenolate C-O (C1) and imine C=N (C7). This is anticipated due to the changes in the hybridization and the iso-electronic nature of the two carbon atoms [159]. Furthermore, these chemical shifts have indicated the coordination of both oxygen and nitrogen to the metal atom [160]. In the spectra of cadmium complex, similar shifts were noticed at  $\delta$  174.4 and so require same description. The signal due to aromatic carbons appeared at  $\delta$  range 114-138 in zinc and at  $\delta$  121-139 in cadmium complexes respectively. This chemical shift can be afforded to the delocalization of the phenolic ring electrons due to complexation [161] (Table 3.21, Figure 3.71-3.73) (Appendix D). The copper complex did not manifest clear spectra.

<sup>13</sup>C NMR spectra of (E)-2-((2-(piperazin-1-yl)ethylimino)methyl)phenol (LSP)

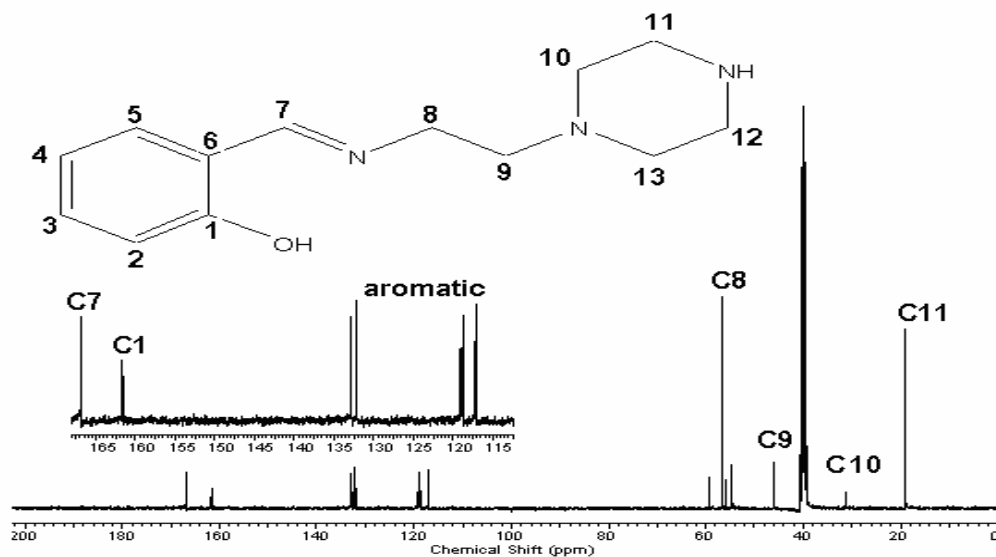


Figure 3.71 <sup>13</sup>C NMR spectra of LSP ligand.

3.4.2. <sup>13</sup>C NMR spectra of (E)-4-chloro-2-((2-(piperazin-1-yl)ethylimino)methyl) phenol (LCS) and its Zn and Cd complexes.

Table 3.22 <sup>13</sup>C NMR spectral data for LCS and its complexes  $\delta$  (ppm)

Compound	C1	C7	C8	C9	C10	C11	arC
LCS	162.8	166.5	58.6	46.4	20	19	117-133
[Zn(LCS)Cl <sub>2</sub> ]	150.3	175.6	58.2	46.1	36	31	116-136
[Cd(LCS)Cl <sub>2</sub> ]	169.4	173.4	60.8	50.2	42	38	104-134

The <sup>13</sup>C NMR spectrum of the ligand LCS displayed peaks at  $\delta$  166.5 that can be ascribed to phenolic carbon (C1). The imine carbon (C7) appeared at  $\delta$  162.8 and the signals at  $\delta$  range 20- 60.8 are attributable to methylene CH<sub>2</sub> (C8, C9, C10 and C11) [162]. The resonance at  $\delta$  43 and 44 in the spectra of zinc and at  $\delta$  134 in the spectra of cadmium can be due to impurities. The aromatic carbons were evidenced at  $\delta$  range 117-133. In the spectra of zinc and cadmium complexes of this ligand, the resonance observed at  $\delta$  150.3 and 169.4 can be assigned to phenolate (C1) respectively [163]. Signals at a high field of  $\delta$  175.6 in zinc and at  $\delta$  173.4 in cadmium spectra are attributed to the imine carbon absorption (C7). These signals appear at down field position in the spectra of the ligand

which signifies the involvement of imine nitrogen atom in complexation [164]. The position of methylene CH<sub>2</sub> carbon atoms (C8, C9, C10 and C11) changes slightly in the spectra of zinc and cadmium complexes when compared with the spectra of the free ligand which could be due to geometrical changes that occurs in the ligand structure. The aromatic carbons (arC) appeared at  $\delta$  range 116-136 for zinc and at  $\delta$  range 104-134 for cadmium complex, which also supports the structural changes expected after complexation [165] (Table 3.22, Fig. 3.74-3.76). Paramagnetic was obtained for the copper complex (Appendix D).

<sup>13</sup>C NMR spectra of (E)-4-chloro-2-((2-(piperazin-1-yl)ethylimino)methyl)phenol (LCS)

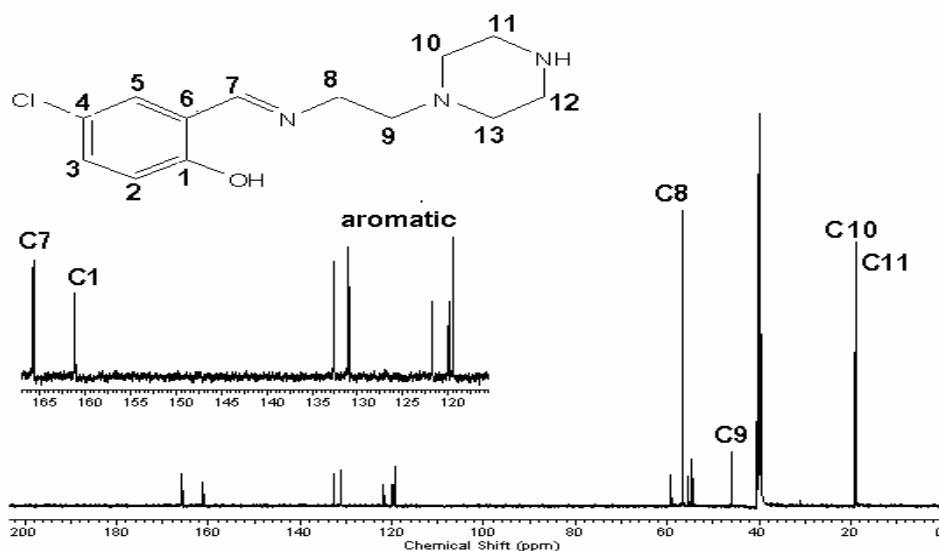


Figure 3.74 <sup>13</sup>C NMR spectra of LCS ligand.

### 3.4.3 <sup>13</sup>C NMR spectra of (E)-4-bromo-2-((2-(piperazin-1-yl)ethylimino)methyl) phenol (LBS) and its Zn and Cd complexes.

Table 3.23 <sup>13</sup>C NMR spectral data for LBS and its complexes  $\delta$  (ppm)

Compound	C1	C7	C8	C9	C10	C11	arC
LBS	160.2	165.2	72.2	32.4	31	24	117-133
[Zn(LBS)Cl <sub>2</sub> ]	136.1	172.8	56.4	44.1	31	20	105-137
[Cd(LBS)Cl <sub>2</sub> ]	137.5	170.5	60.1	51.2	32	19	101-138

The spectral data demonstrated by the ligand LBS in  $^{13}\text{C}$  NMR showed a signal at  $\delta$  160.2 due to phenolic carbon atom. This signal appeared down field at  $\delta$  136.1 and at  $\delta$  137.5 in the spectra of its zinc and cadmium complexes respectively, which indicates deprotonation of phenolic proton and the coordination of phenolic oxygen to the metal ion (C1). The signal observed at  $\delta$  165.2 in the ligand spectra can be ascribed to the imine  $\text{C}=\text{N}$  (C7). This signal has shifted to  $\delta$  172 in the spectra of zinc complex and to  $\delta$  170.5 in the cadmium complex spectra, thus confirming the participation of imine nitrogen in the complexation [166]. The geometrical adjustments observed due to shifts in the position of aromatic protons (arC) appeared at  $\delta$  range 105-137 and at  $\delta$  range 101-138 in the spectra of zinc and cadmium complexes respectively. This is evident when compared with the  $\delta$  range 117-133 noticed in the ligand spectra and the changes observed in the position of methylene  $\text{CH}_2$  (C8, C9, C10 and C11) at the  $\delta$  range 20-72.2 in the spectra of the ligand and its complexes of zinc and cadmium [167]. The peaks that appeared due to impurities were observed at  $\delta$  124 in the ligand spectra and at  $\delta$  104 and 100 in the spectra of zinc and cadmium respectively. (Table 3.23, Figure3.77-3.79) (Appendix D).

$^{13}\text{C}$  NMR spectra of (E)-4-bromo-2-((2-(piperazin-1-yl)ethylimino)methyl)phenol (LBS)

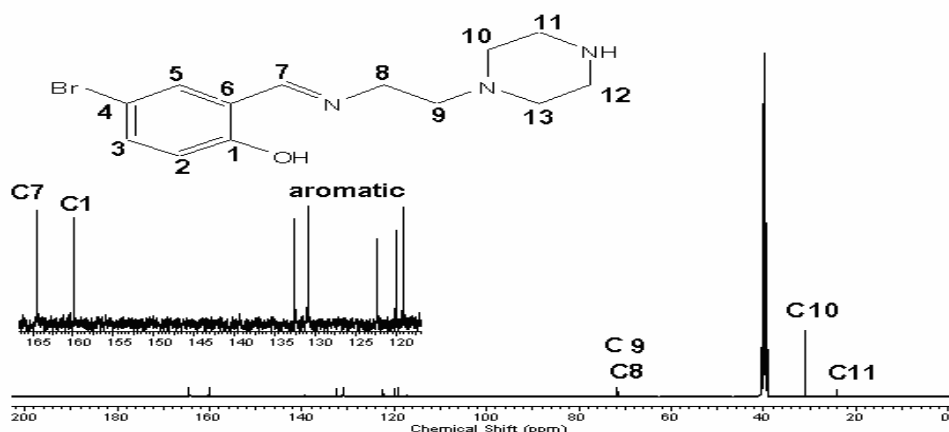


Fig. 3.77  $^{13}\text{C}$  NMR spectra of LBS ligand.

3.4.4. <sup>13</sup>C NMR spectra of (*E*)-4nitro-2-((2-(piperazin-1-yl)ethylimino)methyl) phenol (LNS) and its Zn and Cd complexes.

Table 3.24 <sup>13</sup>C NMR spectral data for LNS and its complexes  $\delta$  (ppm)

Compound	C1	C7	C8	C9	C10	C11	arC
LNS	165.4	180.2	53	47	58	19	114-134
[Zn(LNS)Cl <sub>2</sub> ]	133.8	170.6	50	42	32	19	117-135
[Cd(LNS)Cl <sub>2</sub> ]	168.2	177.8	59	54	50	32	119-136

The <sup>13</sup>C NMR spectra of the ligand LNS shows a signal at  $\delta$  165.4 that could be assigned to the phenolic carbon C-OH (C1) vibrations. The signal at  $\delta$  180.2 can be assigned to iminic C=N carbon (C7) whereby the aromatic carbons (arC) appeared at  $\delta$  range 124-134. Other signals observed at the  $\delta$  range 19-59 could be attributed to methylene CH<sub>2</sub> (C8, C9, C10 and C11) due to conformational changes observed on complexation [168]. However, the peak observed at  $\delta$  114 in the ligand spectra,  $\delta$  56 in the spectra of zinc and  $\delta$  42 in the spectra of cadmium complexes presumably arises due to impurities. The position of imine signal in the spectra of zinc and cadmium complexes of this ligand shifted to an up-field band at  $\delta$  170.6 and  $\delta$  177.8 respectively, which could be due to complexation [169]. The phenolate carbon appeared at  $\delta$  133.8 in spectra of zinc and at  $\delta$  168.2 in the spectra of cadmium complexes. The signal due to aromatic carbon showed resonance at  $\delta$  range 117-135 and  $\delta$  119-136 in the spectra of zinc and cadmium complexes respectively (Table 3.24, Fig. 3.80-3.82). The slight resonance shifts of methylene groups in the spectra of the complexes when compared to that of the ligand has suggested a long bond length between the tertiary nitrogen of piperazine and the central metal ion. This is confirmed by x-ray structural elucidation (Appendix D).

<sup>13</sup>C NMR spectra of (E)-4-nitro-2-((2-(piperazin-1-yl)ethylimino)methyl)phenol (LNS)

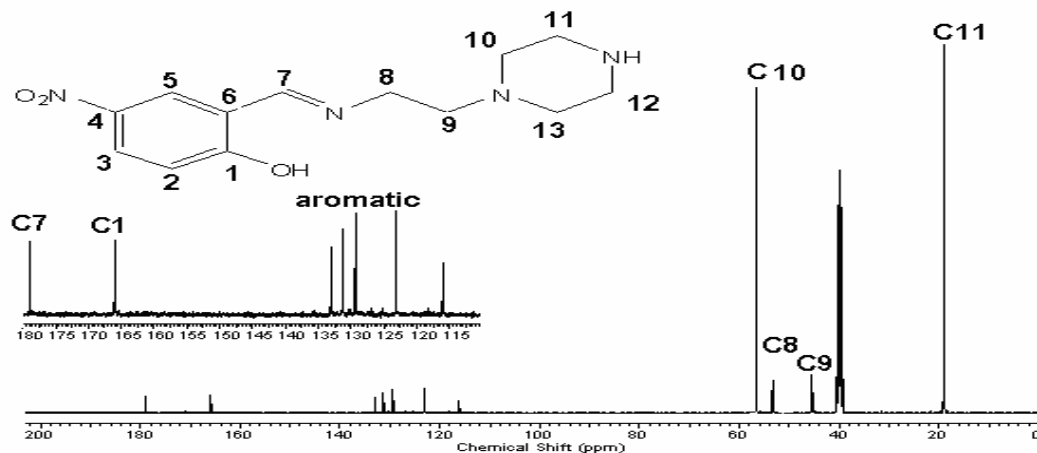


Figure 3.80 <sup>13</sup>C NMR spectra of LNS ligand.

3.4.5. <sup>13</sup>C NMR spectra of (E)-2-((2-(piperazin-1-yl)ethylimino)methyl)benzene-1,4-diol (LDH) and its Zn and Cd complexes.

Table 3.25 <sup>13</sup>C NMR spectral data for LDH and its complexes  $\delta$  (ppm)

Compound	C1	C7	C8	C9	C10	C11	arC
LDH	155.2	167.3	59	54	44	32	118-149
[Zn(LDH)Cl <sub>2</sub> ]	134.6	172.3	58	50	42	31	124-134
[Cd(LDH)Cl <sub>2</sub> ]	136.5	170.4	59	54	52	42	118-137

The <sup>13</sup>C NMR spectra of the ligand LDH demonstrated a chemical shift at  $\delta$  155.2 that was attributed to phenolic carbon (C1). Similar signals were observed at the down field frequencies of  $\delta$  134.6 and  $\delta$  136.5 in the spectra of zinc and cadmium complexes of this ligand respectively. This indicated the formation of phenolate bond due to complexation. In addition, the imine signal that appeared at  $\delta$  167.3 in the ligand spectra has also shifted to a new frequency of  $\delta$  172.3 and  $\delta$  170.4 in zinc and cadmium complexes respectively. This is presumed to be caused by the de-shielding of imine C=N carbon (C7) due to chelation [170]. The shifts of aromatic carbon (arC) atoms from  $\delta$  range 118-149 in the ligand to the  $\delta$  range of 124-134 in zinc complex and  $\delta$  range of 118-137 in the cadmium complex

spectra is evident due chelate formation. The slight resonance shifts noticed in the methylene CH<sub>2</sub> carbons (C8, C9, C10 and C11) from  $\delta$  range 32-59 in the ligand to  $\delta$  range 31-58 in zinc complex spectra and  $\delta$  range 42-59 in the spectra of the cadmium complex [171] (Table 3.25, Fig. 3.83-3.85) indicated the non-involvement of piperazine nitrogen atoms in the coordination with the metal ion. This phenomenon was further confirmed by the x-ray structure of zinc complex (Appendix D).

<sup>13</sup>C NMR spectra of (E)-2-((2-(piperazin-1-yl)ethylimino)methyl)benzene-1,4-diol (LDH)

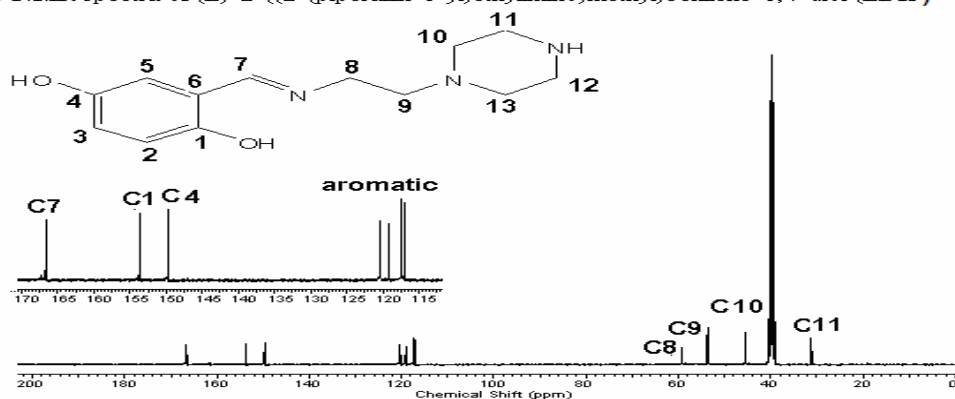


Figure 3.83 <sup>13</sup>C NMR spectra of LDH ligand.

3.4.6. <sup>13</sup>C NMR spectra of (E)-2-((2-(piperazin-1-yl)ethylimino)methyl)benzene-1,3-diol (DHS) and its Zn and Cd complexes.

Table 3.26 <sup>13</sup>C NMR spectral data for DHS and its complexes,  $\delta$  (ppm)

Compound	C1	C7	C8	C9	C10	C11	arC
DHS	157.1	166.4	60	58	50	46	120-148
[Zn(DHS)Cl <sub>2</sub> ]	165.4	175.3	58	50	44	34	104-138
[Cd(DHS)Cl <sub>2</sub> ]	162.2	168.4	60	52	44	19	103-158

Similar to the <sup>13</sup>C NMR spectra of LDH, the ligand DHS showed a resonance peak at  $\delta$  157, which corresponds to the signal of phenolic carbon (C1), this signal appeared at a bit lower frequency of  $\delta$  155.2 in the spectra of LDH, which indicates comparable influences of their ring substituents on the ligand structure [172]. Moreover, the spectra of zinc and cadmium

complexes of this ligand manifested chemical shifts at  $\delta$  165.4 and  $\delta$  162.2 respectively, which can be related to the shift of the band region (C1) observed in the ligand spectra. The signal due to imine C=N (C7) appeared at  $\delta$  166.4 in the spectra of DHS; this is also comparable with the band at  $\delta$  167.3 found in the spectra of LDH. Furthermore, the signal (C7) shifted to  $\delta$  175 in zinc complex of DHS, which is similar to the shift noticed in the spectra of zinc derived from LDH ligand. This suggests structural analogy between the two ligands as expected. However, the cadmium complex of DHS ligand showed  $\delta$  at 168.4 that can also be related with the up-field shifts noticeable in the complexes of the two structurally corresponding ligands [173]. The methylene carbon atoms C8, C9, C10 and C11 were observed at the frequency range  $\delta$  19-60 in the spectra of the ligand (DHS) and its zinc and cadmium complexes. (Table 3.26, Fig. 3.86-3.88) (Appendix D).

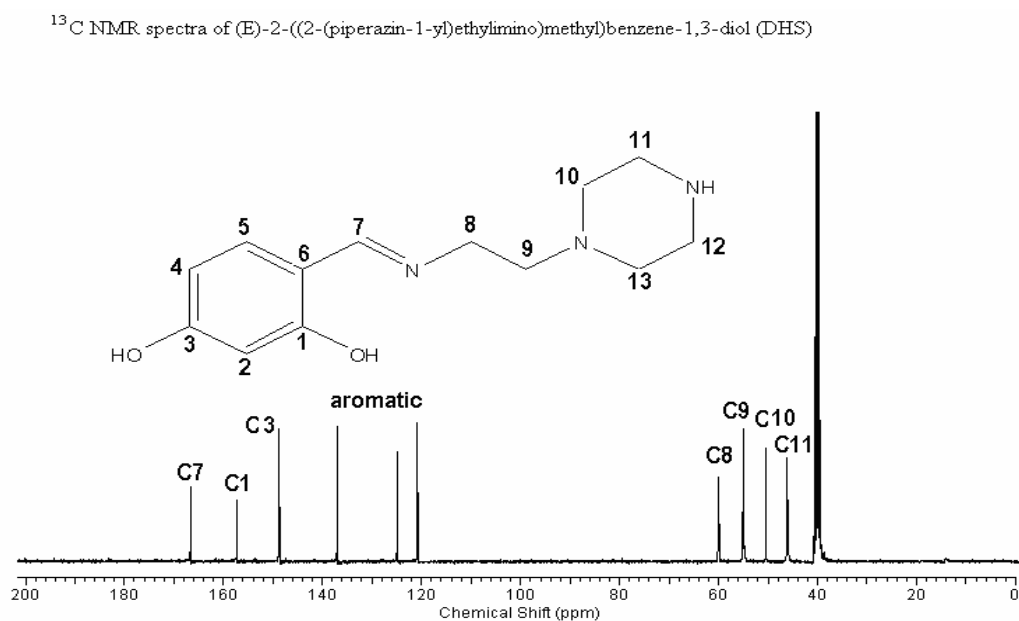


Figure 3.86 <sup>13</sup>C NMR spectra of DHS ligand.

3.4.7. <sup>13</sup>C NMR spectra of (*E*)-4-methoxy-2-((2-(piperazin-1-yl)ethylimino)methyl) phenol (LHM) and its Zn and Cd complexes.

Table 3.27 <sup>13</sup>C NMR spectral data for LHM and its complexes,  $\delta$  (ppm)

Compound	C1	C7	C8	C9	C10	C11	arC
LHM	163.4	167.2	60	58	55	45	115-155
[Zn(LHM)Cl <sub>2</sub> ]	150.6	171.3	67	65	45	19	117-147
[Cd(LHM)Cl <sub>2</sub> ]	142.3	154.5	65	59	51	32	109-121

The <sup>13</sup>C NMR spectra of the ligand LHM displayed a band shift at  $\delta$  163.4, which can be associated to phenolic carbon (C1) [173]. This signal shifts down field to  $\delta$  150.6 and  $\delta$  142.3 in the spectra of zinc and cadmium complexes respectively due to metal-phenolate coordination [174]. The imine carbon (C7) in the ligand spectra appears at  $\delta$  167.2. The signals that appeared at  $\delta$  range 45-60 in the ligand spectra can be associated to methylene CH<sub>2</sub> of C8, C9, C10 and C11) respectively. The signals due to the aromatic carbons (arC) were observed at  $\delta$  range 115-155 in the ligand spectra. However, the spectral data obtained from zinc complex of this ligand show an up-field shift in the position of imine carbon to  $\delta$  171.3 while the cadmium complex showed a down field shift to 154.5 when compared to the position of this carbon atom (C7) in the ligand spectra. This indicates the geometrical variation between the two complexes derived from the same ligand. The down field shift of aromatic carbons to  $\delta$  range 117-147 in zinc and to  $\delta$  109-121 in cadmium complex spectra further proves the expected changes in the bond length and bond order between the two geometrical structures of the complexes [175]. Furthermore, the shift of CH<sub>2</sub> signals to  $\delta$  range 19-67 in zinc complex and at  $\delta$  range 32-65 in cadmium complex provides supportive evidence on the presumed structural adjustments [175]. Resonance peaks at  $\delta$  152 and 156 are attributable to the impurities (Table 3.27, Fig. 3.89-3.91) (Appendix D).

$^{13}\text{C}$  NMR spectra of (E)-4-methoxy-2-((2-(piperazin-1-yl)ethylimino)methyl)phenol (LHM)

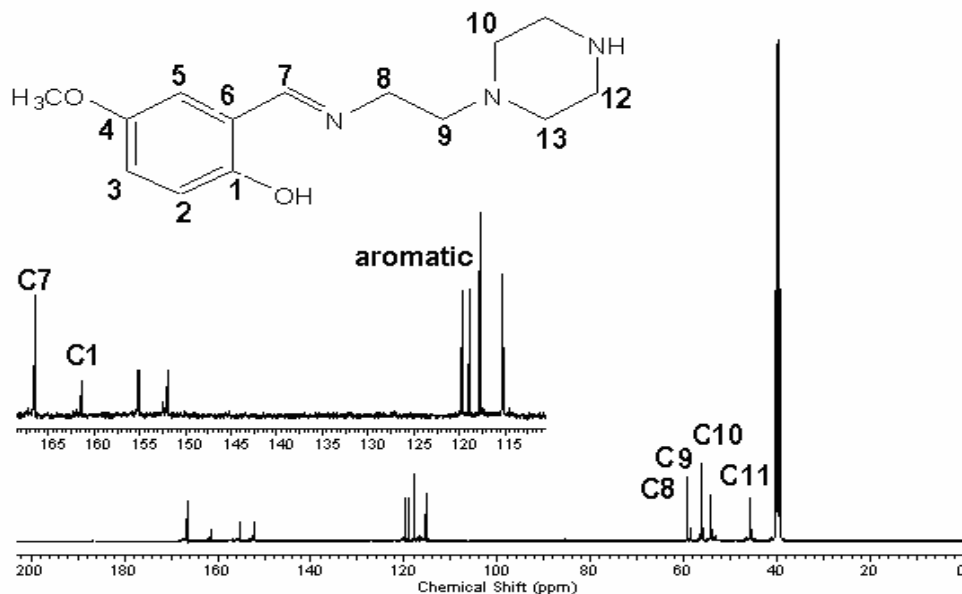


Figure 3.89  $^{13}\text{C}$  NMR spectra of LHM ligand.

3.4.8.  $^{13}\text{C}$  NMR spectra of (E)-5-methoxy-2-((2-(piperazin-1-yl)ethylimino)methyl) phenol (HMS) and its Zn and Cd complexes.

Table 3.28  $^{13}\text{C}$  NMR spectral data for HMS and its complexes,  $\delta$  (ppm)

Compound	C1	C7	C8	C9	C10	C11	arC
HMS	147.6	158.2	60	50	45	28	116-139
$[\text{Zn}(\text{HMS})\text{Cl}_2]$	165.3	184.2	56	48	32	19	104-165
$[\text{Cd}(\text{HMS})\text{Cl}_2]$	164.4	193.2	54	49	31	19	102-164

Unlike the spectra of ligand LHM, the  $^{13}\text{C}$  NMR spectra of HMS ligand show signals at  $\delta$  147.6 and  $\delta$  158.2 that can be interrelated to phenolic C-OH (C1) and imine C=N (C7) carbons respectively. These signals appeared at high field frequencies of  $\delta$  163.4 and  $\delta$  167.2 in the spectra of its analogue ligand LHM, which indicates the influence of substituents position on the aromatic ring [176]. The methylene  $\text{CH}_2$  at C8, C9, C10 and C11 were observed at  $\delta$  range 28-60 in the ligand spectra. These carbon atoms resonate at  $\delta$  range 19-32 in the spectra of its zinc and cadmium complex which indicate similar conformational changes in those complexes. Moreover, the aromatic carbons appeared at  $\delta$

range 116-139 in the spectra of the ligand. This resonance signal shifted to a high-field frequency of  $\delta$  165.3 and  $\delta$  164.4 in the zinc and cadmium complexes respectively and can be assigned to phenolate coordination [177]. The signal due to metal-imine bonding (C7) also appears at a high field  $\delta$  of 184.2 and  $\delta$  193.2 in the spectra of zinc and cadmium complexes respectively when compared to the chemical shift of 158.2 ppm in the spectra of the free ligand. The signals noticeable at  $\delta$  42 and 53 in the spectra of cadmium complex are attributable to the impurities (Table 28, Fig. 3.92-3.94) (Appendix D).

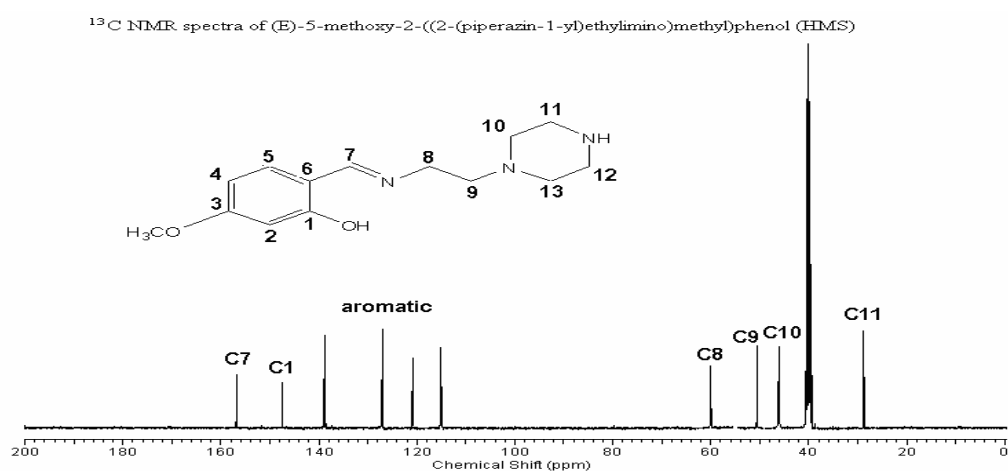


Figure. 3.92 <sup>13</sup>C NMR spectra of HMS ligand.

### 3.4.9. <sup>13</sup>C NMR spectra of (E)-2-(1-(2-(piperazin-1-yl)ethylimino)ethyl)phenol (2HP) and its Zn and Cd complexes.

Table 3.29 <sup>13</sup>C NMR spectral data for 2HP and its complexes  $\delta$  (ppm)

Compound	C1	C7	C8	C9	C10	C11	C12	arC
2HP	164.6	173.2	54	60	58	48	20	116-133
[Zn(2HP)Cl <sub>2</sub> ]	128.4	139.5	46	59	55	19	17	114-132
[Cd(2HP)Cl <sub>2</sub> ]	137.4	158.3	49	61	57	32	19	128-136

The <sup>13</sup>C NMR spectra of the ligand 2HP illustrated a signal due to the phenolic carbon at  $\delta$  164.6 (C1). The resonance band due to imine carbon appears at  $\delta$  173.2 (C7) whereby the aromatic carbons (arC) and the methylene carbon atoms (C9, C10, C11 and C12) were

observed at  $\delta$  range 116-133 and  $\delta$  range 20-60 respectively in the spectra of the ligand. The band signal that appeared at  $\delta$  54 can be ascribed to the methyl group of the keto-imine.  $\text{CH}_3\text{-C=N}$  (C8) [178]. The spectra of zinc complex obtained from 2HP ligand exhibited a low field signal shift at  $\delta$  128.4 and  $\delta$  139.5 that could be attributed to metal-phenolate (C1) and metal-nitrogen coordination respectively. The resonance shifts noticeable in the spectra of zinc at  $\delta$  46 could be ascribed to the methyl group of the imine whereby the methylene  $\text{CH}_2$  carbon atoms (C9, C10, C11 and C12) appeared at  $\delta$  range of 17-59. In the spectra of cadmium complex, these peaks appeared at  $\delta$  49 and at  $\delta$  range 19-61 attributable to iminic methyl group and the methylene carbon atoms of the aminoethylpiperazine. This presumably indicates the involvement of phenolic oxygen, iminic nitrogen and the tertiary nitrogen atom of the piperazine moiety in coordination with the metal atom. The aromatic carbon signals appeared at a low frequency of  $\delta$  range 114-132 in the spectra of zinc and at a bit high frequency of  $\delta$  range 128-136 in the spectra of cadmium complex. (Table 29, Fig. 3.95-3.97) (Appendix D). This can be attributed to the changes in the bond length [179] probably between the tertiary nitrogen of piperazine moiety and the central metal ions upon complex formation. The peak at  $\delta$  34 can be due to impurities.

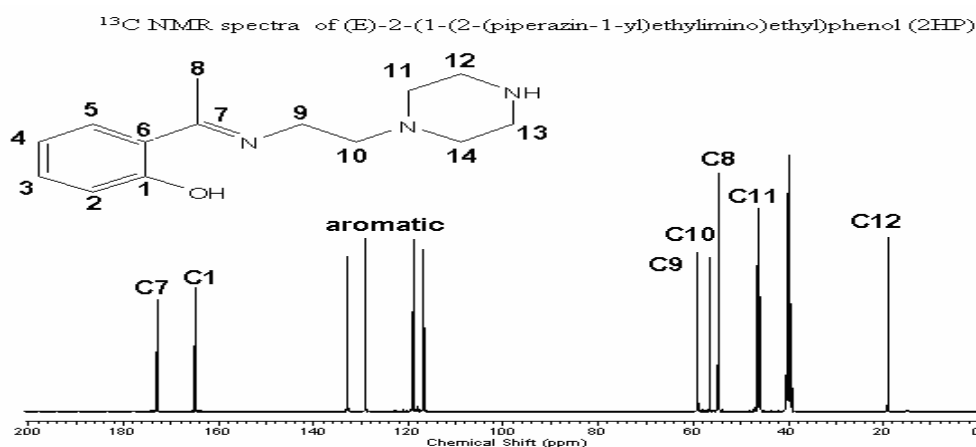


Figure 3.95 <sup>13</sup>C NMR spectra of 2HP ligand.

3.4.10. <sup>13</sup>C NMR spectra of (*E*)-4-(1-(2-(piperazin-1-yl)ethylimino)ethyl)benzene-1,3-diol (DHP) and its Zn and Cd complexes.

Table 3.30 <sup>13</sup>C NMR spectral data for DHP and its complexes,  $\delta$  (ppm)

Compound	C1	C7	C8	C9	C10	C11	C12	arC
DHP	162.1	170.9	56	66	64	32	19	126-138
[Zn(DHP)Cl <sub>2</sub> ]	124.2	176.2	56	54	46	31	18	116-126
[Cd(DHP)Cl <sub>2</sub> ]	138.2	144.6	49	57	52	32	19	133-144

The <sup>13</sup>C NMR spectral data for the ligand DHP showed chemical shifts at  $\delta$  162.1 which could be ascribed to the phenolic carbon (C1). This signal became shielded after complexation and appears at low field frequencies  $\delta$  124.2 and at  $\delta$  138.2 in the spectra of its zinc and cadmium complexes. The ligand spectra also showed the resonance of imine carbon (C7) at  $\delta$  170.9 whereby the methyl group of the keto-imine (C8) [180] appeared  $\delta$  56 and methylene CH<sub>2</sub> (C9, C10, C11 and C12) were noticed  $\delta$  range 19-66. The band signal observed due to the double resonance between methylene CH<sub>2</sub> and the solvent DMSO-d<sub>6</sub> appear at a similar position ( $\delta$  40) with the previously discussed complexes. In the spectra of zinc complex, a high-field shift was noticed at  $\delta$  176.2 that could be attributed to zinc-nitrogen (Zn-N) bonding. This signal shifted in the cadmium spectra to a down field frequency of  $\delta$  144.6 as a result of cadmium-nitrogen (Cd-N) coordination probably due to change in size of the coordinating metal [181]. However, the methyl group of the imine and the methylene carbon atoms also gives new signals in the spectra of zinc ( $\delta$  18-56) and cadmium ( $\delta$  19-57) complexes (Table 30). This could be due to the decrease in the electron density upon complexation. This is supported by the shifts of the aromatic carbons (arC) to a  $\delta$  range 116-126 and  $\delta$  range 126-138 in the spectra of zinc and cadmium complexes respectively. The involvement of piperazine nitrogen in complexation with the

central atoms remained is not evident in both spectra (Table 3.30, Fig.3.98-3.100). (Appendix D).

<sup>13</sup>C NMR spectra of (E)-4-(1-(2-(piperazin-1-yl)ethylimino)ethyl)benzene-1,3-diol (DHP)

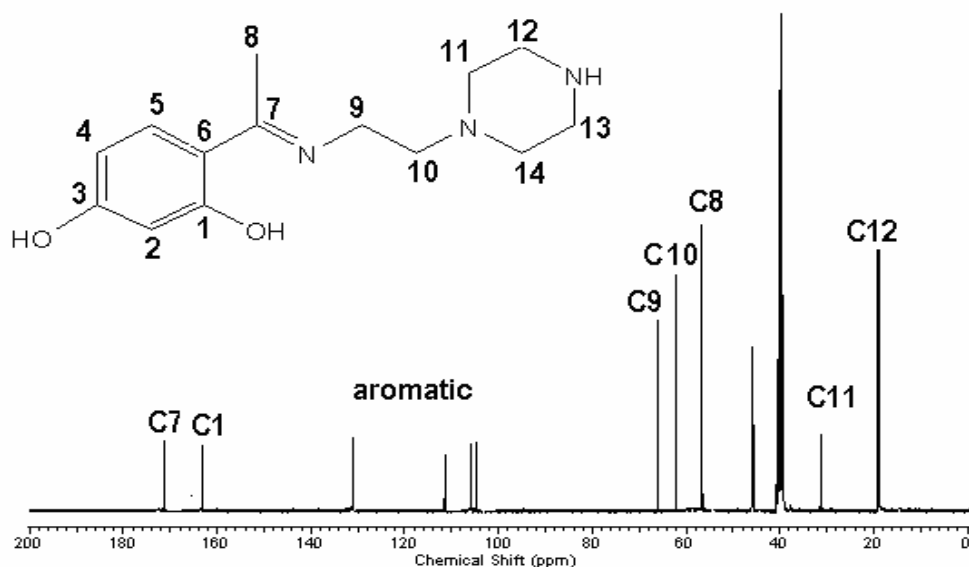


Figure 3.98 <sup>13</sup>C NMR spectra of DHP ligand.

### 3.5 UV-visible spectra of the Schiff bases and their complexes

The electronic spectra of the ligands and their complexes of Cu, Zn and Cd in DMSO were recorded at room temperature in the UV range 200-900 nm and their absorption band maxima together with the tentative band assignments are allocated and listed in Table 31-40 and the spectra shown in the Figure 101-140.

#### 3.5.1 UV-visible spectra of the ligand LSP and its Cu, Zn and Cd complexes

The electronic spectra of the ligand LSP and its complexes of copper, zinc and cadmium with their absorption band assignments are shown in Table 31 and Figure 101-104

Table 3.31 UV-visible spectra of LSP and its Cu, Zn and Cd complexes:

Compounds	Concentration	Wavelengths	Remark
LSP	$9.87 \times 10^{-4}$	406	$n-\pi^*$
		319	$\pi-\pi^*$
		302	CT
		243	$\pi-\pi^*$
Cu(LSP)	$1.09 \times 10^{-3}$	674	$d-d$
		408	$n-\pi^*$
		367	LMCT
		204	$\pi-\pi^*$
Zn(LSP)	$1.08 \times 10^{-3}$	413	$n-\pi^*$
		338	LMCT
		266	$\pi-\pi^*$
		207	$\pi-\pi^*$
Cd(LSP)	$9.6 \times 10^{-4}$	407	$n-\pi^*$
		341	LMCT
		260	$\pi-\pi^*$
		222	$\pi-\pi^*$

The electronic spectral data of the ligand LSP and its complexes of Cu, Zn and Cd in DMSO were recorded at room temperature. The spectra of the ligand comprised four absorption band maxima. The medium intensity band at 406 nm can be ascribed to  $n-\pi^*$  transition [45,182]. This band has noticeably shifted to 408 nm, 413 nm and 407 nm in the spectra of copper, zinc and cadmium complexes of this ligand due to complexation. The band at 319 nm could be assigned to  $\pi-\pi^*$  electronic transitions in the aromatic ring. The intensity of this band has increased due to imine chromophore; which led to the appearance of a band at 302 nm as a result of charge transfer (CT) in the imine region [25,183]. The band at 243 nm can be related with  $\pi-\pi^*$  electronic transitions of a piperazine moiety. The absorption maxima displayed at 367 nm, 338 nm and 341 nm in the spectra of Cu, Zn and Cd complexes respectively, can be attributed to the ligand-metal charge transfer (LMCT) bands originating from 302 nm in the ligand spectra which indicates chelate formation. However, the spectra of the complexes show high-intensity bands at low wavelengths (Table 31) which supports the possible coordination of the metal ions with the ligand LSP

[184]. To compare the variations in the absorption maxima among the complexes of LSP ligand, more concentrated solutions were used. This led to the appearance of a band at 674 nm in the spectra of copper complex, which is characteristic of ligand field (*d-d*) transition [25,185]. The spectra of zinc and cadmium complexes did not show this kind of transition even at high concentrations. This is expected due to the complete *d*-orbital electronic configuration of the two metal atoms (Table 3.31, Fig. 3.101-3.104) (Appendix E).

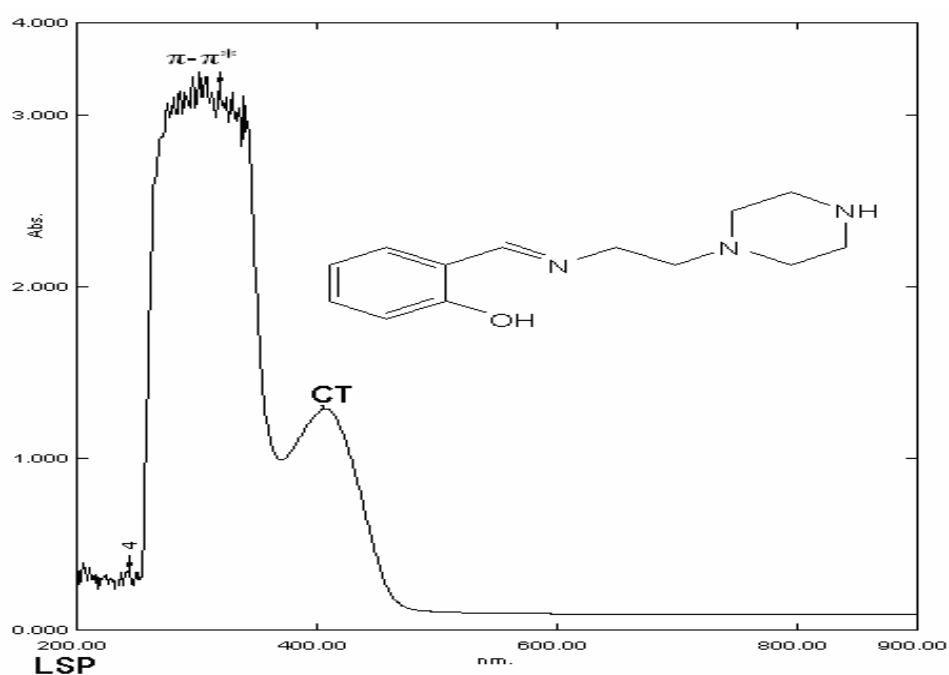


Figure 3.101 UV-visible spectra of LSP ligand

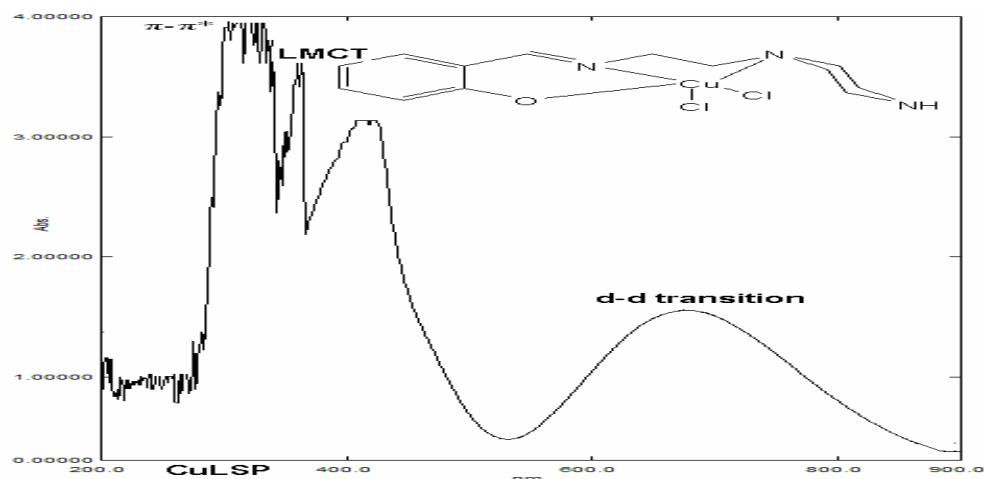


Figure 3.102 UV-visible spectra of  $[\text{Cu}(\text{LSP})\text{Cl}_2]$  complex.

### 3.5.2 UV-visible spectra of the ligand LCS and its Cu, Zn and Cd complexes

The electronic spectra of the ligand LCS and its complexes of copper, zinc and cadmium with their absorption band assignments are shown in Table 32 and Figures 105-108.

Table 3.32 UV-visible spectra of LCS and its Cu, Zn and Cd complexes:

Compounds	Concentrations	Wavelengths	Remark
LCS	$1.12 \times 10^{-3}$	416	$n-\pi^*$
		371	CT
		264	$\pi-\pi^*$
		223	$\pi-\pi^*$
Cu(LCS)	$9.97 \times 10^{-4}$	683	$d-d$
		431	$n-\pi^*$
		340	LMCT
		253	$\pi-\pi^*$
Zn(LCS)	$9.93 \times 10^{-4}$	421	$n-\pi^*$
		311	LMCT
		276	$\pi-\pi^*$
		254	$\pi-\pi^*$
Cd(LCS)	$8.86 \times 10^{-4}$	400	$n-\pi^*$
		328	LMCT
		280	$\pi-\pi^*$
		226	$\pi-\pi^*$

The UV spectrum of the ligand LCS showed four broad band maxima at 416 nm and 371 nm due to  $n-\pi^*$  and charge transfer (CT) electronic transitions. Other absorption bands

appeared at lower wavelengths of 264 nm and 223 nm which can be ascribed to  $\pi-\pi^*$  electronic transitions in the phenolic ring and piperazine moiety respectively [186]. In the spectra of Cu, Zn and Cd complexes, this absorption maxima shifts appreciably to new wavelengths 431 nm, 421 nm and 400 nm respectively. This high absorption can be due to the effect of chlorine substituents on the phenolic ring. Similar absorption is observed in the band region of 416 nm in the spectra of the free ligand. The bathochromic shifts of the bands at 340 nm in copper, 311 nm in zinc and at 328 nm in cadmium complexes could be attributed to the ligand-metal charge transfer (LMCT). This absorption has also originated from the charge transfer region at 371 nm in the ligand spectra. The absorption band at 683 nm in the spectra of copper complex is attributed to the ligand field  $d-d$  transition [147,187]. This absorption is absent in the spectra of Zn and Cd complexes. Moreover, the bands at low wavelength 253 nm noticed in the spectra of copper complex can be associated with ligand  $\pi-\pi^*$  transition (Table 3.32, Fig. 105-108) (Appendix E).

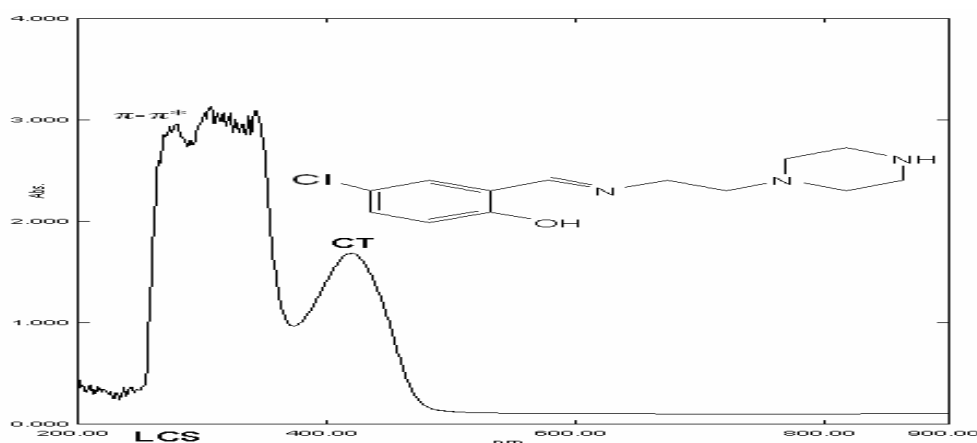


Figure 3.105 UV-visible spectra of LCS ligand

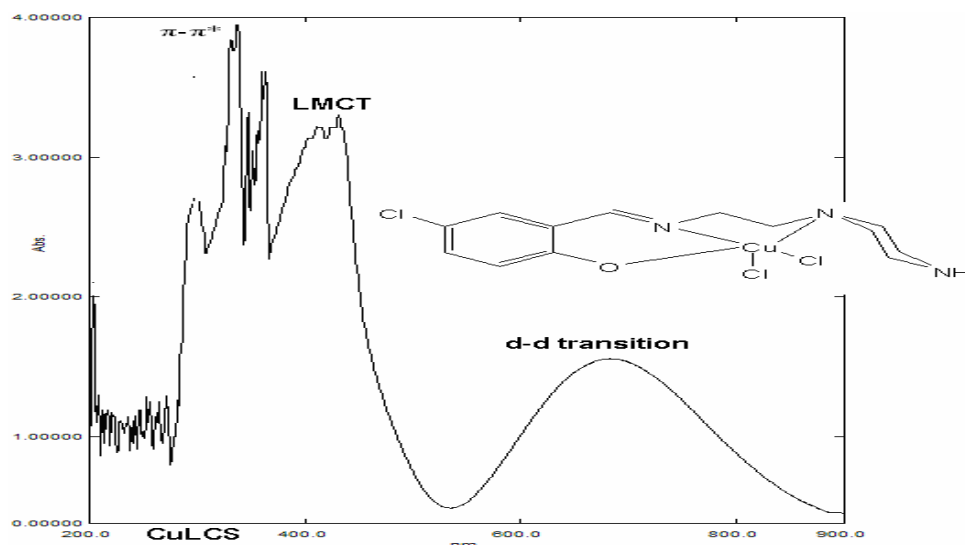


Figure 3.106 UV-visible spectra of  $[\text{Cu}(\text{LCS})\text{Cl}_2]$  complex.

### 3.5.3 UV-visible spectra of the ligand LBS and its Cu, Zn and Cd complexes

The electronic spectra of the ligand LBS and its complexes of copper, zinc and cadmium with their absorption band assignments are shown in Table 33 and Figures 3.109-3.112

Table 3.33 UV-visible spectra of LBS and its Cu, Zn and Cd complexes:

Compounds	Concentration	Wavelengths	Remark
LBS	$9.6 \times 10^{-4}$	416	$n-\pi^*$
		344	CT
		326	$\pi-\pi^*$
		248	$\pi-\pi^*$
Cu(LBS)	$8.97 \times 10^{-4}$	636	$d-d$
		377	LMCT
		274	$\pi-\pi^*$
		208	$\pi-\pi^*$
Zn(LBS)	$8.93 \times 10^{-4}$	448	$n-\pi^*$
		382	LMCT
		267	$\pi-\pi^*$
		237	$\pi-\pi^*$
Cd(LBS)	$1.01 \times 10^{-3}$	400	$\pi-\pi^*$
		323	LMCT
		240	$\pi-\pi^*$
		223	$\pi-\pi^*$

The electronic spectra of the ligand LBS exhibits absorption maxima at 344 nm due to charge transfer of an imine group in the ligand [188]. Another band at 326 nm can be

attributed to  $\pi$ - $\pi^*$  electronic transition due to the effect of bromine substituents on the aromatic ring [189]. The band observed at 416 nm can be associated with  $n$ - $\pi^*$  electronic transition in the piperazine moiety. The spectra of copper, zinc and cadmium complexes exhibits similar absorption bands at high frequencies that can be correlated with  $n$ - $\pi^*$  band absorption found in the ligand spectra. The bands region observed at 377 nm, in copper, 382 nm in zinc and 323 nm in cadmium complexes can be attributed to the ligand-metal charge transfer (LMCT) [190]. Other bands that appear at low wavelengths can be ascribed to  $\pi$ - $\pi^*$  electronic transition of the ligand (Table 32). However, the absorption band at 636 nm in the spectra of copper complex can be due to the ligand field  $d$ - $d$  transition [190]. This absorption is absent in zinc and cadmium spectra as observed in the complexes of the previously described ligands (Table 3.33, Fig. 3.109-3.112) (Appendix E).

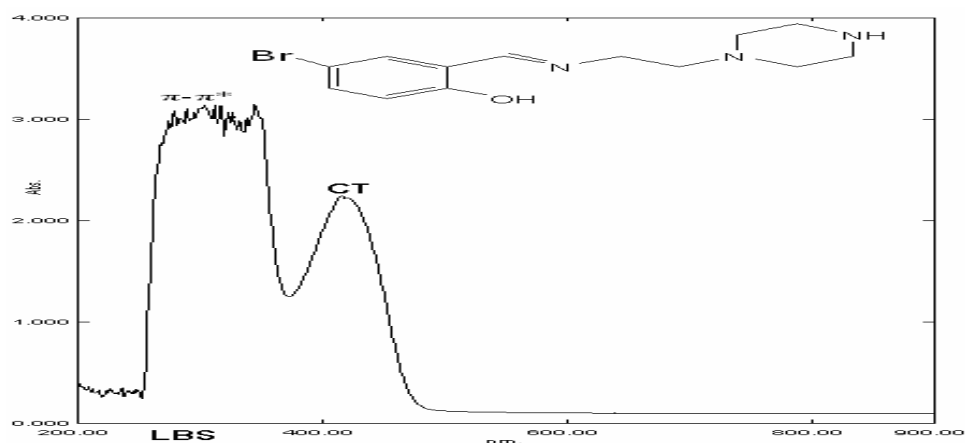


Figure 3.109 UV-visible spectra of LBS ligand

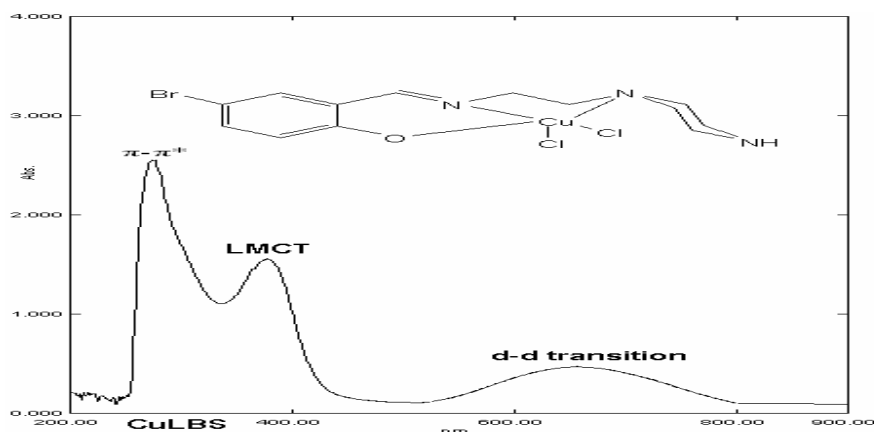


Figure 3.110 UV-visible spectra of  $[\text{Cu}(\text{LBS})\text{Cl}_2]$  complex.

### 3.5.4 UV-visible spectra of the ligand LNS and its Cu, Zn and Cd complexes

The electronic spectra of the ligand LNS and its complexes of copper, zinc and cadmium with their absorption band assignments are shown in Table 33 and Figure 3.113-3.116

Table 3.34 UV-visible spectra of LNS and its Cu, Zn and Cd complexes:

Compounds	Concentration	Wavelengths	Remark
LNS	$1.08 \times 10^{-3}$	413	$n-\pi^*$
		364	CT
		258	$\pi-\pi^*$
		222	$\pi-\pi^*$
Cu(LNS)	$9.71 \times 10^{-4}$	699	$d-d$
		283	LMCT
		265	$\pi-\pi^*$
		203	$\pi-\pi^*$
Zn(LNS)	$9.67 \times 10^{-4}$	434	$n-\pi^*$
		386	LMCT
		260	$\pi-\pi^*$
		214	$\pi-\pi^*$
Cd(LNS)	$1.08 \times 10^{-3}$	475	$n-\pi^*$
		398	LMCT
		258	$\pi-\pi^*$
		234	$\pi-\pi^*$

The electronic spectrum of the ligand LNS shows bands regions at 413 nm and 364 nm that can be assigned to  $n-\pi^*$  transition and charge transfer (CT) in the imine band respectively [191]. The bands that appears at 258 nm and 222 nm could be associated with the  $\pi-\pi^*$

transitions in the phenolic ring and piperazine moiety accordingly. These absorption maxima shift substantially to high wavelengths 434 nm and 386 nm due to ligand-metal charge transfer (LMCT) upon complexation with zinc metal. Similar band shifts to 475 nm and 398 nm are observed in the spectra of cadmium complex. This suggests the possible formations of the tetrahedral geometries by the two complexes [192]. Other absorptions at 260 nm and 214 nm in zinc complex and at 258 nm and 234 nm in the spectra of cadmium complex can be associated with  $\pi$ - $\pi^*$  transitions that was initiated from the ligand moiety. However, the spectra of copper complex at high concentration show an absorption band at 699 nm that could be attributed to the ligand field  $d$ - $d$  electronic transition. The band region at 283 nm can be assigned to ligand-metal charge transfer (CT) whereby the bands at 265 nm and 203 nm are ascribed to the ligand  $\pi$ - $\pi^*$  transitions (Table 34). The absence of a band at 400 nm is presumed to cause a distortion in the geometrical form of this complex [193] in comparison with zinc and cadmium complexes (Table 3.34, Fig. 3.113-3.116) (Appendix E).

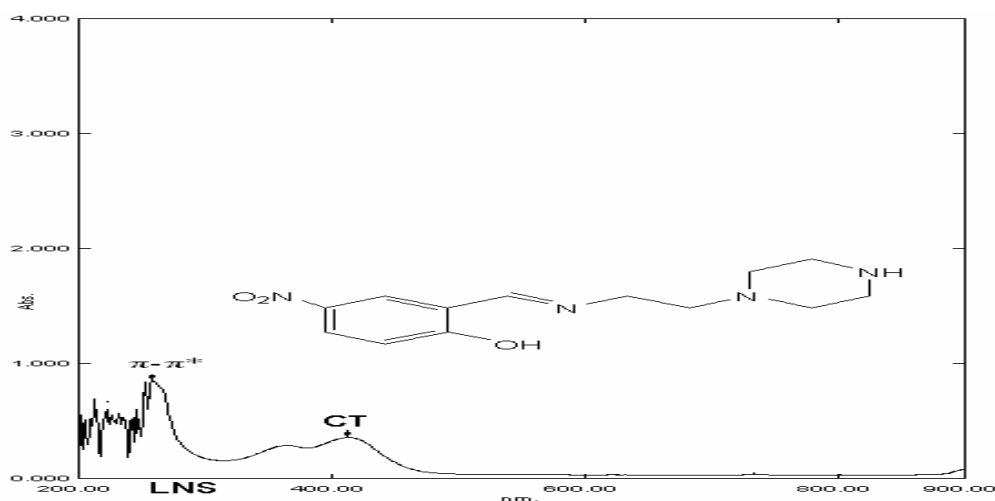


Figure 3.113 UV-visible spectra of LNS ligand

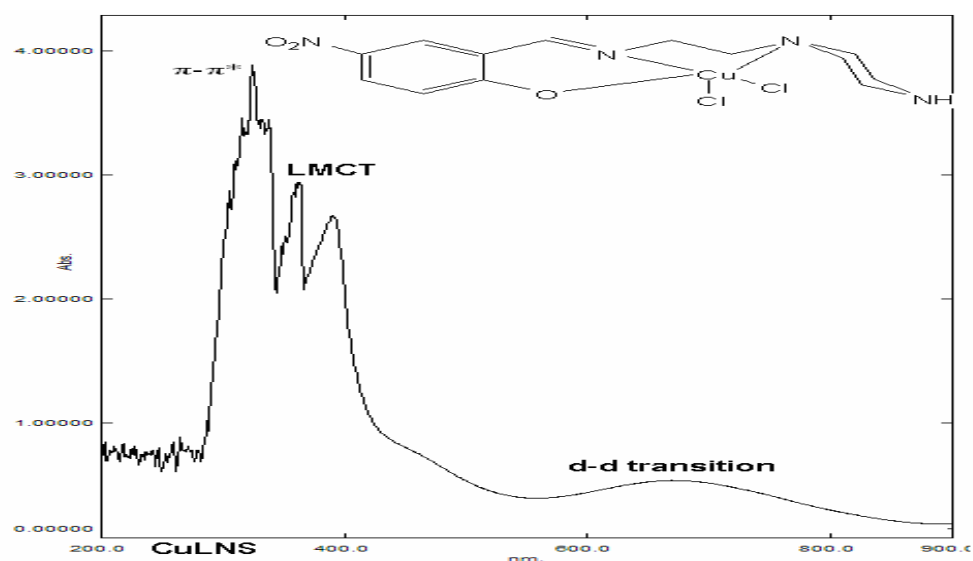


Figure 3.114 UV-visible spectra of [Cu(LNS)Cl<sub>2</sub>] complex.

### 3.5.5 UV-visible spectra of the ligand LDH and its Cu, Zn and Cd complexes

The electronic spectra of the ligand LDH and its complexes of copper, zinc and cadmium with their absorption band assignments are shown in Table 35 and Figure 3.117-3.120

Table 3.35 UV-visible spectra of LDH and its Cu, Zn and Cd complexes:

Compounds	Concentration	Wavelengths	Remark
LDH	1.2 x 10 <sup>-3</sup>	433	n-π*
		345	CT
		263	π-π*
		239	π-π*
Cu(LDH)	1.04 x 10 <sup>-3</sup>	682	d-d
		410	n-π*
		323	LMCT
		291	π-π*
Zn(LDH)	1.04 x 10 <sup>-3</sup>	434	n-π*
		361	LMCT
		261	π-π*
		217	π-π*
Cd(LDH)	9.3 x 10 <sup>-4</sup>	363	LMCT
		267	π-π*
		235	π-π*
		210	π-π*

The UV-visible spectra of the ligand LDH display four different absorption bands. The band region at 345 nm could be attributed to charge transfer (CT) in the ligand. In addition, the shifts at the wavelengths 263 nm and 239 nm could be assigned to the chromophores of the piperazine ring and the  $\pi$ - $\pi^*$  transitions in phenolic ring. These two absorptions are very close to the band observed at 345 nm in the imine region, thus indicating the weak covalent bond formed by the ligand [194]. Other band at 433 nm can be assigned to  $n$ - $\pi^*$  transition. The spectra of the complexes exhibits bands that are correlated with the absorption maxima noticed in the ligand spectra. Copper complex show absorption bands at lower wavelength of 323 nm which can presumably be due to charge transfer between ligand and metal (LMCT) upon coordination. The bathochromic shift observed at 410 nm and 291 nm can be afforded to  $n$ - $\pi^*$  electronic transitions in the phenolic ring and  $\pi$ - $\pi^*$  transitions in the ligand moiety respectively [195]. The absorption band at 682 nm could be due to  $d$ - $d$  transition of copper electrons as described earlier. The spectra of zinc and cadmium complexes display their band maxima at 361 nm and 363 nm respectively, these absorption are comparable to the band region observed in the ligand spectra due to the  $\pi$ - $\pi^*$  electronic transitions. Furthermore, these bands are well defined and can be attributed to intra ligand transitions (LMCT) [196]. The changes observed in the appearance and position of these bands confirms the coordination of the ligand with the metal ions. The band at 217 nm in the spectra of zinc complex and at 210 nm in cadmium complex spectra also supports these deductions and further predicts the tetrahedral geometries for these complexes [197] (Table 3.35, Fig. 3.117-3.120) (Appendix E).

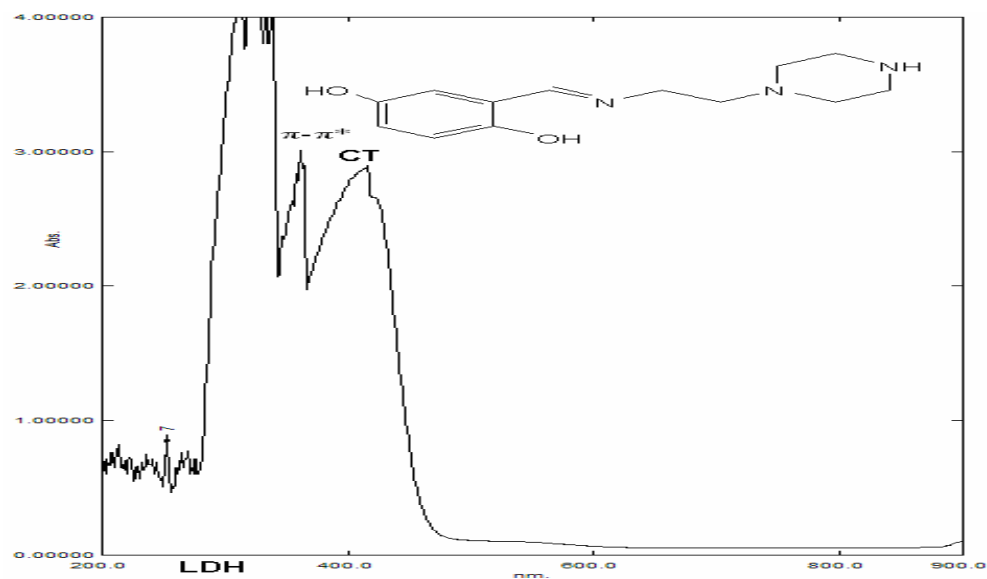


Figure 3.117 UV-visible spectra of LDH ligand

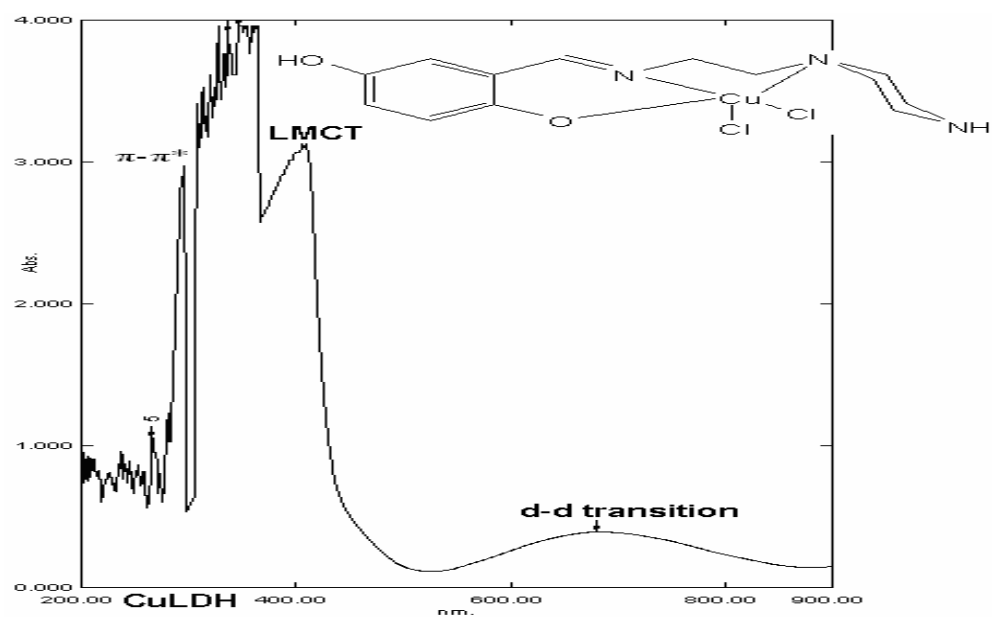


Figure 3.118 UV-visible spectra of  $[\text{Cu}(\text{LDH})\text{Cl}_2]$  complex.

### 3.5.6 UV-visible spectra of the ligand DHS and its Cu, Zn and Cd complexes

The electronic spectra of the ligand DHS and its complexes of copper, zinc and cadmium with their absorption band assignments are shown in Table 36 and Figure 3.121-3.124

Table 3.36 UV-visible spectra of DHS and its Cu, Zn and Cd complexes:

Compounds	Concentration	Wavelengths	Remark
DHS	$1.2 \times 10^{-3}$	389	n- $\pi^*$
		309	CT
		280	$\pi$ - $\pi^*$
		215	$\pi$ - $\pi^*$
Cu(DHS)	$1.04 \times 10^{-3}$	675	<i>d-d</i>
		395	n- $\pi^*$
		337	LMCT
		270	$\pi$ - $\pi^*$
Zn(DHS)	$1.04 \times 10^{-3}$	318	n- $\pi^*$
		298	MLCT
		257	$\pi$ - $\pi^*$
		213	$\pi$ - $\pi^*$
Cd(DHS)	$9.3 \times 10^{-4}$	322	n- $\pi^*$
		274	MLCT
		262	$\pi$ - $\pi^*$
		243	$\pi$ - $\pi^*$

The electronic spectra of DHS ligand display band maxima at 389 nm and 309 nm due to n- $\pi^*$  and CT electronic transitions that is characteristics of the imine absorptions in the ligand. The changes observed in the position of these bands to 337 nm and 395 nm in the spectra of copper complex is presumed due to the coordination between the ligand and the metal atom. In addition, the band at 675 nm of this spectrum can be attributed to the ligand field *d-d* electronic transition. However, the spectra of zinc and cadmium complexes shows similar bands at the wavelengths 318 nm and 298 nm for zinc and the bands at 322 nm and 274 nm for cadmium complexes due to bathochromic shift of the imine group resulting from the metal-ligand charge transfer MLCT upon complexation [189,197]. The weak bands at 280 nm and 215 nm in the ligand spectra are assignable to  $\pi$ - $\pi^*$  electronic transition in the aromatic ring and piperazine moiety respectively. These bands has also shifted to new wavelengths of 257 nm and 213 nm in zinc and to 262 nm and 243 nm in a cadmium spectra with moderate absorption intensities in the form of a shoulder due to spin

allowed  $\pi\text{-}\pi^*$  transition that is typical of the distorted tetrahedral species [197] (Table 3.36, Fig. 3.121-3.124) (Appendix E).

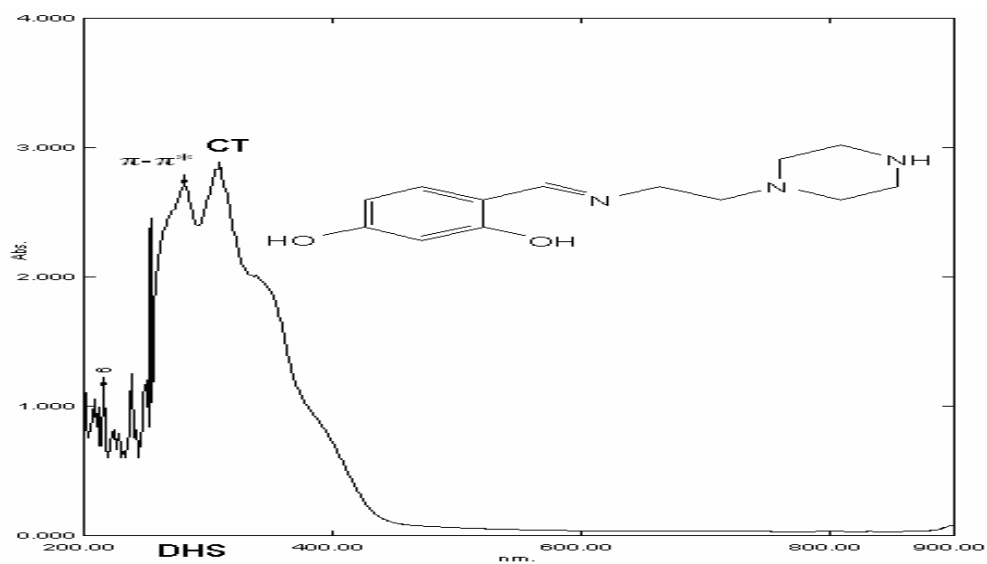


Figure 3.121 UV-visible spectra of DHS

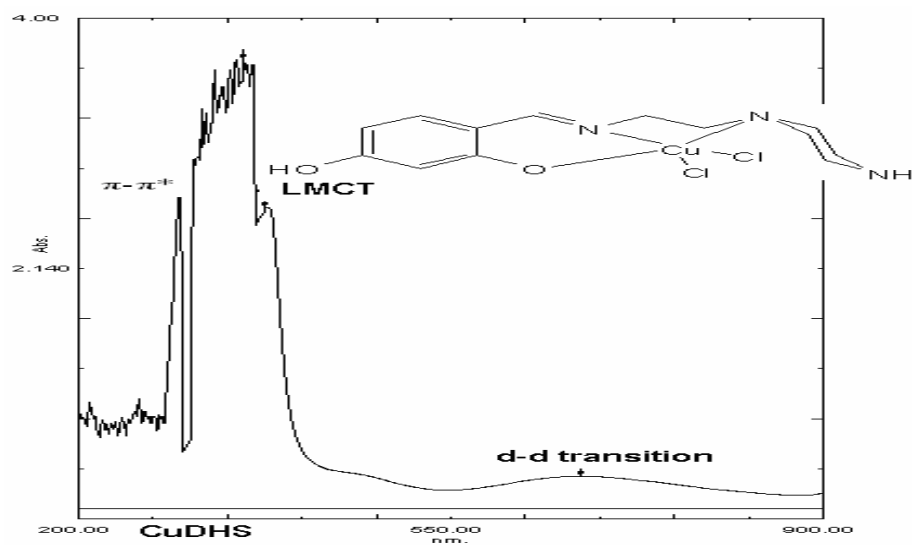


Figure 3.122 UV-visible spectra of  $[\text{Cu}(\text{DHS})\text{Cl}_2]$  complex.

### 3.5.7 UV-visible spectra of the ligand LHM and its Cu, Zn and Cd complexes

The electronic spectra of the ligand LHM and its complexes of copper, zinc and cadmium with their absorption band assignments are shown in (Table 3.37 and Figure 3.125-3.128).

Table 3.37 UV-visible spectra of LHM and its Cu, Zn and Cd complexes

Compounds	Concentration	Wavelengths	Remark
LHM	$8.97 \times 10^{-4}$	434	$n-\pi^*$
		398	$\pi-\pi^*$
		314	CT
		266	$\pi-\pi^*$
Cu(LHM)	$1.14 \times 10^{-3}$	675	$d-d$
		404	$n-\pi^*$
		362	LMCT
		247	$\pi-\pi^*$
Zn(LHM)	$1.0 \times 10^{-3}$	407	$n-\pi^*$
		383	MLCT
		296	$\pi-\pi^*$
		222	$\pi-\pi^*$
Cd(LHM)	$1.12 \times 10^{-3}$	409	$n-\pi^*$
		303	MLCT
		273	$\pi-\pi^*$
		239	$\pi-\pi^*$

The spectral data illustrated by ligand LHM contains 4 absorption band maxima. The band at 434 nm, is distinctive for the  $n-\pi^*$  electronic transition in the ligand moiety. The electronic transition band observed at 314 nm can be due to the charge transfer (CT) of imine in the ligand. Other absorptions at 398 nm and 266 nm can be assignable to  $\pi-\pi^*$  transitions expected to have arisen from the redistribution of electron density within the ligand moiety [198]. The spectra of the complexes show high wavelength band maxima of 404 nm in Cu, 407 nm in Zn and 409 nm in Cd. These absorptions originated from 434 nm in the ligand with an increased energy probably due to changes in the  $n-\pi^*$  electronic transition. These absorptions extend to new bands of 362 nm in Cu, 383 nm in Zn and 303 nm in Cd and could be associated to the ligand to metal charge transfer (LMCT). The medium intensity bands that appear at high energy of 247 nm in Cu, 222 nm in Zn and 239 nm in Cd spectra also supports the covalent coordination expected between the ligand and the metal ions [199]. In addition, the copper complex displays absorption at 675 nm band

region, which could be ascribed to the *d-d* transition (Table 3.37, Fig. 3.125-128) (Appendix E).

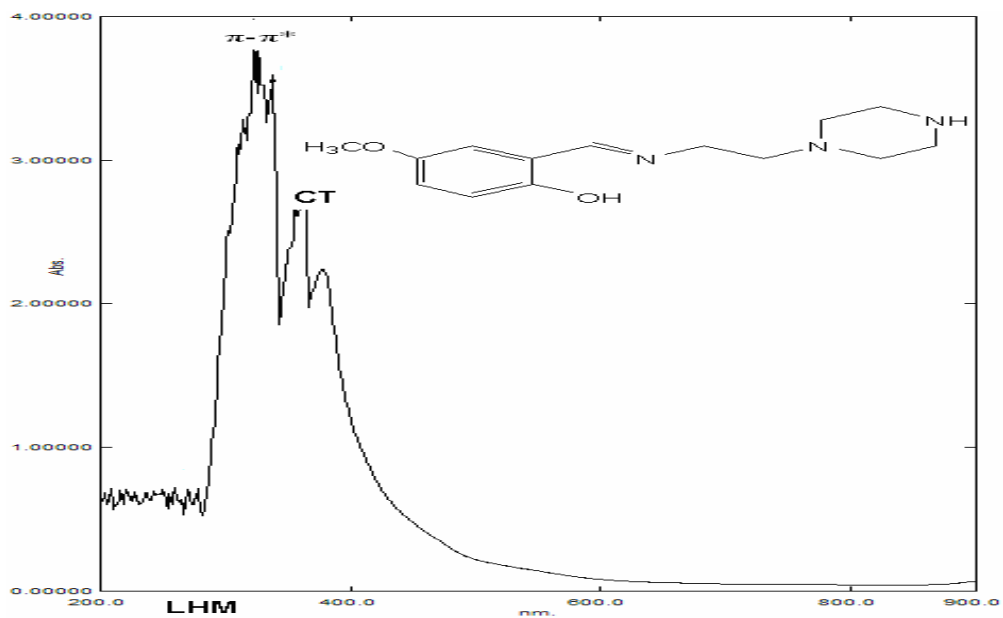


Figure 3.125 UV-visible spectra of LHM ligand.

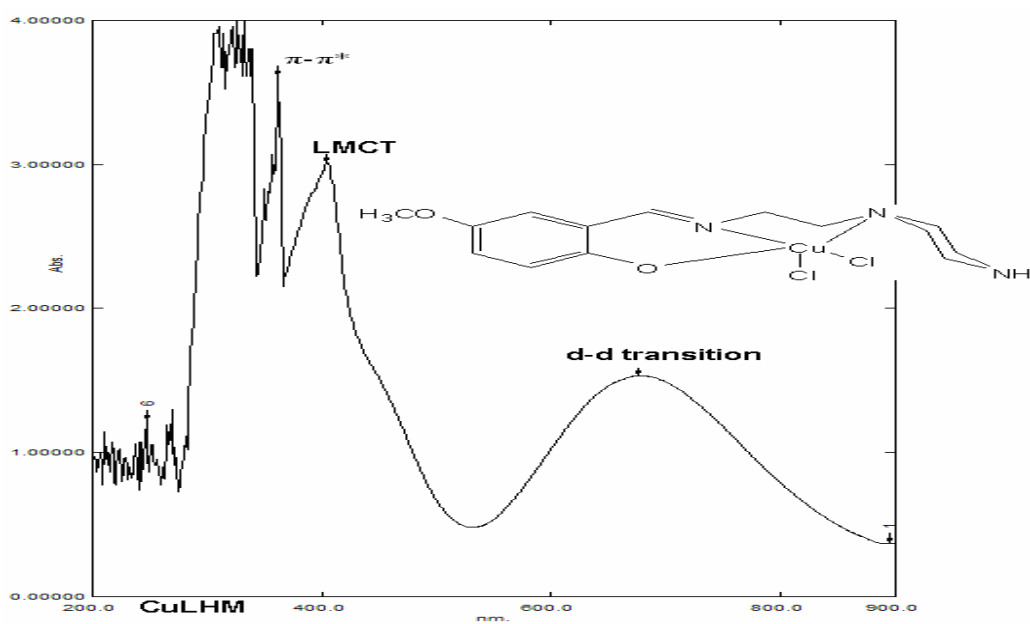


Figure 3.126 UV-visible spectra of  $[\text{Cu}(\text{LHM})\text{Cl}_2]$  complex.

### 3.5.8 UV-visible spectra of the ligand HMS and its Cu, Zn and Cd complexes

The electronic spectra of the ligand HMS and its complexes of copper, zinc and cadmium with their absorption band assignments are shown in Table 38 and Figure 3.129-3.132

Table 3.38 UV-visible spectra of HMS and its Cu, Zn and Cd complexes:

Compounds	Concentrations	Wavelengths	Remark
HMS	$8.97 \times 10^{-4}$	430	$n-\pi^*$
		303	$\pi-\pi^*$
		298	CT
		275	$\pi-\pi^*$
Cu(HMS)	$1.14 \times 10^{-3}$	662	$d-d$
		407	$\pi-\pi^*$
		282	LMCT
		244	$\pi-\pi^*$
Zn(HMS)	$1.0 \times 10^{-3}$	383	$\pi-\pi^*$
		326	$\pi-\pi^*$
		295	LMCT
Cd(HMS)	$1.12 \times 10^{-3}$	406	$\pi-\pi^*$
		297	LMCT
		225	$\pi-\pi^*$

The electronic spectra obtained from HMS ligand, and its complexes of Cu, Zn and Cd have displayed common band maxima at 298 nm, 282 nm, 295 nm and 297 nm respectively. These high energy absorptions (Table 3.38) could be ascribed to charge transfer (CT) in the ligand. These bands are noticed to have shifted to new regions due to ligand-metal charge transfer in the spectra of the complexes. The high wavelength absorption evident at 430 nm in the ligand spectra is assigned to  $n-\pi^*$  transition in the imine center. This band was observed at 407 nm in the spectra of copper, at 383 nm in the spectra of zinc and at 406 nm in the spectra of cadmium complexes as a shoulder that is resulted from the spin allowed electronic transitions upon complexation [200]. The copper complex further exhibits the ligand field electronic ( $d-d$ ) transition at 662 nm. However, the complicated absorptions that appear at high energies in the spectra of the complexes cannot

be explained with any certainty but can seemingly support the expected chelation of the compounds (Table 3.38, Fig. 3.129-3.132) (Appendix E).

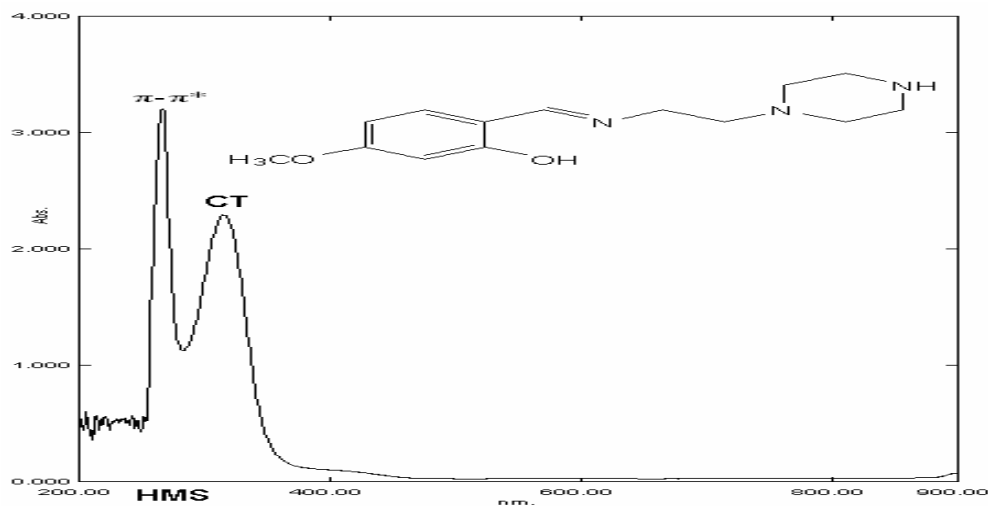


Figure 3.129 UV-visible spectra of HMS ligand.

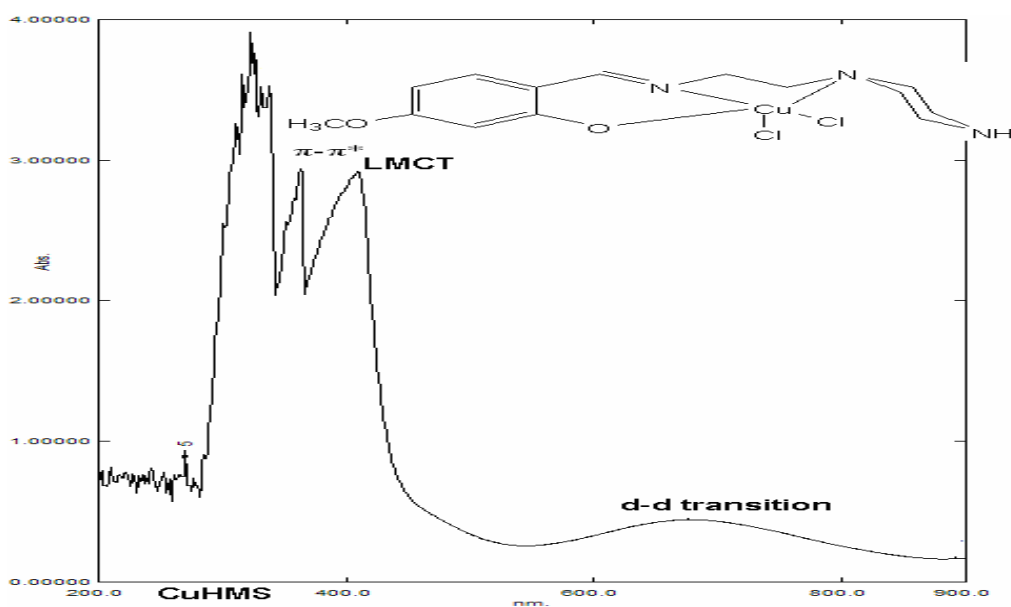


Fig. 3.130 UV-visible spectra of [Cu(HMS)Cl<sub>2</sub>] complex.

### 3.5.9 UV-visible spectra of the ligand 2HP and its Cu, Zn and Cd complexes

The electronic spectra of the ligand 2HP and its complexes of copper, zinc and cadmium with their absorption band assignments are shown in Table 39 and Figure 3.132-3.136.

Table 3.39 UV-visible spectra of 2HP and its Cu, Zn and Cd complexes:

Compounds	Concentration	Wavelengths	Remark
2HP	$1.2 \times 10^{-3}$	395	$n-\pi^*$
		318	$\pi-\pi^*$
		262	CT
		242	$\pi-\pi^*$
Cu(2HP)	$1.05 \times 10^{-3}$	572	$d-d$
		363	$\pi-\pi^*$
		269	LMCT
		208	$\pi-\pi^*$
Zn(2HP)	$1.04 \times 10^{-3}$	400	$n-\pi^*$
		362	$\pi-\pi^*$
		313	$\pi-\pi^*$
		285	LMCT
Cd(2HP)	$9.3 \times 10^{-4}$	382	$n-\pi^*$
		362	$\pi-\pi^*$
		272	LMCT
		261	$\pi-\pi^*$

The UV –visible spectral data shown by the ligand 2HP manifests four band maxima at 395 nm, 318 nm, 262 nm and 242 nm. The intense band at 395 nm can be due to  $n-\pi^*$  electronic transitions. This absorption is intense at the region of the chromophore (HC=N, 262 nm) as a consequence of charge transfer (CT) [201]. The bands that appears at 318 nm and 242 nm could be assigned to the  $\pi-\pi^*$  electronic transitions due to delocalization in the aromatic ring and the chromophores in the piperazine ring respectively [201]. In the spectra of copper complex of this ligand, the bands that emerge at 363 nm and 269 nm are considered as shoulder due to chelate formation [202]. The band regions at 208 nm and 572 nm in the spectra of copper complex can be attributed to chelate ring  $n-\pi^*$  and the ligand field  $d-d$  transitions in copper respectively. The spectra of zinc complex also show four band maxima at 400 nm, 362 nm, 313 nm and 285 nm. The band regions at 400 nm and 313 nm are much closer and can be ascribed to  $n-\pi^*$  electronic transition of the phenyl ring and  $\pi-\pi^*$  electronic transition in the imine position. These bands exhibit an intense absorption at high energy due to ligand-metal charge transfer [203]. The spectra of the cadmium complex

manifested a double resonance absorptions at 382 nm and 362 nm which could be due to  $n-\pi^*$  and  $\pi-\pi^*$  electronic transitions respectively. This predictably originates from the increased ketonic character of the phenolic ring [204]. The high-intensity band at 272 nm is associated with charge transfer from ligand to metal (LMCT) whereby the band at 261 nm can be assigned to  $\pi-\pi^*$  electronic transition in piperazine ring (Table 3.39, Fig. 3.133-3.136) (Appendix E).

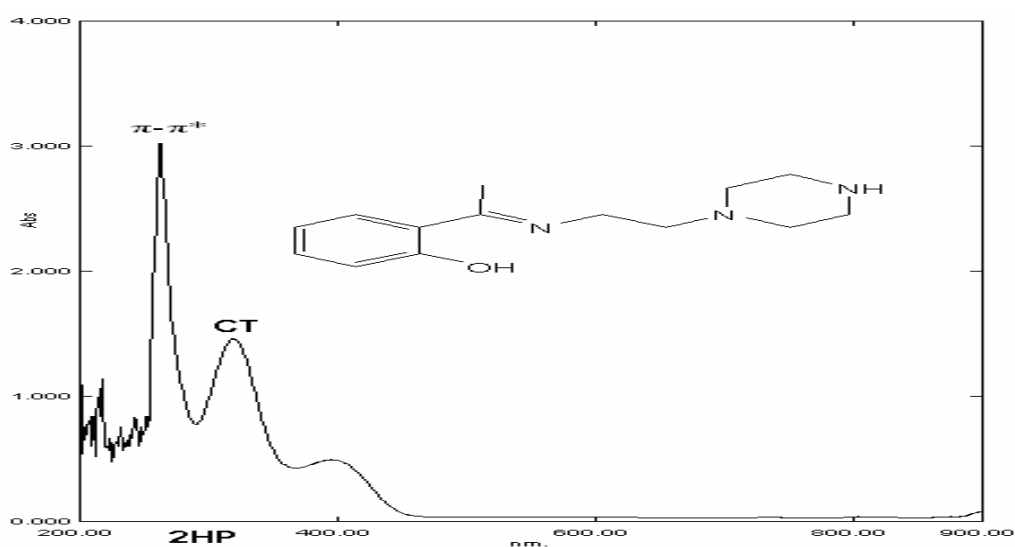


Figure 3.133 UV-visible spectra of 2HP ligand.

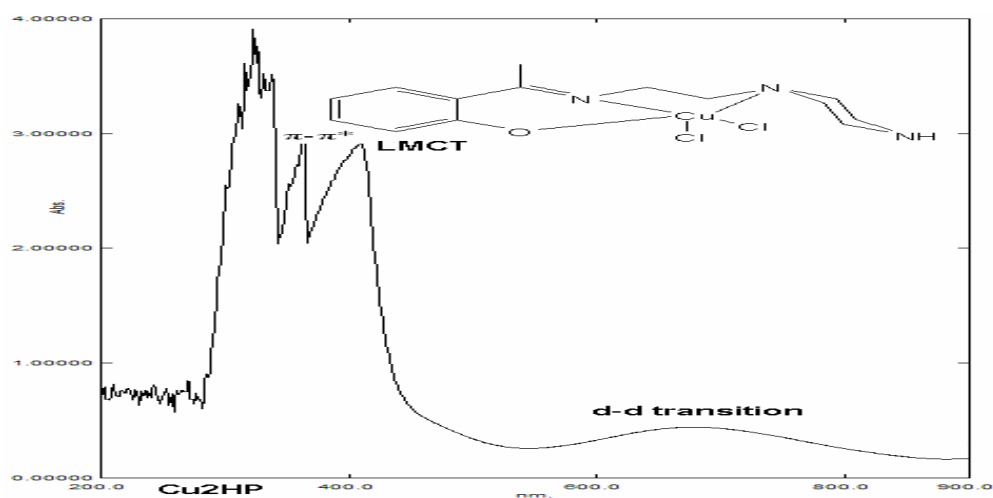


Figure 3.134 UV-visible spectra of  $[\text{Cu}(\text{2HP})\text{Cl}_2]$  complex.

### 3.5.10 UV-visible spectra of the ligand DHP and its Cu, Zn and Cd complexes

The electronic spectra of the ligand DHP and its complexes of copper, zinc and cadmium with their absorption band assignments are shown in Table 40 and Figure 3.137-3.140.

Table 3.40 UV-visible spectra of DHP and its Cu, Zn and Cd complexes:

Compounds	Concentrations	Wavelengths	Remark
DHP	8.97 x 10 <sup>-6</sup>	410	n- $\pi^*$
		346	CT
		215	$\pi$ - $\pi^*$
		206	$\pi$ - $\pi^*$
Cu(DHP)	1.14 x 10 <sup>-3</sup>	634	<i>d-d</i>
		359	LMCT
		343	$\pi$ - $\pi^*$
		224	$\pi$ - $\pi^*$
Zn(DHP)	1.0 x 10 <sup>-3</sup>	375	n- $\pi^*$
		227	LMCT
		256	$\pi$ - $\pi^*$
Cd(DHP)	1.12 x 10 <sup>-3</sup>	382	n- $\pi^*$
		284	$\pi$ - $\pi^*$
		260	LMCT

The electronic spectra of DHP ligand shows 2 absorption bands that correspond to the  $\pi$ - $\pi^*$  electronic transition and a band that can be ascribed to n- $\pi^*$  electronic transitions at the wavelengths 215 nm, 206 nm and 346 nm respectively. The intense absorption at 410 nm band region can be attributed to the charge transfer (CT) in the ligand. The electronic spectra of the copper complex shows three absorption band regions at 359 nm, 343 nm and 224 nm. These bands can be attributable to the charge transfer from ligand to metal (LMCT) and the spin allowed  $\pi$ - $\pi^*$  electronic transitions thus, suggesting a distorted tetrahedral geometry for the complex [197,205]. A weak absorption that appears at 634 nm is assigned to the *d-d* electronic transitions. The spectra of zinc and cadmium complexes display absorption band maxima at 227 nm and 260 nm respectively which are expected due to the ligand to metal charge transfer (LCMT) (Table 40). The bands at 375 nm in zinc and 382 nm in cadmium could be due to n- $\pi^*$  electronic transitions in the chelate ring.

Other absorption bands at 256 nm in the zinc complex spectra and at 284 nm in the spectra of cadmium complex could be assigned to the bathochromic shifts of the chromophores in the piperazine moiety. However, the exact interpretation of the bands that appear at low wavelengths in all the complexes has become complicated due to the deviation of the complexes from regular tetrahedral geometry [206] (Table 3.40, Fig. 3.137-3.140) (Appendix E).

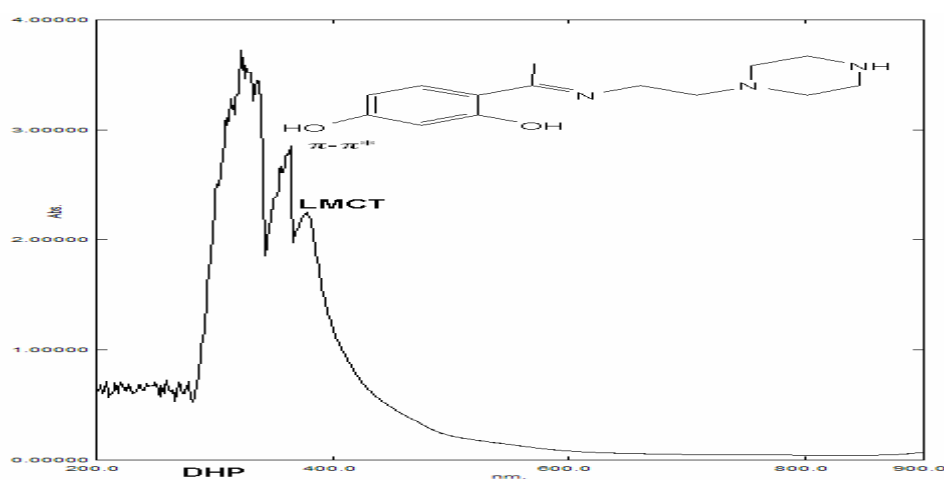


Figure 137 UV-visible spectra of DHP ligand.

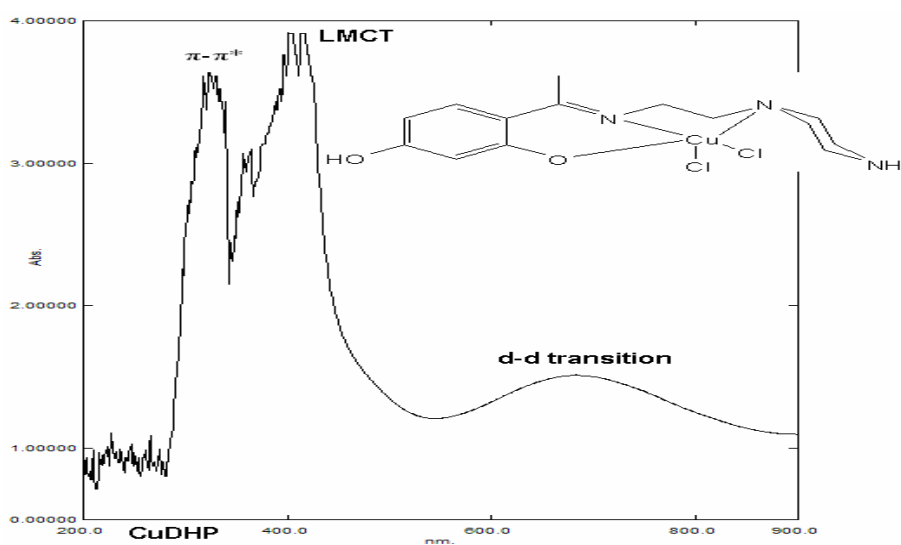


Figure 3.138 UV-visible spectra of [Cu(DHP)Cl<sub>2</sub>] complex.

### 3.6 Thermal studies

The thermal behavior of Cu, Zn and Cd complexes has been studied at the temperature range 50-900°C with interval of 20°C. The complexes exhibited stepwise decomposition activities whereby the mass loss and the temperatures at the first decomposition stage were considered relevant in estimating the thermal stability of each complex for the purpose of biological studies. The thermal behavior of all the complexes is almost the same, and consequently; their inferences became comparable in most instances.

#### 3.6.1 Thermogravimetric data of Cu(LSP), Zn(LSP) and Cd(LSP) complexes

The thermogravimetric data for copper, zinc and cadmium complexes with their tentative assignments are shown in Table 41 and Figure 3.141-3.143

Table 3.41 TGA data of Cu(LSP), Zn(LSP) and Cd(LSP) complexes:

Compounds	M.P /D.T	TGA	Weight loss (%)		Remark
			Observed	Calculated.	
LSP	82	NA			
[Cu(LSP)Cl <sub>2</sub> ]	267	224	14.98	14.58	loss of H <sub>2</sub> O and Cl
[Zn(LSP)Cl <sub>2</sub> ]	269	212	14.41	14.51	loss of H <sub>2</sub> O and Cl
[Cd(LSP)Cl <sub>2</sub> ]	273	231	15.49	12.87	loss of H <sub>2</sub> O and Cl

The thermo-gravimetric curves of the complexes obtained from LSP ligand shows the first weight loss of 14.98 % at 224°C in copper spectra, 14.41 % at 212°C in the spectra of zinc and 15.49 % at 231°C in the spectra of cadmium complexes. The percentage of weight loss observed in each complex is consistent with the calculated values of 14.58 %, 14.51 % and 12.87 % for Cu, Zn and Cd complexes respectively. These mass losses demonstrated by the complexes correspond to the departure of a molecule of water of hydration and a chlorine atom [207]. In addition, the decomposition point recorded from the melting point apparatus gave values slightly above the temperatures observed at the first decomposition stage in the TG analysis. This presumably indicates that the departure of the molecules from the

complexes started and completed within the range of the two different decomposition stages obtained from TGA and melting point apparatus (Table 3.41, Fig. 3.141-3.143) (Appendix F). This has evidently confirmed the high thermal stability of the compounds that is required for further studies.

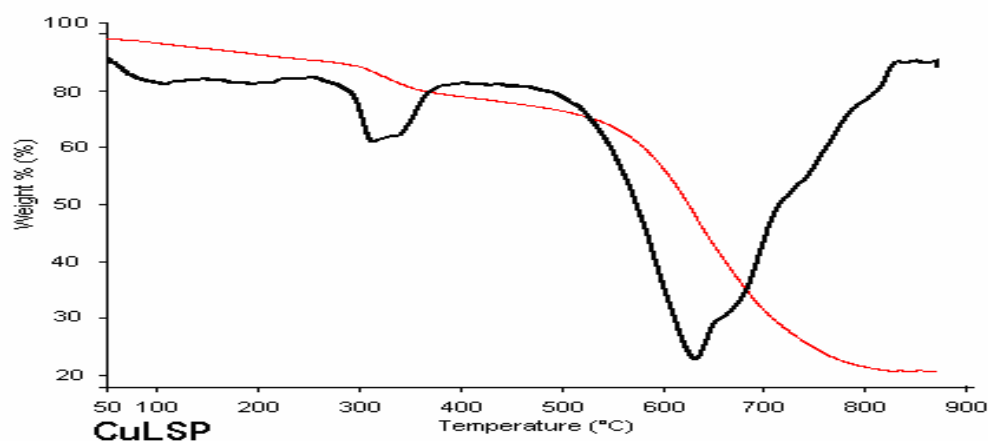


Fig. 3.141 TGA curve of  $[\text{Cu}(\text{LSP})\text{Cl}_2]$  complex.

### 3.6.2 Thermogravimetric data of $\text{Cu}(\text{LCS})$ , $\text{Zn}(\text{LCS})$ and $\text{Cd}(\text{LCS})$ complexes

The thermo-gravimetric data for copper, zinc and cadmium complexes of LCS ligand with their tentative assignments are shown in Table 42 and Figure 3.144-3.146.

Table 3.42 TGA data of  $\text{Cu}(\text{LCS})$ ,  $\text{Zn}(\text{LCS})$  and  $\text{Cd}(\text{LCS})$  complexes:

Compounds	M.P /D.T	TGA	Weight loss (%)		Remark
			Observed	Calculated.	
LCS	86	NA			
$[\text{Cu}(\text{LCS})\text{Cl}_2]$	328	277	13.20	13.33	loss of $\text{H}_2\text{O}$ and $\text{Cl}$
$[\text{Zn}(\text{LCS})\text{Cl}_2]$	293	220	17.49	13.27	loss of $2\text{H}_2\text{O}$ and $\text{Cl}$
$[\text{Cd}(\text{LCS})\text{Cl}_2]$	289	236	11.67	11.86	loss of $\text{H}_2\text{O}$ and $\text{Cl}$

The weight change observed due to thermal effects in the complexes of LCS ligand revealed 13.20 % (calcd. 13.33 %) at 277°C for copper, 17.49 % (calcd. 13.27 %) at 220°C for zinc and 11.67 % (calcd. 11.86 %) at 236°C for the cadmium complexes (Table 42). The weight losses observed in the TG curves of Cu and Cd complexes are inferentially comparable with those noticed in the complexes of LSP ligand, which are correspondingly

related to the loss of molecule of water of hydration and a chlorine atom. The weight changes observed in zinc complex can be accredited to the loss of two molecules of water of hydration and a chlorine atom [207]. The variations in the values of decomposition temperatures noticed between TGA, and the melting point apparatus had confirmed the departure of the molecules with relative molecular weights 52.9, 70.5 and 52.7 in copper, zinc and cadmium complexes respectively. This supposition is supported by the significant increase in decomposition temperature recorded on the melting point apparatus [208] (Table 3.42, Fig. 3.144-3.146) (Appendix F).

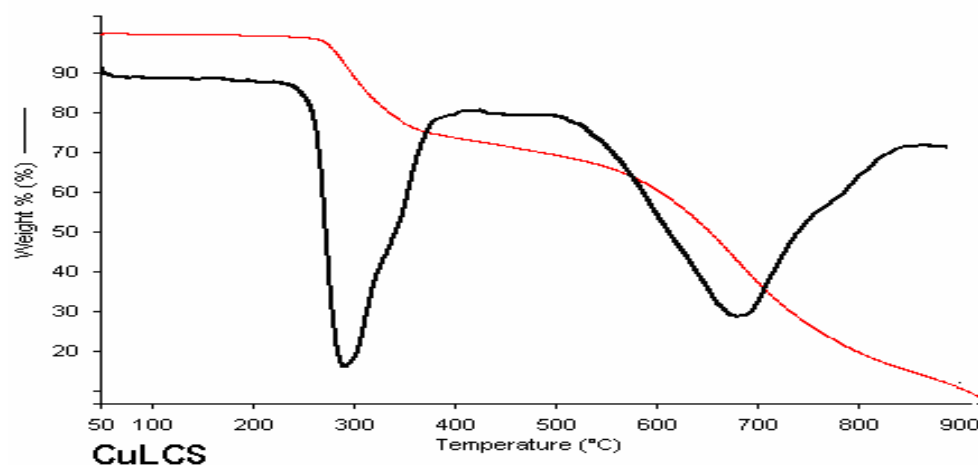


Fig. 3.144 TGA curve of  $[\text{Cu}(\text{LCS})\text{Cl}_2]$  complex.

### 3.6.3 Thermogravimetric data of $\text{Cu}(\text{LBS})$ , $\text{Zn}(\text{LBS})$ and $\text{Cd}(\text{LBS})$ complexes

The thermo-gravimetric data for copper, zinc and cadmium complexes of LBS ligand with their tentative assignments are shown in Table 3.43 and Figure 3.147-3.149

Table 3.43 TGA data of  $\text{Cu}(\text{LCS})$ ,  $\text{Zn}(\text{LCS})$  and  $\text{Cd}(\text{LCS})$  complexes:

Compounds	M.P /D.T	TGA	Weight loss (%)		Remark
			Observed	Calculated.	
LBS	84	NA	Observed	Calculated.	
$[\text{Cu}(\text{LBS})\text{Cl}_2]$	283	236	11.86	12.00	loss of $\text{H}_2\text{O}$ and Cl
$[\text{Zn}(\text{LBS})\text{Cl}_2]$	349	304	11.55	11.96	loss of $\text{H}_2\text{O}$ and Cl
$[\text{Cd}(\text{LBS})\text{Cl}_2]$	343	310	7.24	7.26	loss of $2\text{H}_2\text{O}$

The thermal behavior of the complexes derived from LBS ligand show an initial weight loss of 11.86 % (calcd. 12.00 %) at 236 °C for copper, 11.56 % (calcd. 11.96 %) at 304 °C for zinc and 7.24 % (calcd. 7.26 %) at 310 °C for cadmium complexes (Table 3.43) (Appendix F). These percentages correspond to the mass loss due to disappearance of the molecules with relative molar masses 52.86, 51.69 and 35.89 in Cu, Zn and Cd TG curves respectively. These weight changes can be attributable to the exit of a molecule of water of hydration and chlorine atom in Cu and Zn complexes whereby the mass loss noticed in the spectra of cadmium complex can be attributed to the departure of two molecules of water of hydration [209]. Furthermore, the decomposition temperatures recorded from melting point apparatus show correlated deductions with the previously described complexes. Generally, the complexes showed high thermal stabilities desired for biological studies.

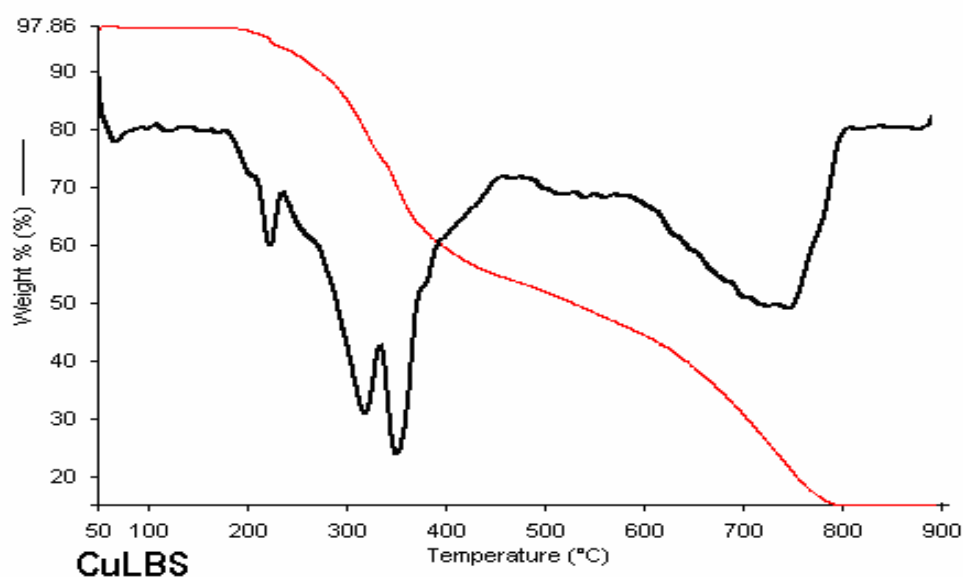


Fig. 3.147 TGA curve of [Cu(LBS)Cl<sub>2</sub>] complex.

### 3.6.4 Thermogravimetric data of Cu(LNS), Zn(LNS) and Cd(LNS) complexes

The thermo-gravimetric data for copper, zinc and cadmium complexes of LNS with their tentative assignments are shown in Table 3.44 and Figure 3.150-3.152.

Table 3.44 TGA data of Cu(LNS), Zn(LNS) and Cd(LNS) complexes:

Compounds	M.P/D.T	TGA	Weight loss (%)		Remark
			Observed	Calculated.	
LNS	62	NA			
[Cu(LNS)Cl <sub>2</sub> ]	210	152	13.16	12.99	loss of H <sub>2</sub> O and Cl
[Zn(LNS)Cl <sub>2</sub> ]	327	285	12.48	12.93	loss of H <sub>2</sub> O and Cl
[Cd(LNS)Cl <sub>2</sub> ]	311	253	11.48	11.61	loss of H <sub>2</sub> O and Cl

The TG curves of Cu, Zn and Cd complexes obtained from LNS ligand show weight changes relative to temperature by 13.16 % (calcd. 12.99 %) at 152°C, 12.48 % (calcd. 12.93 %) at 285°C and 11.48 % (calcd. 11.61 %) at 253°C respectively. These weight losses can be ascribed to the removal of water of hydration and a chlorine atom as observed in the previously described complexes. This deduction is supported by the temperature differences observed between the two decomposition points acquired from TG-analyzer and the melting point apparatus. However, the percentage mass losses could be interconnected to the departure of molecules with the relative molar masses 54.21, 51.61 and 52.87 from Cu Zn and Cd complexes respectively. This may be associated with the easy diffusion behavior of water molecules in the lattice structure of the complexes [207,210] (Table 3.44 and Fig.3.150-3.152) (Appendix F).

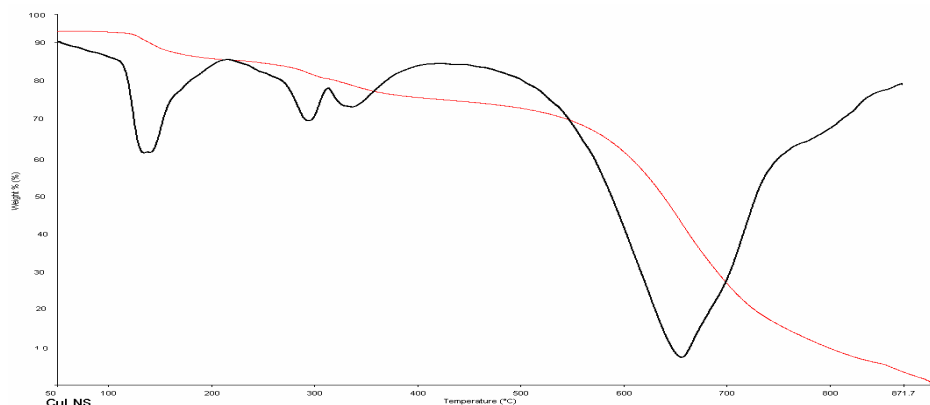


Fig. 3.150 TGA curve of [Cu(LNS)Cl<sub>2</sub>] complex.

### 3.6.5 Thermogravimetric data of Cu(LDH), Zn(LDH) and Cd(LDH) complexes

The thermo-gravimetric data for copper, zinc and cadmium complexes of LDH with their tentative assignments are shown in Table 3.45 and Figure 3.153-155

Table 3.45 TGA data of Cu(LDH), Zn(LDH) and Cd(LDH) complexes:

Compounds	M.P /D.T	TGA	Weight loss (%)		Remark
			Observed	Calculated.	
LDH	128	NA	Observed	Calculated.	
[Cu(LDH)Cl <sub>2</sub> ]	329	261	28.43	27.95	loss of 2H <sub>2</sub> O and 2Cl
[Zn(LDH)Cl <sub>2</sub> ]	213	187	4.93	4.68	loss of H <sub>2</sub> O
[Cd(LDH)Cl <sub>2</sub> ]	245	224	4.45	4.17	loss of H <sub>2</sub> O

The TG measurements performed on the complexes derived from LDH ligand demonstrated mass losses of 18.43%, 4.93% and 4.45 for Cu, Zn and Cd complexes respectively. These percentages differ from the calculated values by  $\pm 0.48$  in the curve of Cu complex,  $\pm 0.25$  in Zn complex curve and  $\pm 0.28$  in the curve of Cd complex. This designates the agreement of the two results which is consistent with the values obtained (Table 3.45) (Appendix F) from the melting point machine [211]. These mass differences correspond to the loss of molecules with relative molar masses of about 70.54, 18.98 and 19.21 in Cu, Zn and Cd TG curves respectively. This is approximately equivalent to the loss of two molecules of water of hydration and chlorine atom in copper complex and a molecule of water of hydration in Zn and Cd complexes. The complexes displayed high thermal stabilities.

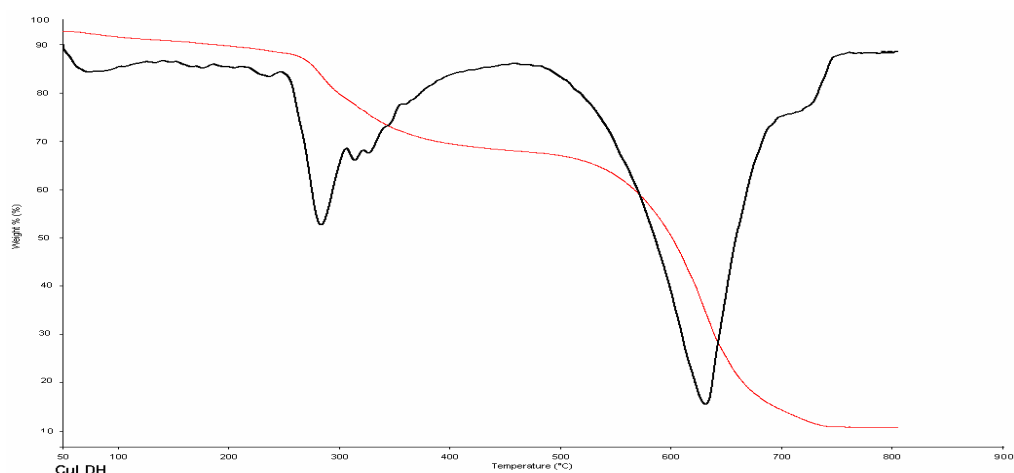


Fig. 3.153 TGA curve of  $[\text{Cu}(\text{LDH})\text{Cl}_2]$  complex.

### 3.6.6 Thermogravimetric data of $\text{Cu}(\text{DHS})$ , $\text{Zn}(\text{DHS})$ and $\text{Cd}(\text{DHS})$ complexes

The thermo-gravimetric data for copper, zinc and cadmium complexes with their tentative assignments are shown in Table 3.46 and Figure 3.156-3.158

Table 3.46 TGA data of  $\text{Cu}(\text{DHS})$ ,  $\text{Zn}(\text{DHS})$  and  $\text{Cd}(\text{DHS})$  complexes:

Compounds	M.P/D.T	TGA	Weight loss (%)		Remark
			Observed	Calculated.	
DHS	118	NA			
$[\text{Cu}(\text{DHS})\text{Cl}_2]$	324	302	4.97	4.70	loss of $\text{H}_2\text{O}$
$[\text{Zn}(\text{DHS})\text{Cl}_2]$	227	208	4.77	4.68	loss of $\text{H}_2\text{O}$
$[\text{Cd}(\text{DHS})\text{Cl}_2]$	229	204	4.67	4.17	loss of $\text{H}_2\text{O}$

The thermal data of the complexes derived from LDH ligand reveals distinctive weight changes in the copper complex by 4.97 % (calcd. 4.70 %) when compared with the weight loss of 28.43 % (calcd. 27.95 %) in its analogue  $[\text{Cu}(\text{LDH})\text{Cl}_2]$  complex (Table 3.46). The weight losses of 4.77 % (calcd. 4.68 %) recorded for zinc and 4.67 % (calcd. 4.17 %) for cadmium complexes are concordance with the values recorded in their analogue complexes derived from LDH ligand and so require same description. The decomposition temperatures at which the weight changes occur in TG analysis are also in conformity with the observed decomposition points recorded on melting point machine. This further proves the high

thermal stability of the complexes derived from DHS ligand [212,213]. Inferentially, the mass losses of 19.04, 18.33 and 20.16 observed in the TG curves of Cu, Zn and Cd complexes respectively correspond to the exit of a molecule of water of hydration in all the complexes (Table 3.46, Fig. 3.156-3.158)

(Appendix F).

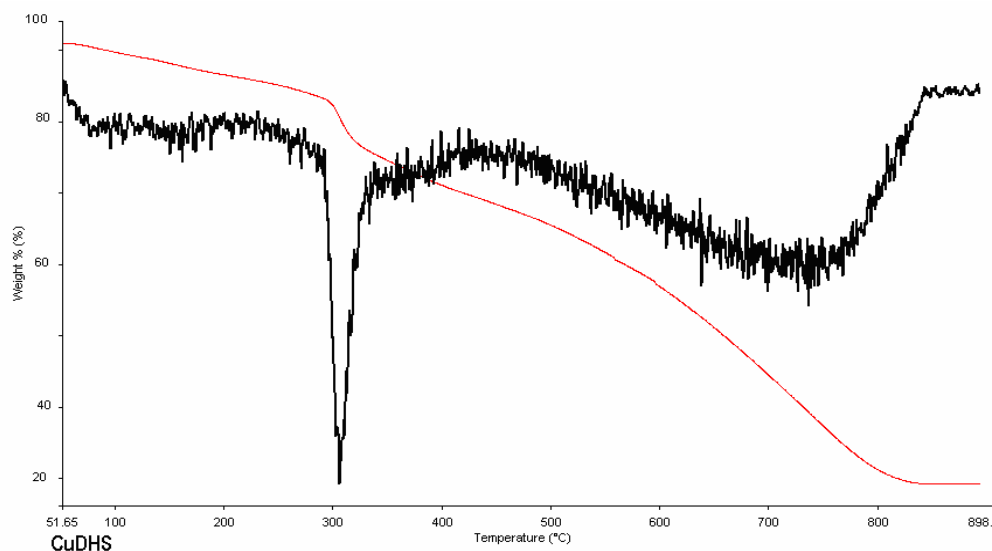


Fig. 3.156 TGA curve of [Cu(DHS)Cl<sub>2</sub>] complex.

### 3.6.7 Thermogravimetric data of Cu(LHM), Zn(LHM) and Cd(LHM) complexes

The thermo-gravimetric data for copper, zinc and cadmium complexes of LHM with their tentative assignments are shown in Table 3.47 and Figure 3.159-3.161

Table 3.47 TGA data of Cu(LHM), Zn(LHM) and Cd(LHM) complexes:

Compounds	M.P/D.T	TGA	Weight loss (%)		Remark
			Observed	Calculated.	
LHM	62	NA	13.23	13.48	loss of H <sub>2</sub> O and Cl
[Cu(LHM)Cl <sub>2</sub> ]	255	201	13.16	13.42	loss of H <sub>2</sub> O and Cl
[Zn(LHM)Cl <sub>2</sub> ]	268	213	8.35	8.08	loss of 2H <sub>2</sub> O
[Cd(LHM)Cl <sub>2</sub> ]	253	214			

The thermal curves obtained from LHM complexes show stepwise degradation behavior (Table 3.47) (Appendix F). Hence, only the first decomposition step of the complexes are

discussed here and the tentative assignments of their weight losses. The weight losses observed by 13.23 % (calcd. 13.48 %) at 201°C in the TG curve of Cu and the loss of 13.16 % (calcd. 13.42 %) at 213°C in the curve of Zn complexes are quite similar and presumably correspond to the departure of the identical molecules from the respective complexes which is seemingly a molecule of water of hydration and chlorine atom. The weight loss of 8.35 % (calcd. 8.08 %) at 214°C in the curve of cadmium complex corresponds to the loss of two water molecules of hydration. The decomposition temperatures acquired from the melting point machine also supports the projected inferences for the weight changes in this TG analysis [214].

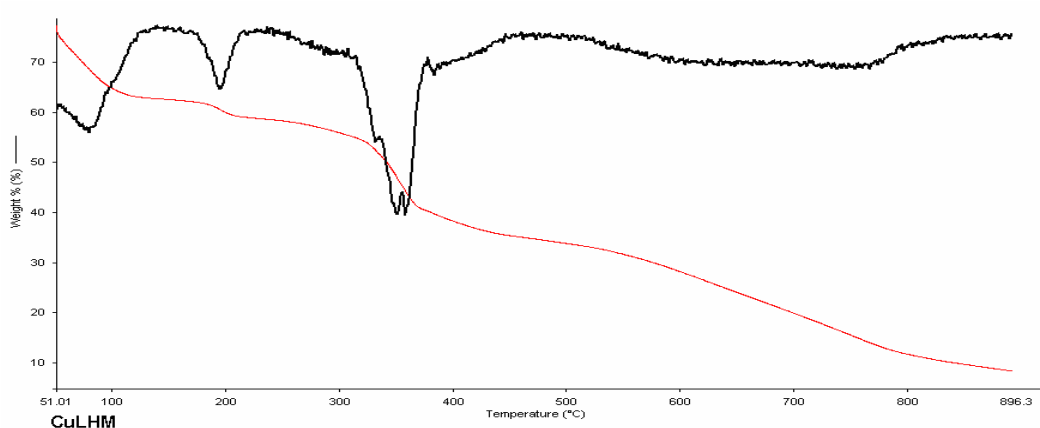


Fig. 3.159 TGA curve of  $[\text{Cu}(\text{LHM})\text{Cl}_2]$  complex.

### 3.6.8 Thermogravimetric data of $\text{Cu}(\text{HMS})$ , $\text{Zn}(\text{HMS})$ and $\text{Cd}(\text{HMS})$ complexes

The thermo-gravimetric data for copper, zinc and cadmium complexes of HMS with their tentative assignments are shown in Table 3.48 and Figure 3.162-3.164

Table 3.48 TGA data of  $\text{Cu}(\text{HMS})$ ,  $\text{Zn}(\text{HMS})$  and  $\text{Cd}(\text{HMS})$  complexes:

Compounds	M.P /D.T	TGA	Weight loss (%)		Remark
			Observed	calculated	
HMS	64	NA			
$[\text{Cu}(\text{HMS})\text{Cl}_2]$	266	228	9.18	9.07	loss of $2\text{H}_2\text{O}$
$[\text{Zn}(\text{HMS})\text{Cl}_2]$	248	192	13.04	13.42	loss of $\text{H}_2\text{O}$ and Cl
$[\text{Cd}(\text{HMS})\text{Cl}_2]$	338	301	7.82	8.07	loss of $2\text{H}_2\text{O}$

The TG curves recorded for the complexes derived from HMS ligand exhibits similar weight losses with its analogue LHM ligand by 9.18 % (calcd. 9.07 %) in the Cu complex curve, 13.04 % (calcd. 13.42 %) in the curve of Zn complex and 7.82 % (calcd. 8.07) in the curve of Cd. The observed temperatures at which these weight changes occurs are comparable with the decomposition temperatures noticed in the complexes derived from LHM ligands except in the cadmium complex which shows increased thermal stability by 87°C. This high temperature observed in Cd complex is further supported by the thermal decompositions points recorded on the melting point apparatus and can be attributed to the atomic size influence. However, the mass losses observed for Cu, Zn and Cd can be afforded to the departure of molecules with the relative molar masses of 36 and 54 which can predictably be two molecules of water of hydration in the case of Cu and Cd curves and a molecule of water of hydration and chlorine atom in the TG curve of zinc complex [210,215] (Appendix F).

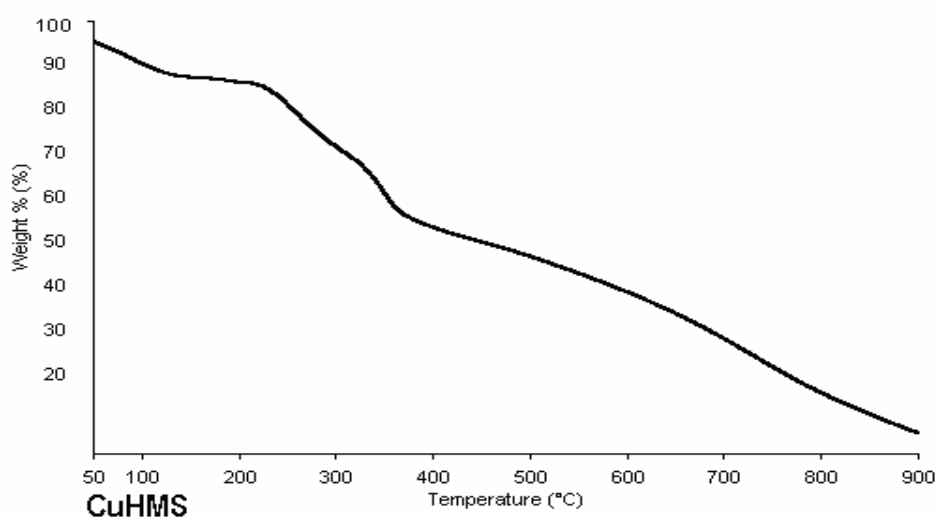


Fig. 3.162 TGA curve of [Cu(HMS)Cl<sub>2</sub>] complex.

### 3.6.9 Thermogravimetric data of Cu(2HP), Zn(2HP) and Cd(2HP) complexes

The thermo-gravimetric data for copper, zinc and cadmium complexes of 2HP with their tentative assignments are shown in Table 3.49 and Figure 3.165-3.167

Table 3.49 TGA data of Cu(2HP), Zn(2HP) and Cd(2HP) complexes:

Compounds	M.P/D.T	TGA	Weight loss (%)		Remark
			Observed	Calculated.	
2HP	61	NA			
[Cu(2HP)Cl <sub>2</sub> ]	269	231	9.96	9.45	loss of 2H <sub>2</sub> O
[Zn(2HP)Cl <sub>2</sub> ]	265	243	4.70	4.70	loss of H <sub>2</sub> O
[Cd(2HP)Cl <sub>2</sub> ]	247	208	8.65	8.38	loss of 2H <sub>2</sub> O

The thermal stability results of Cu, Zn and Cd complexes synthesized from the ligand 2HP exhibits first decomposition temperatures in TG analysis (Table 3.49) (Appendix F). The complexes show comparable weight losses between the observed, and the calculated values. The weight losses of 9.96 % (calcd. 9.45 %) in the Cu complex curve, 4.70 % (calcd. 4.70 %) in the curve of Zn complex and 8.65 % (calcd. 8.38 %) in the curve of Cd complex indicates the possibility of high stability of these complexes. These weight changes correspond to the exit of molecules with relative molar mass of 36 in the curves of Cu and Cd complexes and the possible departure of a molecule with molar mass 18 gmol<sup>-1</sup> in the zinc complex TG curve. This can presumably be the molecule of water of hydration found in the structure of the complexes [51,216]. Despite the low melting point shown by this ligand, its complexes demonstrated high thermal stabilities as supported by the results obtained from the decomposition points recorded on the melting point machine.

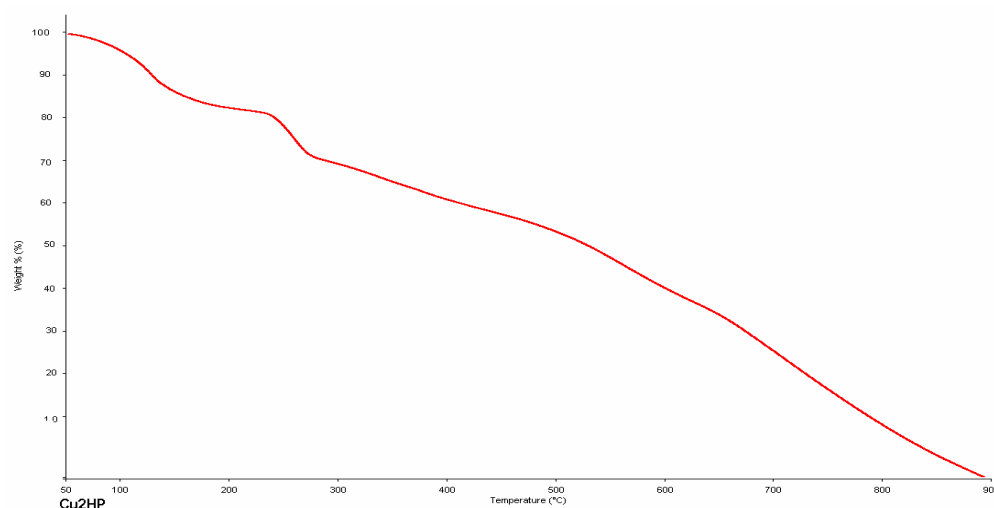


Fig. 3.165 TGA curve of [Cu(2HP)Cl<sub>2</sub>] complex.

### 3.6.10 Thermogravimetric data of Cu(DHP), Zn(DHP) and Cd(DHP) complexes

The thermo-gravimetric data for copper, zinc and cadmium complexes with their tentative assignments are shown in Table 3.50 and Figure 3.168-3.170.

Table 3.50 TGA data of Cu(DHP), Zn(DHP) and Cd(DHP) complexes:

Compounds	M.P/D.T	TGA	Weight loss (%)		Remark
			Observed	Calculated.	
DHP	64	NA	Observed	Calculated.	
[Cu(DHP)Cl <sub>2</sub> ]	255	201	13.39	13.48	loss of H <sub>2</sub> O and Cl
[Zn(DHP)Cl <sub>2</sub> ]	352	306	14.08	13.42	loss of H <sub>2</sub> O and Cl
[Cd(DHP)Cl <sub>2</sub> ]	239	184	12.33	12.00	loss of H <sub>2</sub> O and Cl

The thermal data recorded for the complexes derived from DHP ligand exhibits stepwise decomposition behavior. The first decomposition step observed at the temperature 201°C with mass loss of 13.39 % (calcd. 13.48 %) in the curve of copper complex and the decomposition at 306°C with the mass loss of 14.08 % (calcd. 13.42 %) in the curve of zinc complex indicates the departure of an identical molecule. Similar weight loss is noticed in the curve of cadmium complex at 184°C with mass loss of 12.33 % (calcd. 12.00 %). These weight changes are correspondingly attributed to the disappearance of a molecule with relative molar mass of 54 in all the complexes. The expected loss of a molecule of water of hydration and chlorine atom is assumed considering the behavior of the previous

complexes. The complexes of DHP ligand shows a rise in the stabilities when compared to the complexes obtained from 2HP ligand, which perhaps maybe due to additional ring substituents [217] (Table 3.50) (Appendix F).

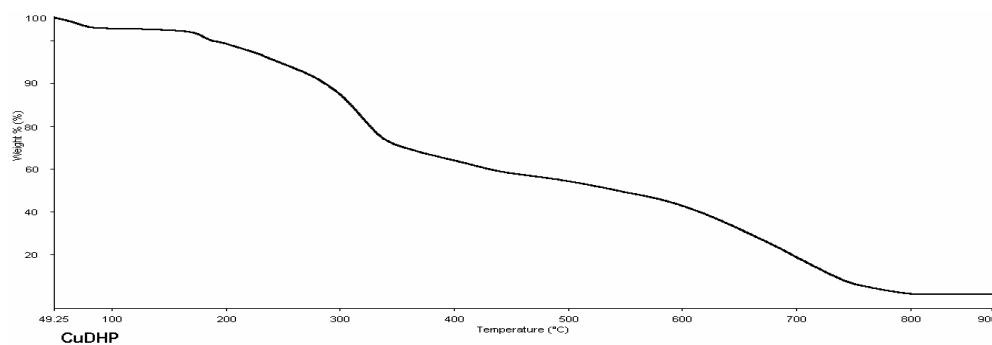


Fig. 3.168 TGA curve of [Cu(DHP)Cl<sub>2</sub>] complex.

### 3.7 X ray diffraction analysis

The crystals obtained were isolated and analyzed for structure determination. Some complexes of zinc and cadmium were successfully isolated, and their spectroscopic data were used as a guide to interpret the possible geometries of other complexes.

#### 3.7.1 Crystal structure and analyses of [Zn(LNS)Cl<sub>2</sub>], [Zn(LDH)Cl<sub>2</sub>] and [ZnHMSCl<sub>2</sub>]

Single crystals for X-ray analysis were obtained from ethanolic solutions of zinc complexes after slow evaporation at room temperature. The crystal data and the details of the X-ray analysis are given in Tables 3.51-3.56. The molecular structures of zinc complexes are shown in Figures 3.171-3.173. The crystal structures contained hydrated water molecules, which are not depicted in the figures. This is evident in the TGA result of all the complexes. The three zinc complexes have zwitter-ionic nature wherein their piperazine secondary nitrogen, N3, stay away from coordination and are protonated to keep the electro-neutrality of the molecules. In [Zn(LDH)Cl<sub>2</sub>], the piperazine tertiary nitrogen, N2, is also away from the coordination environment, thus the zinc atom is four coordinated in a distorted tetrahedral geometry. In the crystal, the zinc metal is connected via N-H...O and

N-H...Cl hydrogen bonds (Tables 3.52, 3.54, 3.56) into layers parallel to the crystallographic *bc* plane. In [Zn(HMS)Cl<sub>2</sub>] and [Zn(LNS)Cl<sub>2</sub>], in contrary, the tertiary nitrogen lone pair electrons are directed towards the metal centers and contribute in the metal chelations *via* long-range interactions, the Zn-N2 distances being 2.591(2) and 2.7299(13) Å for [Zn(HMS)Cl<sub>2</sub>] and [Zn(LNS)Cl<sub>2</sub>] respectively. All the complexes have comparable Zn-N distance. The geometries of the resulting pseudo-five-coordinate complexes are intermediate between square-pyramidal and trigonal-bipyramidal as indicated by Addison  $\tau$  values [218] of 0.56 for [Zn(HMS)Cl<sub>2</sub>] and 0.39 for [Zn(LNS)Cl<sub>2</sub>]. In the crystal structure of [Zn(HMS)Cl<sub>2</sub>], the molecules of the metal complex are connected through N-H...O and N-H...Cl hydrogen bonds (Table 3.56) into layers in the *ab* plane. In the crystal of [Zn(LNS)Cl<sub>2</sub>], pairs of the metal complex molecules are linked through N-H...Cl hydrogen bonds (Table 3.51) (Appendix G) to form centro-symmetric dimers.

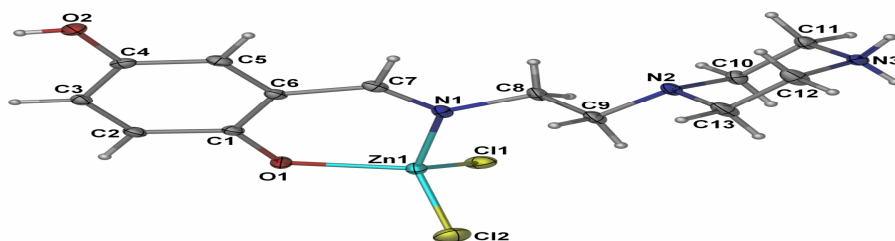


Figure 3.171 The molecular structure of [Zn(LNS)Cl<sub>2</sub>] with thermal ellipsoids at 50% probability level.

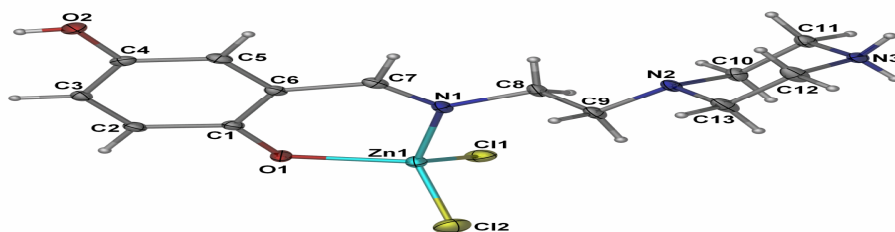


Figure 3.172 The molecular structure of [Zn(LDH)Cl<sub>2</sub>] with thermal ellipsoids at the 50% probability level

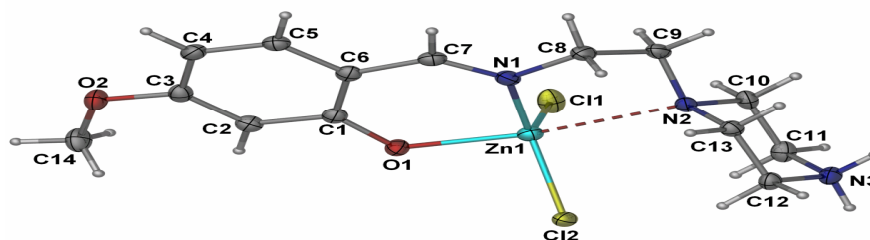


Figure 3.173 The molecular structure of  $[\text{Zn}(\text{HMS})\text{Cl}_2]$ , with thermal ellipsoids at the 50% probability level.

### 3.7.2 Crystal structure and analyses of $[\text{Cd}(\text{LSP})\text{Cl}_2]$ and $[\text{Cd}(\text{LHM})\text{Cl}_2]$

The X-ray structure of cadmium complex obtained from LSP ligand  $[\text{Cd}(\text{LSP})\text{Cl}_2]$  exhibits that the piperazine ring adopts a chair conformation and the ligand is bound to the metal ion in a NNO-tridentate fashion. The cadmium(II) atom is penta-coordinated by the Schiff base ligand and two chloride atoms in a highly distorted square planar geometry (index  $\tau = 0.38$ ). The piperazine nitrogen atom, N3, which stays away from coordination, is protonated, implying the zwitter-ionic nature of the complex. In the crystal structure, intermolecular N—H $\cdots$ O, N—H $\cdots$ Cl and C—H $\cdots$ Cl hydrogen bonds are connected to the adjacent molecules into infinite three-dimensional network (Fig. 3.174). Moreover, intramolecular C—H $\cdots$ Cl hydrogen bonding are observed. The crystal structure contains void spaces with the size of  $199 \text{ \AA}^3$  (6.2% of the cell volume) within which there is no evidence for included solvent (Table 3.58,3.59,3.62) (Appendix G).

Akin to the X-ray structure of cadmium complex obtained from LSP ligand, the  $[\text{Cd}(\text{LHM})\text{Cl}_2]$  complex also shows the piperazine ring moiety with a chair conformation and bonded to only one of the ring N atoms. The Schiff base ligand coordinates to the metal atom through *N,N,O*-mode, along with two Cl atoms and makes a distorted square-

pyramidal cadmium(II) complex. The distortion from the ideal geometry is evident from the  $\tau$  index of 0.30 ( $\tau$  is 0 for an ideal square-pyramid and is 1 for a perfect trigonal-bipyramid,) [218]. The other ring N atom stays away from the chelation, and is protonated to keep the electro-neutrality of the molecule, thus the complex can be described as a zwitter-ion. In the crystal, C—H $\cdots\pi$  interactions link the molecules into infinite chains along the *a* axis and these are connected into a three-dimensional network *via* N—H $\cdots$ O, N—H $\cdots$ Cl and C—H $\cdots$ Cl hydrogen bonds (Table 3.60, 3.61, 3.62 and Fig. 3.175) (Appendix G).

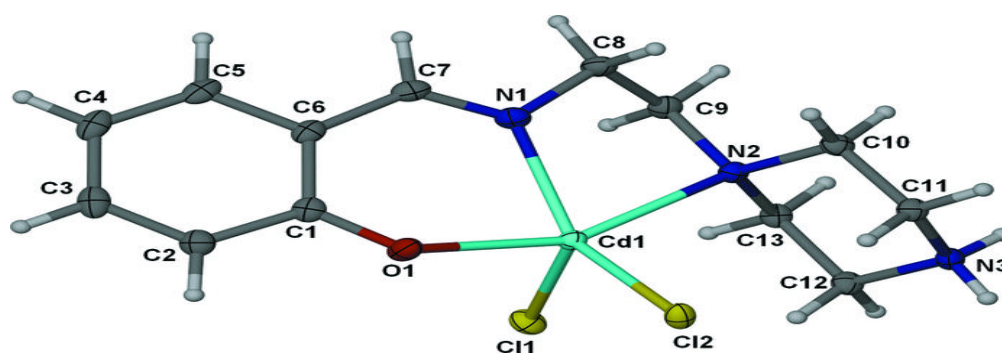


Figure 3.174 The molecular structure of [Cd(LSP)Cl<sub>2</sub>], with thermal ellipsoids at the 50% probability level.

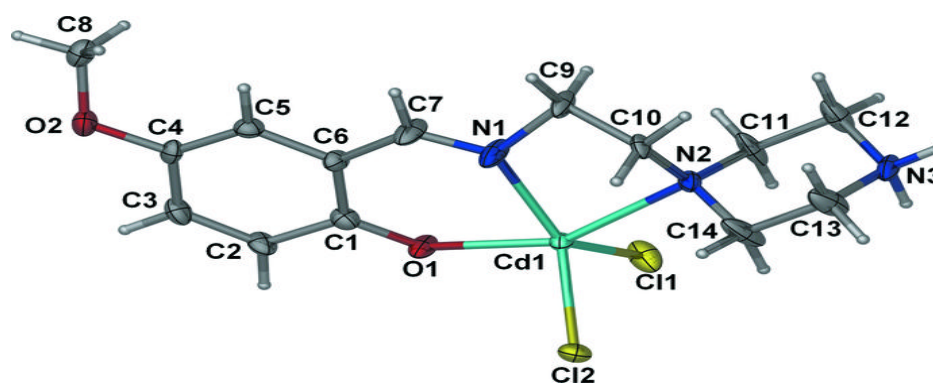


Figure 3.175 The molecular structure of [Cd(LHM)Cl<sub>2</sub>], with thermal ellipsoids at the 50% probability level.

**CHAPTER FOUR**

**BIOLOGICAL STUDIES**

## **4. Biological studies**

### **4.1. Introduction**

#### *4.1.1. Acute toxicity studies*

The analysis on the toxicity level of chemical compounds is the most important step required for further biological studies [219]. The toxicity level of the Schiff bases and their metal complexes were evaluated at the maximum dose of 2000 mg/kg/body weight. The compounds were administered orally to the 24 h fasted rats and monitored closely after every 30 minutes up to 8 h of post treatment. It was observed that the compounds did not cause any gross behavioral changes like convulsion, dizziness or respiratory distress. No mortality was recorded for the period of 14 days which indicated that the lethal dose of the compounds is above 2000 mg/kg body weight in rats and that the compounds can be considered to be less harmful at this dose.

#### *4.1.2 Acetylcholinesterase inhibition*

The neurodegenerative disorder characterized by the nerve cell dysfunctions and loss of neurons in the central nervous system was first discovered in 1907 by a German scientist, Alois Alzheimer, and was named as Alzheimer's disease (AD). Millions of people are reported to fall victims of this traumatic problem worldwide [220]. In the early stages, the patient is faced with a decline in cognitive functions, exclusively short-term memory, which later results in the incapability to read, speak and/or think rationally [221]. Recent reports on curative approaches to this ailing disease are based on the assumption of a cholinergic mechanism, with particular emphasis on acetylcholinesterase inhibition [221,222]. Indeed, many scientific trials have been conducted in order to discover a typical and non-toxic drug for the treatment of AD. The most commonly used drugs for the treatment of AD is tacrine which is recognized to possess so many side effects that in most

cases they lead to the withdrawal of the medication. Other drugs like donepezil, rivastigmine, galanthamine, caproctamine and memantine were also used for the treatment of AD, but are known for their unfavorable effects like hepatotoxicity, gastrointestinal disturbance, dizziness, diarrhea, vomiting and nausea [223-225]. The key factor likely implicated in many diseases is oxidative stress caused by free radicals produced as a result of an imbalance in antioxidants produced by the cells [226]. This suggests that treatment of AD should involve acetylcholinesterase inhibitors and antioxidants that can scavenge the excess free radicals and antagonize the consequences of oxidative stress [227,228]. In addition, the literature reported that many standard drugs contain a polyamine backbone in their structures and that the AChE gorge is lined with various preserved aromatic residues which in principle can form cation- $\pi$  bonds with a basic polyamine counterpart [229,230]. This study therefore sought to synthesize and characterize some new compounds capable of AChE binding site inhibition and compares their activity with that of standard drugs like tacrin and propidium. These compounds have flexidentate behavior and contain secondary and tertiary amines in their structures akin to the secondary amino function found in tacrine dimer [231] and the tertiary amino group of donepezil [232]. Moreover, the compounds were tested for antioxidant activities using the FRAP and DPPH assays due to arising demands for compounds that are safe and possess dual AChE inhibition and antioxidant activities [233,234].

#### *4.1.3 Anti-ulcer studies*

Gastric mucosal erosion was theorized to be associated with the imbalance between the aggressive factors (physical, chemical or psychological) in the lumen and protective mechanisms [235] in the duodenal mucosa causing chronic inflammation that lead to a defect in the regulation of gastrin production [236]. Gastrointestinal problems have now

become a global problem and many studies were conducted towards fixing it [237]. The ability of some ulcer models to suppress the production of prostaglandins and thromboxanes, and cause irreversible inactivation of the cyclooxygenases (which is essential for the production of prostaglandins) has provided a means for intense investigation [238-240]. It was suggested that cytokines such as tumor necrosis factor-alpha (TNF- $\alpha$ ), interleukin-6 (IL-6) and interleukin-10 (IL-10) play important roles in the acute phase inflammation as well as in maintenance and regulation of the severity of gastric ulcers [241]. The ulceration bestowed by ethanol causes an intense infiltration in the submucosa, decrease mucus, depletes sulfhydryl groups and decrease blood flow which ensures in serious damage to gastric mucosa [242]. This ulcer model has found relevance in scientific research for providing means of determining the mechanistic action of many compounds in gastroprotective efficacy. On the other hand, zinc being an essential element which plays an imperative role in cell-mediated immune functions. Zinc is employed as a cofactor for metalloenzymes, superoxide dismutase, collagenase, alcohol dehydrogenase, alkaline phosphate, and spermatogenesis and in growth in children [243,244]. It is also required for the proper functioning of mucosal cells and can arrest the advancement of gastrointestinal diseases by free radical scavenging and interruption of the inflammatory process as an antioxidant and anti-inflammatory agent. Zinc deficiency can cause poor wound healing, loss of taste and smell and elevation in ROS [245,246]. Zinc complexes were reported to have anti-ulcer activity and used as drugs for the treatment of gastrointestinal injuries in Japan [247]. This study therefore, considers the therapeutic potentials of piperazine derivatives and the role played by zinc in wound healing to synthesize novel compounds with combine protective activities [248,249].

#### ***4.1.4 Anti-cancer studies***

Cancer has become the major source of mortality throughout the world due to its resistance to many therapeutic approaches. Treatment of cancer is one of the major challenges in the scientific research today [250]. It is the leading cause of death in the United States [251] and found in various forms including the cancers of the lung, breast, skin, prostate etc [252]. Cancer is considered as the unwanted cell growth due to genetic mutations [253] as a consequence of inheritance or environmental changes. The current chemotherapeutic agents used in the treatment of cancer are associated with many side effects including damage to the healthy cells and tissues. This prompted the interest of many researchers to bring compounds that can kill the cancer cells and have less toxic effects to the healthy cells. However, cancer cell sometimes become resistant to chemotherapy due to cellular modifications that involves augmented expression of drug detoxifying enzymes and drug bioavailability [254]. Furthermore, compounds containing piperazine moiety were reported to have shown anticancer activities [255] in different cancer cell lines and this has motivated the interest of this study in evaluating the anticancer activities of the synthesized compounds as well as their toxicity level.

### **4.2. Experimental**

#### ***4.2.1 Protocol for acute toxicity***

In this study, twenty four *Sprague Dawley* rats of 7-8 weeks old weighed ( $165 \pm 15$  g) were assigned into two groups of twelve rats each (six male and six female rats per group) and labeled as control and treatment groups. The animals were fasted for 24 h and orally received a single dose of the compound 2000 mg/Kg/body weight, and continued fasting for 3–4 h after dosing. Daily clinical examinations of the animals did not show any significant signs of toxicity like tremor, eyes mucus, body weight changes or autonomous

saliva release. No mortality was recorded at any time of observation for the period of two weeks. The study was conducted according to the “International Guidelines for Testing of Chemicals Oral Toxicity” [256] and was approved by the Animal Ethics Committee of University of Malaya. In addition, only the less toxic compounds were used for further biological evaluations.

#### 4.2.2. AChE assay

The anti-cholinesterase activities of the ligands were evaluated by Ellmann’s method with slight modifications, using acetylthiocholine as a substrate [257] and 5,5’-dithiobis[2-nitrobenzoic acid](DTNB). Sodium phosphate buffer (pH 8.0, 110  $\mu$ L) was added into the 96 wells followed by sample solution (20  $\mu$ L), DTNB (0.126 mM, 50  $\mu$ L) and AChE enzyme (0.6 U/mL, 20  $\mu$ L). The mixture was incubated for 50 minutes at 37 °C. The reaction was then initiated by the addition of acetylthiocholine iodide (0.120 mM, 50  $\mu$ L). The hydrolysis of acetylthiocholine was monitored by the formation of yellow 5-thio-2-nitrobenzoate anion as the result of the reaction of DTNB with thiocholine, released by the enzymatic hydrolysis of acetylthiocholine, at a wavelength of 412 nm every 30 s for 25 min using a 96-well microplate plate reader (TECAN Infinite M200, Mannedorf, Switzerland). Test compounds were dissolved in analytical grade DMSO. Tacrine and propidium iodide was used as reference standards [258]. The reactions were performed in triplicate and monitored with a spectrophotometer. The percent inhibition of the enzyme activity due to the presence of increasing test compound concentration was obtained from the expression;  $100 - (v_i/v_o \times 100)$ , where  $v_i$  is the initial rate calculated in the presence of inhibitors and  $v_o$  is the enzyme activity.

#### 4.2.2.1 Docking studies

The crystal structure of hAChE (pdb id: 1B41) shows that this enzyme possesses a deep narrow gorge which penetrates halfway into the enzyme, where the catalytic site resides [259]. Conversely, hAChE shares a certain degree of similarity with both mAChE and TcAChE, especially the active-site gorge due to their high degree of sequence identities of 87% and 53%, respectively. Generally, the catalytic site of AChE consists of five regions, which are the peripheral anionic site (PAS), the acyl pocket, the esteratic site (ES), the oxyanion hole (OH) and the anion subsite (AS). A similar catalytic site is also observed in hAChE, PAS (Tyr 72, Tyr 124, Tyr 341, Asp 74 and Trp 286 residues), the acyl pocket (Phe 297, Phe 295 and Phe 338 residues), CT (Ser 203, His 447 and Glu 202 residues), OH (Gly 121, Gly 122 and Ala 204 residues) and AS (Trp 86 and Glu 202 residues). A molecular docking simulation (Figure 3.177, Appendix I) showed that the Schiff bases LHM and DHP are well positioned at the active-site gorge. The hydrophobic interaction between these Schiff bases and the alkyl linker and the rich aromatic contents (Tyr 124, Tyr 341, Tyr 337, Phe 338, Phe 297 and Trp 286) along the gorge could potentially direct the phenyl ring to penetrate deep into the anionic site and oxyanion hole regions in the choline-binding site. This interaction is further intensified, where three hydrogen bonding were found between the Schiff bases (LHM and DHP) and the residues in the active site. This includes hydrogen bonding between the tertiary nitrogen of the piperazine ring with Tyr 124 residue at a distance of 2.42 Å. Two hydrogen bonding interactions between the imine group and two amino residues along the gorge which are Tyr 124 (3.05 Å) and Tyr 337 (2.91 Å) were also observed during the docking experiment.

### *4.2.3. Ulcerogenic studies*

#### *4.2.3.1 Dose selection*

A preliminary study for dose fixation was conducted using 20 mg/kg of the compounds (Cu and /or Zn complex) to 24 h fasted rats prior to ethanol induced ulceration. It was observed that 20 mg/kg of the compounds did not significantly prevent the damaging effects of ethanol. Increasing the dosage to 30 mg/kg was observed to give a better protection. Furthermore, treatment with some of the zinc complexes for 3, 7 and 10 days showed continuous inhibition of the ulcer area. Thus, the dose of 30 mg/kg was then considered as the low dose and the treatment extend to 14 days to further ascertain the active dosage that can give the highest protection against the damaging effects of ethanol.

#### *4.2.3.2 Protocol for ulcer studies*

Animals were fasted for 24 h before ethanol-induced ulceration and orally pre-treated as follows; Group 1 and 2 received the vehicle, carboxymethylcellulose (CMC) after 14-days treatments with food and water alone. Group 3 rats were treated with omeprazole (20 mg/kg) dissolved in CMC prior to ethanol administration. Group 4, 7 and 8 were given the compounds dissolved in CMC for two weeks. Group 5 and Group 6 were given the compounds at single doses of 30 and 60 mg/kg, respectively, dissolved in CMC prior to ulcer induction to assess the gastric tolerability of the compounds. One hour after this treatment, animals in Group 2, 3, 5, 6, 7 and 8 were orally gavaged with 95% ethanol at the dose of 5 mL/kg. Group 4 rats were not given ethanol and served as the normal control group. All the animals were sacrificed after 30 minutes by cervical decapitation under anesthesia with xylazine and ketamine. Serum was collected for biochemical analyses.

#### 4.2.4 Antioxidant studies

The antioxidant activities of the Schiff bases were evaluated according to FRAP and DPPH assays described below

##### 4.2.4.1. FRAP (ferric reducing antioxidant power) Assay

The activities of the compounds were assessed using modified FRAP method [260]. The stock solutions contained 300 mM acetate buffer (3.1 g  $C_2H_3NaO_2 \cdot 3H_2O$  and 16 mL  $C_2H_4O_2$ ), pH 3.6, 10 mM TPTZ (2,4,6-tripyridyl-s-triazine) solution in 40 mM hydrochloric acid and 20 mM ferric chloride hexahydrate solution. The fresh working solution was prepared by mixing acetate buffer (25 mL), TPTZ (2.5 mL), and ferric chloride hexahydrate solution (2.5 mL). The temperature of the solution was raised to 37 °C before use and allowed to react with the FRAP solution (300  $\mu$ L) in the dark. The colored product (ferrous tripyridyltriazine complex) was monitored at a wavelength of 593 nm. The standard curve was linear between 100 and 1,000  $\mu$ M ferrous sulphate. Results are expressed in  $\mu$ M ferrous/g dry mass and compared with that of ascorbic acid and butylatedhydroxytoluene.

##### 4.2.4.2. DPPH (1,1-Diphenyl-2-picrylhydrazyl) Assay

The scavenging activities of the compounds on DPPH were recorded according to the reported procedure [261]. The compounds showed final concentrations within the range of 0–25  $\mu$ g/mL in methanol. One milliliter of 0.3 mM DPPH ethanol solution was added to sample solution (2.5 mL) of different concentrations and used as stock solutions for the test; meanwhile, methanol (1 mL) was added to samples (2.5 mL) to make the blank solutions. The negative control (blank) consisted of DPPH solution (1 mL) plus methanol (2.5 mL). These solutions were allowed to react at room temperature for 30 min in the dark.

The absorbance was read at 518 nm and converted into percentage antioxidant activity according to the following equation:

$$\% \text{ Inhibition} = [(A_B - A_A)/A_B] \times 100.$$

Where:  $A_B$ : absorption of blank sample,  $A_A$ : absorption of tested samples. The kinetics of DPPH scavenging activity was determined and the  $IC_{50}$  calculated using ascorbic acid as a positive control.

#### 4.2.5 Anticancer studies

The cancer studies were performed on four different human cancer cell lines *viz* prostate (PC3), lung (A-549), breast (MCF-7) and liver (HepG2) using some selected zinc complexes. The toxicity profiles of the compounds were assessed using MTT (microculture tetrazolium) viability assay [262]. The compounds were prepared at various concentrations and added in triplicates to 96-well plate containing untreated cell controls and blank cell-free controls. After 44 h of incubation, 5 mg/mL of MTT was added to each well and the plates were incubated for further 4 h and then removed. The solvent DMSO was added into each well to solubilize the formazan crystals and the absorbance was read at 595 nm using spectrophotometer (Tecan Infinite M 200 PRO, Mannedorf, Switzerland). The percent viability of the cells was calculated for each complex [263] to determine the  $IC_{50}$  and the values obtained were compared with the control. The inhibitory rate of cell death was calculated by the following formula:

$$\text{Growth inhibition} = \text{OD control} - \text{OD treated} / \text{OD control} \times 100.$$

The cytotoxic effects of the compounds on cancer cells were expressed as  $IC_{50}$  values (the drug concentration reducing the absorbance of treated cells by 50% with respect to untreated cells).

#### 4.3 Results and discussions

The oral administration of the synthesized Schiff bases and their metal complexes of copper and zinc for 2 weeks did not signify change in the biochemical parameters such as renal function indices like creatinine, urea, anion gap sodium and carbon dioxide (Table 3.63). Both the normal rats and the rats treated with the compounds had manifested the level of biochemical indices within the normal range (Appendix H). However, the liver enzymes AST, ALT, ALP and triglyceride rises significantly in the rats that received non substituted Schiff bases (LSP and 2HP) and their complexes of Cu and Zn compared to the rats administered with the substituted Schiff bases (LCS, LBS, LNS, LDH, DHS, LHM, HMS and DHP) and their complexes of Cu and Zn, than the normal rats. This indicated damage caused by the compounds in the liver cells [264]. These effects were reduced in the analogue complexes that contained ring substituents in their structures, thus displaying the influence of ring substituents on the activity of the compounds [265,266]. Other liver indices like total protein count, albumin, globulins, total cholesterol, total and conjugated bilirubin did not significantly change (Table 3.64) at the dose of 2000 mg/kg/body weight. The histological evaluations also prove the low toxic effects of the compounds (Fig.3.176, Appendix H).

The enzymatic data for human AChE inhibition had identified the Schiff bases LHM and DHP as the most potent inhibitors with  $IC_{50}$  45.4 and 21.8 respectively among the two series of the Schiff bases. The Schiff bases like LCS ( $IC_{50} = 29.8$ ) and LNS ( $IC_{50} = 28.4$ ) are competing with one of the reference drugs, propidium which showed  $IC_{50}$  of 28.2. Other Schiff bases; LSP, LBS, LDH, DHS and HMS gave  $IC_{50}$  of 13.5, 26.2, 25.6, 18.3 and 27.5 respectively. These values are below the  $IC_{50}$  of 28.2 and 76.6 determined for the reference drugs propidium and tacrine, respectively. However, none of the Schiff bases had

exhibited activity higher than the tacrine drug; therefore, the overall activity can be considered as moderate inhibitory activities. The ability of the compounds to inhibit the acetylcholinesterase activity can be attributed to the influence of the substituents on phenyl ring [267]. Furthermore, the results demonstrated that the compounds with ring substituents at the *para* position to the phenolic functional groups are more active inhibitors than those with substituents at the *meta* position. Thus, the activity increases from the none-substituted (LSP) through meta-substituted (DHS and HMS) to the *para*-substituted (LCS, LBS, LNS, LDH and LHM) Schiff bases. This increase in the inhibitory activities also suggests anti-inflammatory activity of the compounds [268]. The enzyme-ligand binding interactions of the most active inhibitors were investigated by molecular docking studies (Fig. 3.177, Appendix I).

The antioxidant activities of the Schiff bases were established using FRAP and DPPH assays. The compounds demonstrated relatively moderate activities in both assays when compared with the reference standards, vitamin C and BHT. The compounds generally showed activities higher than BHT in FRAP assay, except LSP Schiff base that showed frap value of 120, which is lower than 181 noticed with the BHT. However, the Schiff base LHM was identified as the most active with frap value of 1365, this is higher than the frap values of 293.3, 355.3, 840, 720, 689, 1119, 852, and 932 observed with 2HP, DHP, LCS, LBS, LNS, LDH and HMS respectively but still lower than the frap value of 1974 noticed with vitamin C. In the DPPH assay, the Schiff bases LSP, LCS, and LBS showed  $IC_{50}$  of 8, 19 and 18, which is lower than the  $IC_{50}$  of both BHT, 21 and vitamin C, 55 used as reference standards. Other Schiff bases; LNS, LDH, DHS, LHM and HMS exhibited  $IC_{50}$  of 25, 26, 22, 35 and 28 respectively. These values are slightly lower than the frap value of vitamin C but still higher than the frap value of BHT. This suggests potentials of the

compounds to inhibit oxidation chain reactions by removing the free-radical intermediates through hydrogen atom transfer (HAT) as well as by single-electron transfer (SET) in FRAP and DPPH assays respectively [269].

The protective activity of the compounds against the necrotic effects of ethanol were ascertained by comparing the number of lesions found in the gastric of the rats treated with ethanol and those in the treatment and control groups (Appendix J, Fig. 3.178). It is apparent that the compound significantly and dose-dependently protects the mucosal membrane against ethanol-induced injury (Fig. 3.178 C-F). This protection was high in rats that received the compounds for two weeks (Fig. 3.178 E-F) than those given a single dose of the compounds (Fig. 4D) and/or omeprazole (Fig. 3.178 C). The ability of a mucosa membrane to protect the gastric walls depended solely on equilibrium between the aggressive and the protective factors [270-272]. The compounds administered to the rats had strengthened the protection of mucosal membrane from the damaging effects of ethanol. This was evidenced by the inhibition of leucocytes infiltration of gastric wall (Fig. 3.179 C-F) when compared with the ulcerated rats (Fig. 3.179 B). These rats showed a severe disruption to the surface epithelium, necrotic lesions which penetrate deeply into mucosa, extensive edema of submucosal layer and leucocytes' infiltration. Two-week treatment with these compounds in ulcer induced groups has notably enhanced the mucus secretion (Fig. 3.180 C-D) when compared with the normal rats (Fig. 3.180 A). Ethanol served as the ulcer model that is used for evaluating the protective and healing activity of many drugs [273]. It effectively reduced the level of NO in the gastric mucosa, affects the flow of gastric blood and finally resulted in the development of hemorrhagic necrosis. [274-275]. This leads to an increased flow of Na<sup>+</sup> and K<sup>+</sup>, amplified pepsin secretion, and enhances loss of H<sup>+</sup> ions and histamine in the lumen [276]. The chemo-preventive activity

of the compounds can be presumed to bring changes noticeable in the acute phase C-reactive proteins and HDL. The serum level of AST and ALT were elevated significantly in the ulcerated rats indicating the level of inflammation in the liver. In contrast, the level of these enzymes decreased significantly in the rats pre-treated with the synthesized compounds and omeprazole (Appendix J, Table 3.65). Furthermore, pre-treatment with omeprazole and the synthesized compounds led to the rise in the gastric pH, improved the production of mucus and caused flattening of mucosal folds (Table 3.66). The single doses of the compounds showed a decreased activity compared to omeprazole whereby two-week treatments with the compounds gave better protection. The possible changes in the level of cytokines IL-6, TNF- $\alpha$  and IL-10 were investigated (Table 3.67). The observed increase in the production of IL-6 and TNF- $\alpha$  in plasma can be afforded to the necrotizing effects of ethanol [277]. This effect was mild in the animals treated with omeprazole and the compounds at all doses. However, a slight increase was noticed in the single doses of these compounds, this rise was not significant when compared to the ethanol induced ulcerated rats. The increase in the level of NO, IL-10 (Table 3.66) and inhibition of acid secretion to fix the inflammation and mucosal erosion caused by ethanol [278] can be treated by continuous treatments with the compounds for the period of 14 days. Nitric oxide (NO) was reported to have an ability of inhibiting the neutrophil infiltration and provide a protective barrier to the gastric mucosa against ethanol attack [279]. In addition, the potential anti-ulcer drugs can exert their protective effect against mucosal lesions through inhibition of neutrophil infiltration in the ulcerated gastric tissue [280]. Furthermore, neutrophil accumulation in a gastric mucosa has been shown to induce microcirculatory abnormalities. However, the results of this study demonstrated the ability of Zinc complexes to inhibit the level of pro-inflammatory mediator (TNF- $\alpha$  and IL-6) and neutrophil infiltration. This is

similar to the reported activity of plant extract against indomethacin induced ulceration [281]. This anti-inflammatory activity could also be a key factor in the prevention of gastric ulcer as reported [282]. To further substantiate the mechanism of action of these compounds, MDA level was evaluated (Table 3.67). The current study also showed an appreciable reduction of MDA level in the treatment groups compared with the ulcerated rats. This also suggests the ability of the compounds to prevent the formation of reactive oxygen species (ROS) and consequently, stopped the lipid peroxidation process in the gastric mucosa [282].

The cytotoxic activities of the 1-(2-salicylaldiminoethyl)piperazine complexes were studied in vitro against four human cancer cell lines viz: lung (A-549), prostate (PC3), liver (HepG2) and breast (MCF-7) cancer by 3-(4,5-dimethylthiazole-2-yl)2,5-diphenyl-2H tetrazolium bromide assay (MTT Assay). Cells were treated for 48 h with varying concentrations (0, 1.56, 3.125, 6.25, 12.5, 25, 50 and 100) of the investigated compounds in 5% DMSO. The results indicated that the compounds have acquired different IC<sub>50</sub> values ranging from  $37.01 \pm 5.87$  to  $76.50 \pm 11.3$  and  $>100$  (Table 3.68). These values are by far better than the values showed by the free Schiff bases. However, both the free Schiff bases and their complexes manifested activities lower than the referenced drugs (Appendix K, Table 3.68) which confirmed the non competing behavior of these compounds with the standard drugs and thus, can only be considered as potential therapeutics for cancer treatment when modified and the activity enhanced further. Additionally, the morphological changes of the cell lines were observed using normal inverted microscope to assess the extent of the cytotoxic effect between the cells treated with the compounds and the untreated cells. The Treated cells showed the blebbing of the cell membrane (growth

inhibition and shrinkage of the cells) whereby the untreated cells remained confluent throughout the incubation period (Fig.3.181).

## Conclusion

In conclusion, Schiff bases of piperazines and their complexes of copper(II), zinc(II) and cadmium(II) have been successfully synthesized and characterized. The structures of the prepared compounds were elucidated by spectroscopic techniques involving CHN, IR, NMR, UV-Visible, TGA and X-ray diffraction analysis. The purity of the compounds was evaluated using mass spectra and boiling points/ decomposition temperature determinations. Beside the difficulties experienced in isolating the compounds in a solid form, also, most of the compounds did not produce diffraction quality crystals. Moreover, the copper complexes did not display clear spectra in the NMR analysis. This may probably arise from the paramagnetic nature of the copper ion. After confirming the structures of the synthesized compounds, both the Schiff bases and their metal complexes were further screened for various biological activities such as anti-ulcer, acute toxicity, anti-oxidant, anti-cancer and acetylcholinesterase inhibitions. The complexes of zinc manifested an outstanding anti-ulcer activity and less toxic when compared with that of copper and cadmium complexes. In addition, the metal ions zinc and copper were selected for anti-ulcer studies base on their ability to improve wound healing and serve as cofactors for many metallo-enzymes. Generally, the compounds exhibited moderately good activities in all the assays, except for the cadmium complexes which was limited to only cytotoxic (anticancer) evaluations and found to have killed all the cell lines under study due to its high toxic effect. However, new complexes of the Schiff bases reported in this work need to be synthesized and further biological studies conducted to fully ascertain their chemotherapeutic mechanisms. This is due to the fact that all compounds reported to have contained piperazine moiety in their structure were found to be biologically active.

Therefore, the result of this work has proven the ability of piperazine derive compounds to show various activities in different biological assays.